INFINITE ELEMENTS IN FINITE ELEMENT METHOD

by

Aykut Erkal

B.S., in Civil Engineering, Yıldız Technical University, 1998

M.S., in Civil Engineering, Boğaziçi University, 2001

Submitted to the Institute for Graduate Studies in
Science and Engineering in partial fulfillment of
the requirements for the degree of
Doctor of Philosophy

Graduate Program in Civil Engineering

Boğaziçi University

2007

Dedicated to

My Beloved Sisters Tülay Erkal, Hanife Erkal de Jong

and Brother Ahmet Erkal

ACKNOWLEDGEMENTS

I would like to express my most sincere gratitude to my Thesis Supervisor Prof. Dr. Semih Tezcan for his invaluable guidance, continuous support, motivation and for the influence he has had on my professional growth. His breadth of experience, professionalism as a researcher will always be a source of inspiration for me.

My sincere gratitude is also due to the members of my Advisory Committee, Prof. Dr. Yalçın Aköz, Asst. Prof. Dr. Bilge Doran, Asst. Prof. Dr. Kutay Orakçal, Asst. Prof. Dr. Nilüfer Özyurt for their useful suggestions and improvements.

I would also like to thank my friends Ali Aksoy, Zuhal Özdemir, Fuat Aras, Ali Kasay Enünlü, Yavuz Tokmak, Seyit Çeribaşı, Cenk Güngör, Ufuk Hancılar, and Ayşe Aydın for their helpful supports and friendship.

Heartfelt thanks are due to my beloved Sisters Tülay Erkal, Hanife Erkal de Jong and also to my Brother Ahmet Erkal for their continuous support and endless affection. Finally, I am also grateful to all and every member of my family for all their generous love and support during these years. Thanks for always being there for me.

ABSTRACT

INFINITE ELEMENTS IN FINITE ELEMENT METHOD

It is natural and common to idealize stress or field problems into finite element models with rigid boundaries remote from the area of interest. However, the degree of accuracy of solutions may be significantly increased, if infinite elements extending to infinity are used all along the rigid boundaries.

Infinite elements are introduced and also the history and development of these elements are discussed in detail. The classification of the infinite elements is made as, a) Mapped infinite elements, and b) Decay function infinite elements. Firstly, uni-dimensional infinite elements are described and after the geometric and field variable interpolation of these elements are expressed; the strain matrix and the stiffness matrix are explicitly obtained. In this presentation, a total of 23 different types of 1-D (5), 2-D (13), and 3-D (5) infinite elements have been investigated. Their geometrical configurations, coordinate mapping and field variable mapping functions are presented explicitly in a systematic fashion.

In order to emphasize the high performance and accuracy of the infinite elements, four distinct case studies have been presented. Firstly, the deflection and stress analyses of a point load and a circular uniform distributed load acting on a semi-infinite axi-symmetrical medium have been presented with and without infinite elements. The results have been compared with the exact solution by Boussinesq. Secondly, a square plate loading on the axi-symmetric half space has been analyzed by using solid finite and 3-D dynamic infinite elements. Thirdly, the calculation of the vertical vibration of a square rigid plate resting on a semi-infinite half-space has been given. Finally, for the Boussinesq problem, a sensitivity analysis is performed using not only various mesh sizes but also springs all along the truncated boundaries and the results are compared. It is amply demonstrated that the use of infinite elements provides unprecedented high degree of accuracy.

ÖZET

SONLU ELEMANLAR YÖNTEMİNDE SONSUZ ELEMANLAR

Sonlu elemanlar yönteminde, gerilme problemlerinin ya da tabiatta karşılaştığımız bazı problemlerin modellenmesinde; ilgilenilen bölgeden uzakta, sonsuza uzanan sınırların sabitlenmesi çok sık olarak kullanılmaktadır. Ancak, bu problemlerin sonsuza uzanan sınırlarında sonsuz elemanlar kullanılması durumunda, daha gerçekçi ve doğru sonuçlar elde edilebilmektedir.

Önce sonsuz elemanların genel bir tanımı verilmiş, daha sonra bu elemanların bulunuşu ve tarihsel gelişiminden detaylı olarak bahsedilmiştir. Yine bu elemanların, a) Haritalanan sonsuz elemanlar ve b) Azalan fonksiyonlu sonsuz elemanlar olarak sınıflandırılması yapılmıştır. Öncelikle, bir boyutlu sonsuz elemanlar tarif edilmiştir. Daha sonra geometrik ve bilinmeyen değişken interpolasyonunun tanımlanmasının ardından, gerilme ve stifnes matrisleri oluşturulmuştur. Bu tezde, toplam 23 farklı sonsuz eleman tipi 1 Boyutlu (5), 2 Boyutlu (13), ve 3 Boyutlu (5) incelenmiştir. Bu elemanların geometrik ve bilinmeyen değişken interpolasyon fonksiyonları son derece sistematik ve anlaşılır bir biçimde sunulmuştur.

Sonsuz elemanların son derece yüksek performans ve doğru sonuçlar verdiklerini gösterebilmek amacıyla, dört değişik örnek çalışma verilmiştir. İlk olarak, yarı sonsuz aksi-simetrik ortama etkiyen tekil yük ve dairesel düzgün yayılı yük analizleri sonsuz elemanlar kullanılarak ve kullanılmadan yapılmıştır. Sonuçlar, Boussinesq'in kesin çözümü ile karşılaştırmalı olarak sunulmuştur. Daha sonra, üç boyutlu sonlu ve üç boyutlu sonsuz elemanlar kullanılarak, yarı sonsuz ortamdaki kare bir plağın analizi verilmiştir. Daha sonra, yarı sonsuz ortamdaki kare bir plağın düşey titreşimi verilmiştir. Son olarak, Boussinesq problemi için hassaslık analizi yapılmıştır. Ayrıca, problemin sonsuza giden sınırlarında yaylar kullanılmıştır ve sonuçlar irdelenmiştir. Örnekler göstermiştir ki, sadece sonlu elemanlar kullanıldığında sonuçlar, problemin kesin çözümüne uzak kalırken; sonsuz elemanların kullanılması ile kesin çözüme çok yakın değerler elde edilmektedir.

TABLE OF CONTENTS

LIST OF FIGURES

LIST OF TABLES

LIST OF SYMBOLS

a	Distance between nodes
A	Area
B	Width of plate
$[B]$	Strain matrix
C	Constant
$[C]$	Auxiliary matrix of exponential functions
$[c]$	Consistent damping matrix
C_x, C_z	Dimensions of compliances
C_0	Coefficient of viscosity
$\{d\}$	Nodal displacement vector
$[D]$	Material elasticity matrix
d_i	Nodal displacements
ds	Differential of s along the boundary
dV	Differential of volume
E	Modulus of elasticity
$[E]$	Inverse of auxiliary matrix of exponential functions
E_p	Modulus of elasticity of plate
E_s	Modulus of elasticity of soil
$\{F\}$	Vector of joint loads
$\{f\}_X$	Fixed end reactions of body loads
$\{f\}_S$	Fixed end reactions of surface loads
$\{f\}_{\varepsilon_0}$	Fixed end reactions of initial strains
$\{f\}_{\sigma_0}$	Fixed end reactions of initial stresses
$\{f\}_T$	Fixed end reactions of temperature loads
$\{f\}_0$	Fixed end reactions of known displacements

$[G]$	Strain matrix
G_i	Growth function being unity at node i
G_s	Shear modulus of soil
J	Jacobian
$[J]$	Jacobian matrix
$[K],[k]$	Stiffness matrix
k_L	Wave propagation number
L	Arbitrary distance of the exponential decay $\left(e^{-x/L}\right)$
L_i	Lagrange shape function being unity at node i
l_x, m_x, n_x	Direction cosines of *x*-axis
$[M]$	Consistent mass matrix
M_i	Product of two shape functions being unity at node i
$[N]$	Shape functions matrix
N_i	Shape function of field variables being unity at node i
p	Uniformly distributed load
P	Point load
$\{P\}$	Load vector
$P(x)$	Polynomial
r	Radial distance
R	Radius
$[S]$	Stress matrix
$[t]$	Direction cosines matrix
$[T]$	Transformation matrix
$\{u\}$	Generic displacements vector
u_i	Generic displacements
V	Volume
V_L	Wave propagation velocity
V_p	P-wave velocity
V_s	S-wave velocity

x_i	Distance in x direction
$\{x\}$	Vector of nodal coordinates
α	Positive constant
α_i, β_i	Polynomial constants
γ	Constant
∇^2	Second order laplace operator
$[\underline{\Delta}]$	Operator matrix to differentiate the shape functions
ε	Strain component
$\{\varepsilon\}$	Vector of strains
λ	Lame constant
ν	Poisson's ratio
η	Hysteresis damping ratio
ρ	Mass density
σ	Stress component
τ	Shear stress
ω	Angular frequency of vibration
ξ, η, ζ	Local non-dimensional coordinates

1. FINITE ELEMENTS IN ENGINEERING

1.1. Basic Concept of Finite Element Method

Many physical phenomena in engineering and science are described in terms of partial differential equations. In general, solving these equations by classical analytical methods for arbitrary shapes is almost impossible. The finite element method however, is a numerical approach by which these partial differential equations are solved approximately. From an engineering standpoint, the finite element method is a numerical approach for solving a variety of engineering problems, such as stress analysis, heat transfer, fluid flow and electromagnetics by computer simulation.

Millions of engineers and scientists wordwide use the finite element method to predict the behavior of structural, mechanical, thermal, electrical and chemical systems for both design and performance analyses. Its popularity can be gleaned by the fact that over $1 billion is spent annually in the United States on finite element method software and computer time. A 1991 bibliography (Noor, 1991) lists nearly 400 finite element books in English and other languages. A web search in 2006 for the phrase “finite element” using the Google search engine yielded over 14 million pages of results. Mackerle (http://ohio.ikp.liu.se/fe) lists 578 finite element books published between 1967 and 2005. (Fish and Belytschko, 2007)

The basic idea behind the finite element method is to divide the body into finite elements, often just called elements, connected to each other at their nodes, and obtain an approximate solution. The same basic approach is used in other types of problems. In stress analysis, the field variables are the displacements; in chemical systems, the field variables are material concentrations; in electromagnetics, the potential field. In fluid mechanics problems, the nodal unknowns may, for instance, be fluid pressures due to fluid fluxes (Logan, 2002). The same type of mesh is used to represent the geometry of the structure or component and to develop the finite element equations, and for a linear system, the nodal values are obtained by solving large systems (from 10^3 to 10^6 equations are common today, and in special applications, 10^9) of linear algebraic equations.

For problems involving complicated geometries, loadings, material properties, it is generally not possible to obtain analytical mathematical solutions. Analytical solutions are those given by a mathematical expression that yields the values of the desired unknown quantities at any location in body and are thus valid for an infinite number of locations in the body. These analytical solutions generally require the solution of ordinary or partial differential equations, which, because of the complicated geometries, loadings, and material properties, are not usually obtainable. Hence, the numerical methods are needed, such as the finite element method, for acceptable solutions. The finite element formulation of the problem results in a system of simultaneous algebraic equations for solution, rather than requiring the solution of differential equations. These numerical methods yield approximate values of the unknowns at discrete numbers of points in the continuum. Hence, this process of modeling a body by dividing it into an equivalent system of smaller bodies or units named finite elements interconnected at points common to two or more elements (nodal points or nodes) and/or boundary lines and/or surfaces is called discretization. In the finite element method, instead of solving the problem for the entire body in one operation, equations are formulated and combined to obtain the solution of the whole body.

An example of how a finite element model represents a complex geometrical shape is shown in Figure 1.1. It is very difficult to find the exact response (stresses and displacements) of the machine under any specified loading condition; this structure is approximated as composed of several pieces as shown in Figure 1.1 in the finite element method. In each piece or element, a convenient approximate solution is assumed and the conditions of overall equilibrium of the structure are derived. The satisfaction of these conditions will yield an approximate solution for the displacements and stresses (Rao, 1989).

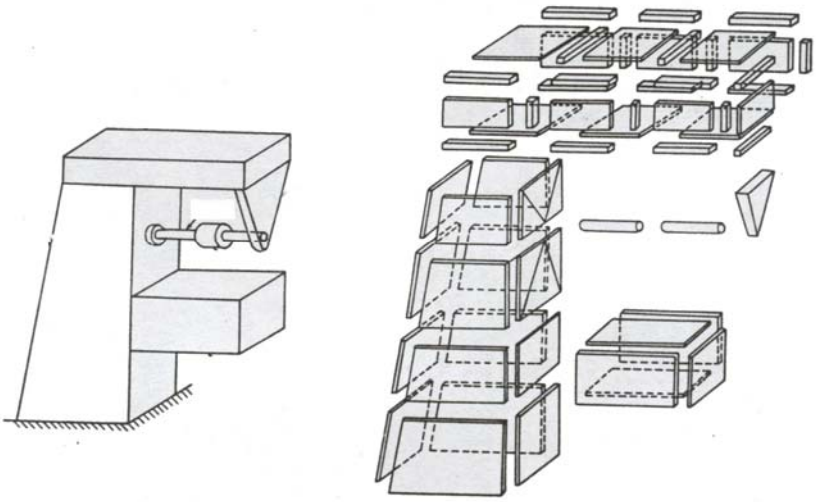

Figure 1.1. Representation of finite elements (Courtesy of Rao, 1989)

1.2. Brief History and Development of Finite Element Method

Advances in aircraft engineering lead to originate the basic idea of finite element method. The modern development of the finite element method began as early as in the 1940s in the field of structural engineering with the pioneering work by Hrennikoff (1941). Hrennikoff presented a solution of elasticity problems using the 'frame work' method. A rectangular finite element model is modeled by means of uni-dimensional lattice bars as originally introduced by Hrennikoff. A typical Hrennikoff lattice cell contains four uni-dimensional flexural bars rigidly connected to each other at the corners. They can carry torsional moments also. The two diagonal bars, however, can only transfer bending moments at their ends.

McHenry (1943) used a lattice of one-dimensional elements for the solution of stresses in continuous solids. He published in a paper in 1943 but not widely recognized for many years. Courant (1943) proposed setting up the solution of stresses in a variational form. Then he introduced piecewise interpolation (or shape) functions over triangular sub-regions making up the whole region as a method to obtain approximate numerical solutions (Logan, 2002).

The general finite element method was developed in the 1950s in the aerospace industry. The major players were Boeing and Bell Aerospace in the United States and Rolls Royce in the United Kingdom. M. J. Turner, R. W. Clough, H. C. Martin and L. J. Top published one of the first papers that laid out the major ideas in 1956 (Turner et al., 1956). They derived stiffness matrices for truss elements, beam elements, and two dimensional triangular and rectangular elements in plane stress and outlined the procedure commonly known as the direct stiffness method for obtaining the total structure stiffness matrix. Along with the development of the high-speed digital computer in early 1950s, the work of Turner et al. prompted further development of finite element stiffness equations expressed in matrix notation. The phrase 'finite element' was first introduced by Clough (1960) when both triangular and rectangular elements were used for plane stress analysis.

Several capable researchers recognized the finite element method's potential early, most notably O. C. Zienkiewicz and R. H. Gallagher (at Cornel). O. C. Zienkiewicz built a renowned group at Swansea in Wales that included B. Irons, R. Owen and many others who pioneered concepts like the isometric element and nonlinear analysis methods. Other important early contributors were J. H. Argyris and J. T. Oden.

Engineers used the method for approximate solution of problems in stress analysis, fluid flow, heat transfer, and other areas in early 1960s. Field problems such as determination of the torsion of a shaft, fluid flow, and heat conduction were solved by Zienkiewicz and Cheung (1965). In the late 1960s and early 1970s, the finite element analysis was applied to nonlinear problems and large deformations.

The finite element method is rapidly becoming an essential and integral part for the solution of medical problems, such as orthopedics, dentistry, etc. Finite element technology consists of a library of element models, a process for combining these models into a mathematical model of an engineering system, and a set of algorithms for numerical solution of equations. This method supported by computer software and by knowledge based on application experiences. The real application of finite element methods requires not only the superiority of the theory but also a significant computer programming effort (Harmandar, 2002).

1.3. Applications of Finite Elements

The range of applications of finite elements is too large to list, but to provide an idea of its versatility, following may be listed:

- Stress and thermal analyses of industrial parts such as electronic chips, electric devices, valves, pipes, pressure vessels, automotive engines and aircraft;
- Seismic analysis of dams, power plants, cities and high-rise buildings;
- Crash analysis of cars, trains and aircraft;
- Fluid flow analysis of coolant ponds, pollutants and contaminants, and air in ventilation systems;
- Electromagnetic analysis of antennas, transistors and aircraft signatures;
- Analysis of surgical procedures such as plastic surgery, jaw reconstruction, correction of scoliosis and many others.

The finite element method was developed for the analysis of aircraft structures as stated earlier. This method is applicable to a wide variety of boundary value problem in engineering. A boundary value problem is one in which a solution required in the domain of a body subject to the satisfaction of prescribed boundary conditions on the dependent variables or their derivatives. A general list of fields of applications of finite element method is given in Table. For each field of application the problem is formulated in anyone of the following types:

- Equilibrium problems
- Eigenvalue problems
- Propagation or transient problems

In an equilibrium problem, it is necessary to find the steady state displacement or stress distribution if it is a solid mechanics problem; the temperature or heat flux distribution if it is a heat transfer problem; and finally the pressure or velocity distribution if it is a fluid mechanics problem.

Eigenvalue problems are sometimes called characteristic value problems and occur in the analysis of homogeneous differential equations. Time will not appear explicitly in eigenvalue problems. These problems can be considered as extensions of equilibrium problems in which critical values of certain constraints are to be determined in addition to the corresponding steady state configurations. The natural frequencies or buckling loads and mode shapes are determined for the solid mechanics or structures problem; the stability of laminar flows for the fluid mechanics problem; and the resonance characteristics for the electrical circuit problem.

The propagation or transient problems are time dependent. The response of a body under time varying force in the area of solid mechanics and under sudden heating or cooling in the field of heat transfer comprise this type of problems (Harmandar, 2002).

Table 1.1. Fields of applications of the finite element method

Area of Study	Equilibrium Problems	Eigenvalue Problems	Propagation Problems
Civil Engineering Structures	• Static analysis of trusses, frames, folded plates, shell roofs, shear walls, bridges and prestressed concrete structures	• Natural frequencies and modes of structures • Stability of structures	• Propagation of stress waves • Response of structures to aperiodic loads
Aircraft Structures	• Static analysis of aircraft wings, fuselages, fins, rockets, spacecraft and missile structures	• Natural frequencies, flutters, and stability of aircraft, rocket, spacecraft and missile structures	• Response of aircraft structures to random loads, dynamic response of aircraft and spacecraft to aperiodic loads
Heat Conduction	• Steady state temperature distribution in solids and fluids	-	• Transient heat flow in rocket nozzles, internal combustion engines, turbine blades, fins and building structures
Geomechanics	• Analysis of excavations, underground openings, rock joints and soil structure interaction problems. • Stress analysis in soils, dams, layered piles and machine foundations	• Natural frequencies and modes of dam reservoir systems and soil-structure interaction problems	• Time-dependent soil-structure interaction problems. • Transient seepage in soils and rocks. • Stress wave propagation in soils and rocks
Hydrodynamics	• Analysis of hydraulic structures and dams	• Sloshing of liquids in rigid and flexible containers	• Rarefied gas dynamics • Magneto hydrodynamic flows
Biomedical Engineering	• Stress analysis of eyeballs, bones and teeth • Mechanics of heart valves	-	• Impact analysis of skull • Dynamics of anatomical structures
Nuclear Engineering	• Analysis of nuclear pressure vessels and containment structures • Steady state temperature distribution in reactor components	• Natural frequencies and stability of containment structures • Neutron flux distribution	• Response of reactor containment structures to dynamic loads • Unsteady temperature distribution in reactor components

2. HISTORY OF INFINITE ELEMENTS

2.1. Introduction to Infinite Elements

In several fields of engineering and science, a large number of problems have domains that are assumed to extend to infinity. The analysis extends to large distances in one or more directions to represent the far field domain.

Such an unbounded medium appears in a wide variety of practical engineering problems, such as soil-structure interaction, consolidation and settlement of soils, ground freezing problems, seepage and ground water flow, contaminant or pollutant diffusion, sediment transport and fluid flow, wave diffraction and refraction, wave propagation, hydrodynamic pressure on dams and off-shore structures, underground structures and thermal transient problems.

Some examples are water waves behind a breakwater, an airplane wing moving through air, diffraction of water waves around an island, a building or dam supported by the ground, aerofoil in flowing water and some of which can be seen in Figure 2.1 through 2.5.

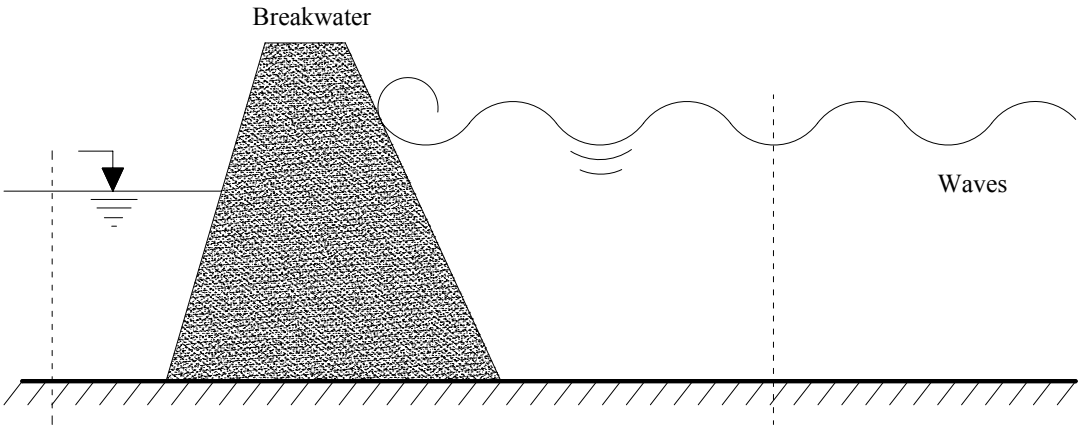

Figure 2.1. Water waves behind a breakwater

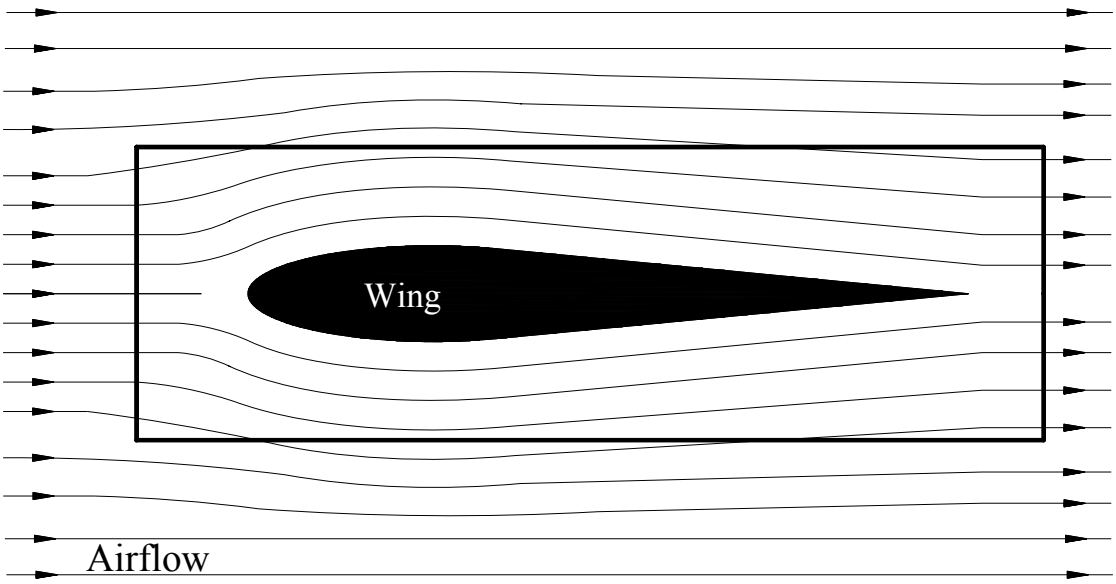

Figure 2.2. Depiction of airflow over a wing

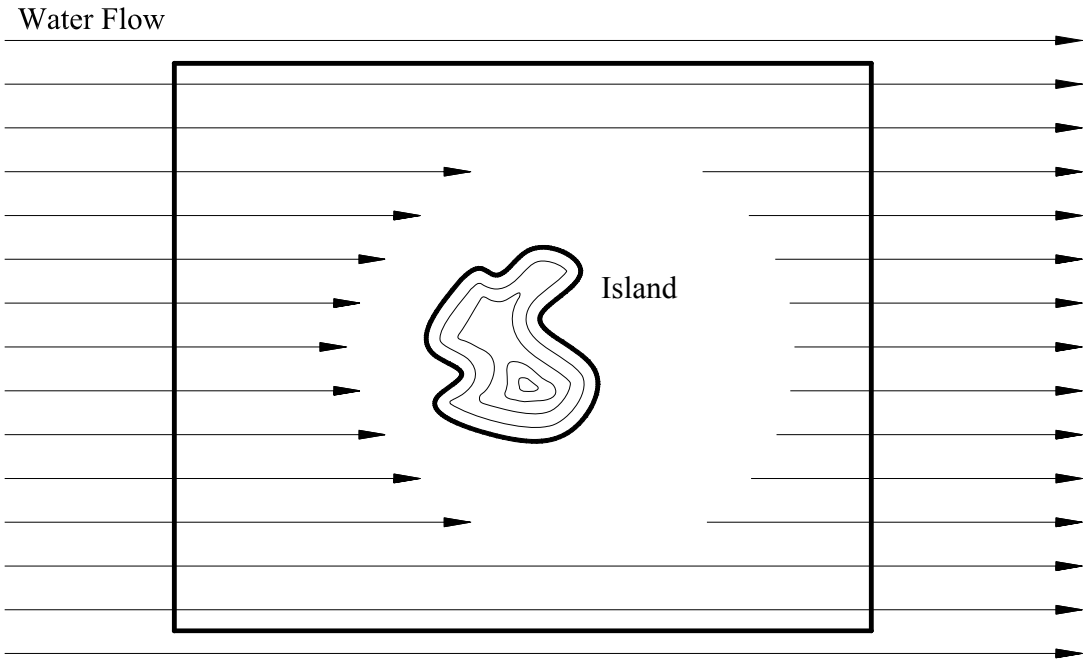

Figure 2.3. Diffraction of water waves around an island

One solution to these problems is to truncate the domain of analysis at large but finite distances from the place of load application. In traditional finite element analysis, these problems are analyzed by extending the conventional finite element mesh outward to a point where the influence of the place of load application is small enough to be neglected, and applying either fixed or movable displacement or constant stress boundary conditions

there. This approach generally requires experimentation with several grid sizes and assumed boundary conditions. The disadvantage in such schemes is that a very large number of node points may be involved simply in modeling the remote region where the perturbation in the stress or displacement field is virtually zero and the method is not suitable for many dynamic analyses.

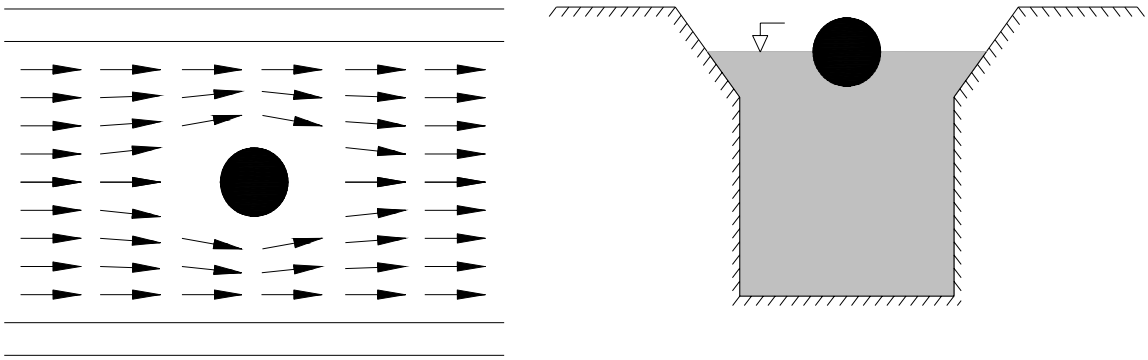

Figure 2.4. Aerofoil in flowing water

To analyze such problems efficiently by the finite element method, infinite elements are introduced to be used combined with the finite elements in order to discretize the domain of analysis. One of the purposes of an infinite element is to model an unbounded domain economically. Reciprocal form of shape functions are introduced over infinite elements which then decays to zero at infinity. Several types of element shape functions which extend to infinity are utilized to generate infinite elements.

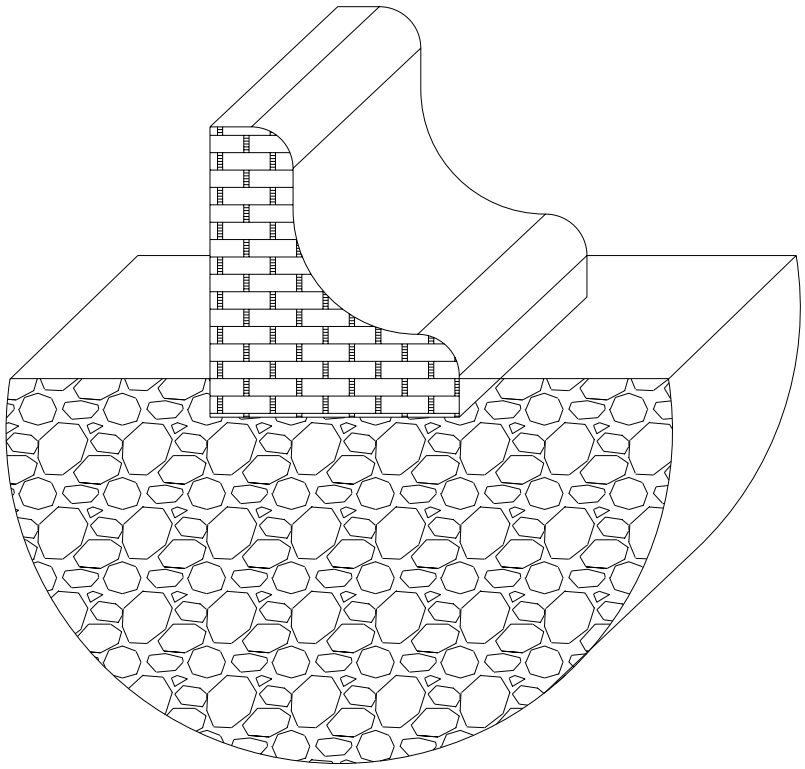

Figure 2.5. A dam supported by the ground

2.2. Origin of Infinite Elements

It is easy to classify infinite elements as static type or dynamic type, as the methods needed for the two types are quite different. Here, the static type and dynamic type will be discussed, although some static types can be used for some dynamic problems. In addition, the infinite elements will be classified as mapped or decay function type.

The first infinite element produced was that of Ungless and Anderson, in 1973. They called their element an infinite finite element. The idea behind the infinite element of Ungless and Anderson was the use of a shape function which varied as $1/(1+r)$ in the radial or r direction. As they remark, this is sufficiently simple for most of the manipulations to be handled analytically. Their infinite finite element is three dimensional and has a triangular base, which is defined to be in the local *xy* plane, and is extended from this base to infinity. It is therefore approximately a triangular prism in shape, with the z direction (which is defined as being perpendicular to the base) being infinite. The element is sketched in Figure 2.6. As Ungless and Anderson (1973) point out, the simple shape function chosen can lead to incompatibilities between adjacent elements, if the bases of

adjacent elements are not parallel. The edges of the elements, in the infinite direction are defined as radiating from some pole. The element matrices are formed using analytical integration in the *xy* plane and numerical integration in the *z* direction. The integration scheme used is a trapezoidal rule scheme, in which the integral is first mapped onto the range [-∞,∞]. The element was tested on the familiar Boussinesq point load on a half space problem, with a hemispherical region around the load removed, to avoid problems with the singularity under the load. Good results were obtained for loads parallel to the free surface and normal to it. Some are shown in Figure 2.7.

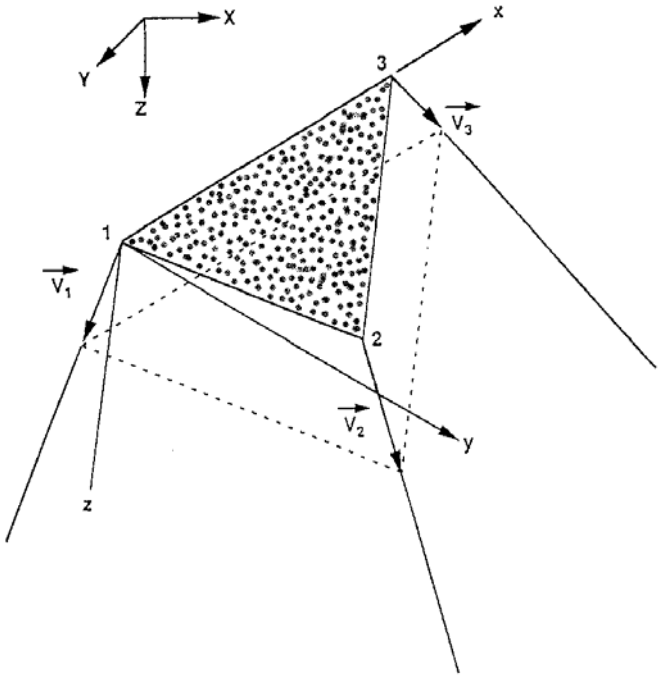

Figure 2.6. Geometry of Ungless and Anderson (1973) infinite element

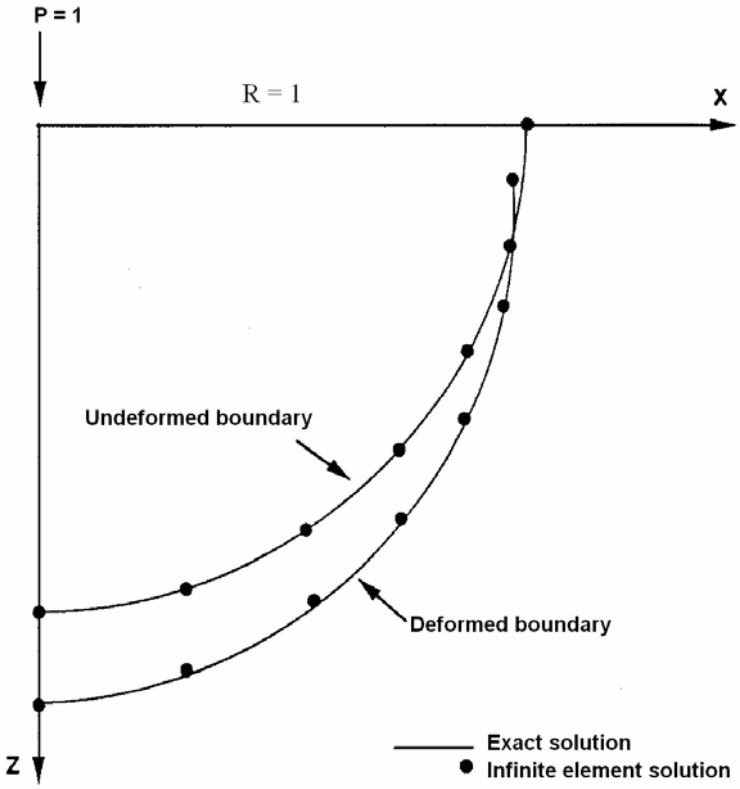

Figure 2.7. Displacements due to a vertical point load on elastic half space obtained by Ungless and Anderson (1973)

The second published work on infinite elements was a paper, by Zienkiewicz and Bettess, in 1975. The original formulation of infinite elements by Bettess is quite different. It is described in the two papers by Bettess in 1977 and 1980. The element domain is extended to infinity, using as a basis any original finite element. The shape function is then multiplied by a decay function which is appropriate for the particular problem type. The arrangement is as shown in Figure 2.8.

In this type of infinite element the shape function is multiplied by a decay function, so that the desired behavior at infinity is obtained. The first decay functions used by Bettess were of an exponential type, and typical terms in the infinite element matrices thus had the form of a polynomial multiplied by an *exp (-r)* term. These types of integrals can be found analytically, and so infinite elements of a rectangular form, which extended to infinity in one or more directions were developed. They were first applied to some simple one dimensional examples and then they were applied to more complicated two dimensional and axi-symmetric problems.

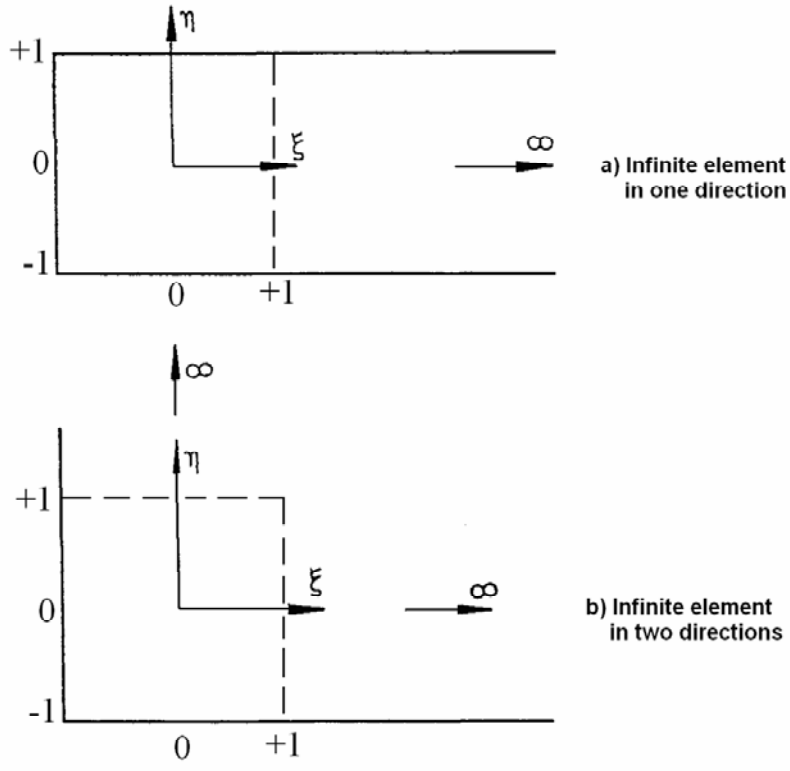

Figure 2.8. Geometry of typical decay function infinite elements (Bettess, 1980)

Bettess (1977) applied the technique to a simple two-dimensional viscous flow problem, that of a cylinder rotating in an infinite viscous liquid. The cylinder has a unit radius. The element mesh for flow around a cylinder can be seen in Figure 2.9. The results for element velocities in the x and y directions along various sections through the quadrant are shown in Figure 2.10 with comparisons with the exact solution.

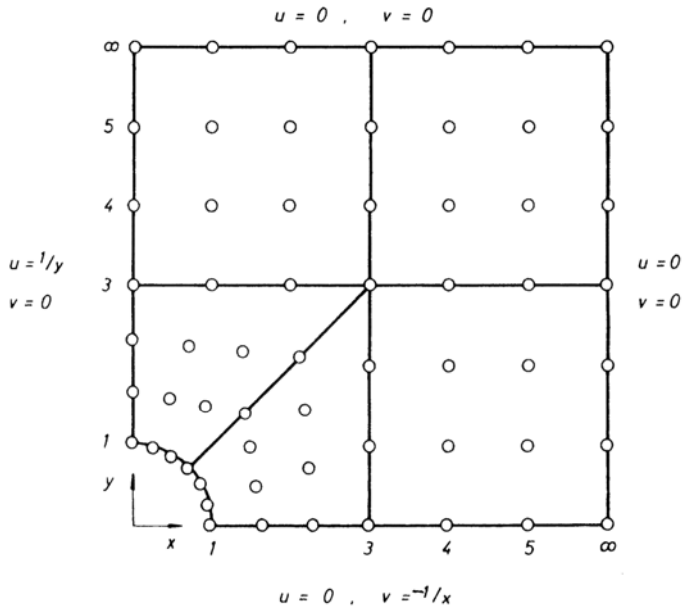

Figure 2.9. Element mesh for flow around a cylinder (Bettess, 1977)

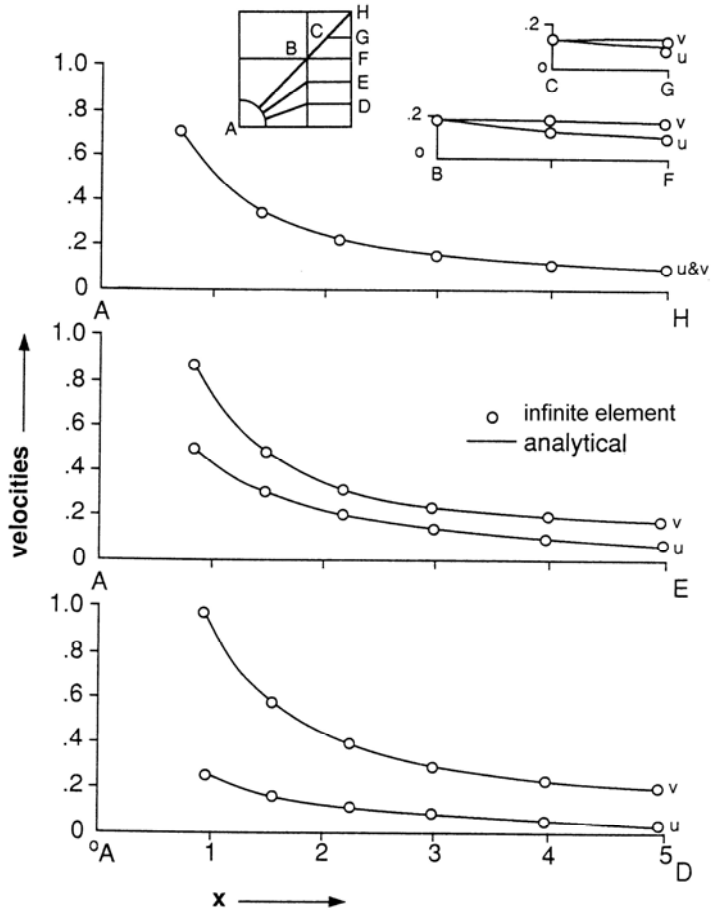

Figure 2.10. Velocities around a cylinder: u and v are velocities in the *x* and *y* directions (Bettess, 1977)

Although the necessary integrations can be carried out analytically, it is also possible to use numerical integration methods, which lead to the possibility of parametric elements.

2.3. Infinite Element Classification

Infinite element formulations are constructed following two main lines of development. Although detailed discussion will be made in chapter 3, these are briefly explained here: A) Decay Function Infinite Elements: These are produced by the help of decay functions in conjunction with the ordinary finite element shape functions. These use standard shape functions for geometry and "decay shape functions" for the field variables (*e.g.* displacement components), so that the element remains of finite size while the field variables decay. B) Mapped Infinite Elements: These consist of mapping of the element from finite to infinite domain. Many mappings are possible, and the first is that of Beer and Meek (1981). Opinions vary, but the Zienkiewicz mapping is seen by Bettees as the best available, because of its simplicity and theoretical advantages. These use standard shape functions for the field variables but "growth shape functions" for the geometry. The latter grow without bound as a natural coordinate approaches a certain value.

Somewhere in between these approaches is the idea of using a series of the form $1/r$, $1/r^2$,$1/r^3$, etc. This idea, taken to the first term by Ungless and Anderson, is implicit in the method of Wood (1976). All these methods have their attractive features and it is always possible to choose a problem for which a given method will give the best answer.

2.4. Studies and Development of Infinite Elements

By using a specially devised mapping, Beer and Meek (1981) analyzed several sample problems for openings in infinite media with comparisons with either theoretical or boundary element solutions which include the infinite boundary in their solution technique.

The geometry of the element is described by conformal mapping of the element including the infinite portion on to the usual, non-dimensional square or cube.

$$x_i = N_i \, x_{ij} \tag{2.1}$$

where, x_i is the current point and N_i are the shape functions. Beer and Meek applied their new element to the determination of the stresses and displacements induced by an excavation in a pre-stressed medium. They considered two types of openings: circular and rectangular. The stresses and displacements necessary to give a traction-free excavation surface are then determined. They obtained excellent agreement between their results and the analytical solution of the problem.

Beer and Meek (1981) also dealt with spherical opening in an elastic solid. They applied these elements to the elasto-plastic analysis of tabular ore body extraction at the Mount Isa mine in Australia. They have since developed alternative methods which involve linking finite elements to boundary integrals.

Chow and Smith (1981) developed serendipity infinite elements to analyze static and periodic problems in geomechanics. Askar and Lynn (1984) developed infinite elements with proper decaying shape functions for ground freezing problems in different spatial domains:

$$N_i = \left(\frac{a}{r}\right)^4 \prod_{\substack{j=1 \\ j\neq i}}^{n-1} \left(\frac{\theta - \theta_j}{\theta_i - \theta_j}\right) \tag{2.2}$$

The use of the infinite elements for ground freezing problems resulted in a considerable savings in the number of elements and nodes used in the mesh; consequently savings also resulted in the computer storage and cost. Damjanić and Owen (1984) used mapped infinite elements for modeling unbounded thermal transient problems. They solved three problems, namely 1) Linear infinite strip with prescribed boundary temperature, 2) Buried cable problem, 3) Spherical cavity problem. They saved substantial computational time with accurate results.

Simoni and Schrefler (1987) applied mapped infinite elements in two consolidation problems and they achieved excellent agreement between infinite elements and analytical solutions. Zhao and Valliappan (1993) presented a time-dependent infinite element which can be used to simulate transient seepage problems in infinite media. In order to examine

the accuracy and efficiency of the infinite elements, they solved both a one-dimensional transient seepage problem in a semi-infinite medium and a two-dimensional transient seepage problem in a full plane using the finite and infinite element technique.

Medina (1981) used an axisymmetric infinite element in order to analyze the Boussinesq and Cerruti problems which deal with vertical and horizontal point loading on an elastic half space. His shape functions in the infinite direction were similar to those of Ungless. He used Gauss-Laguerre numerical integration, in the problem co-ordinates, over an infinite domain, and paid particular attention to the number of integration points needed. Medina also obtained results for a vertically loaded rigid circular plate on an elastic half space, and they compared well with the exact solution. The problem geometry, mesh used and resulting displacements are shown in Figure 2.11.

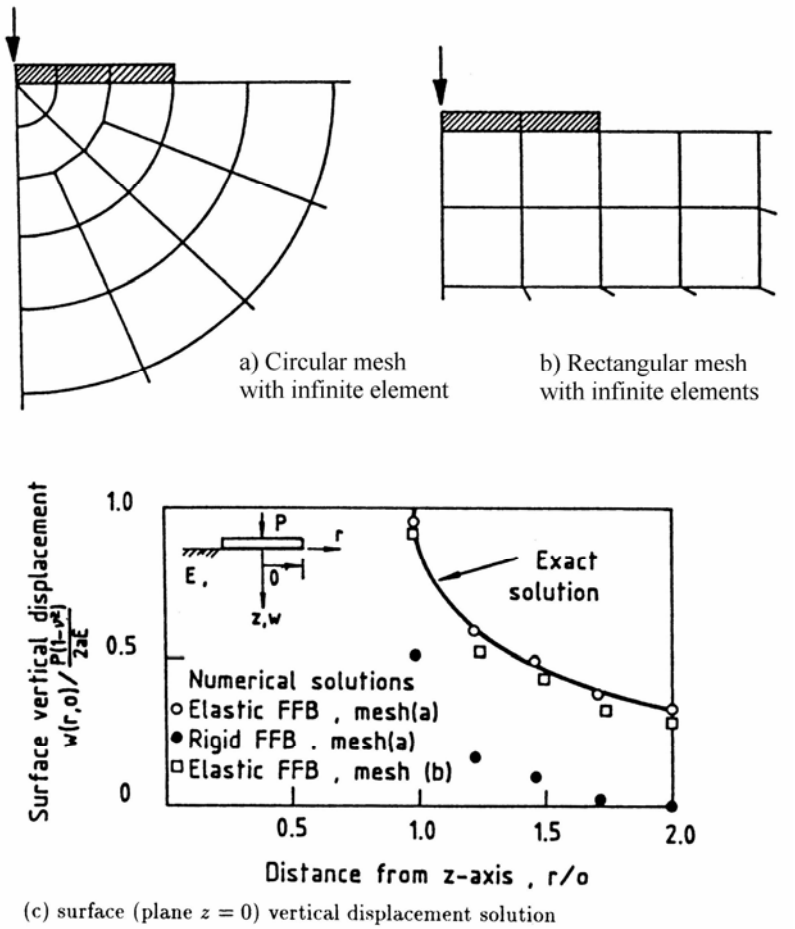

(c) surface (plane $z = 0$) vertical displacement solution

Figure 2.11. Vertically loaded rigid circular plate by Medina (1981)

Bettess and et al. (1982) developed some useful techniques for testing infinite elements. They devised simple one-dimensional test problems in order to test and evaluate infinite element formulations. The crux of the method is that a one dimensional problem is posed which is made artificially to contain decay of the solution. The first results, obtained using the Zienkiewicz form of mapped infinite elements, were published by Zienkiewicz and et al (1983).

Also, Lynn and Hadid (1981) built up a series of infinite elements, which combined terms of the form $1/r^n$ in the shape functions, and applied them to several unbounded elasticity problems. They solved the case of a circular load on an elastic half space and a ring load. They compared their results with those of the exact solution and excellent performances of the element are obtained. Figure 2.12 shows the non-dimensional surface deflection of an elastic half-space under a ring load using infinite elements, compared with the exact solution.

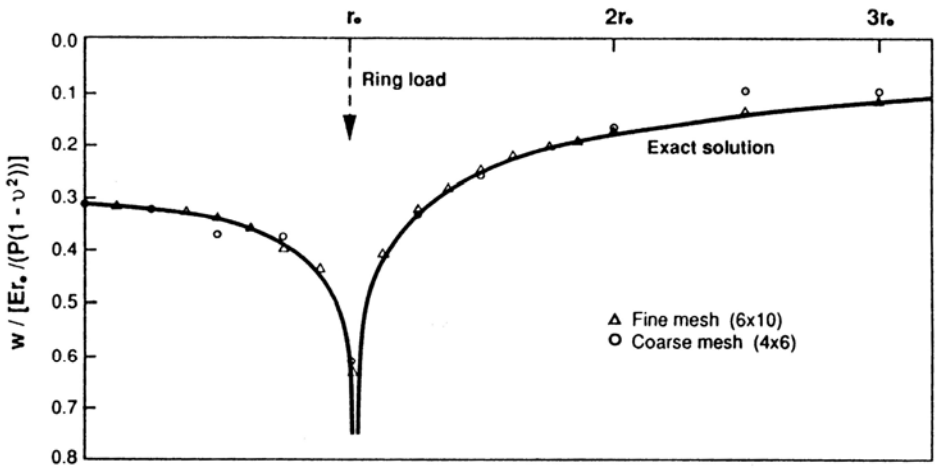

Figure 2.12. Surface deflection of elastic half-space due to a ring load

A Static Infinite Element which classes the decay function and mapped infinite elements as descent and ascent shape functions respectively was described by Curnier (1983), and Curnier showed that they can be made equivalent under certain conditions. For the Flamant problem of a line load acting on an elastic half space and the Boussinesq problem, Curnier gave some results. Good agreement is obtained with analytical solutions of both line load and point load, even that for the plane problem, which has the logarithmic behavior.

Kumar gave static infinite element formulation in 1985 and he used infinite elements in the analysis of underground openings in 1986.

3. CLASSES OF INFINITE ELEMENTS

Infinite elements are actually the same as finite elements that have one or more dimensions of infinite extent in physical space. Informally one can say that some nodes of these elements “go to infinity”. Many physical problems deal with an unbounded medium. The main application of these elements is obviously the treatment of media of infinite extent, where “infinite” in practice means that the domain that influences the solution (the influence domain) is much larger than the domain of interest. These are collectively called unbounded domain problems.

In all these problems a conventional finite element mesh (the computational domain) must be terminated somewhere short of infinity. For many static problems simple truncation at a rigid boundary may work satisfactorily, but it may be unclear where such truncation should take place. A computational compromise is often at work in these situations, as follows: If the truncation boundary is placed too near to the area of interest, the computational effort is saved but the solution accuracy can suffer; if the truncation boundary is placed far away from the area of interest, the solution accuracy is improved but the computation expense may become excessive.

In dynamic problems a rigid boundary reflects a wave, regardless of the size of the mesh; therefore, the model actually misrepresents the reality. Various techniques have been used to treat unbounded problems, both static and dynamic, with various degrees of sophistication. An example of single load P on axially symmetric body of infinite extent can be seen in Figure 3.1 (a). The crudest model is the rigid boundary mesh truncation illustrated in Figure 3.1 (b). Infinite elements can be used in the model as seen in Figure 3.1 (c) and they produce very accurate results in static problems with rather small computational expense. In other words, infinite elements permit satisfactory results to be obtained from fewer elements than would be otherwise required.

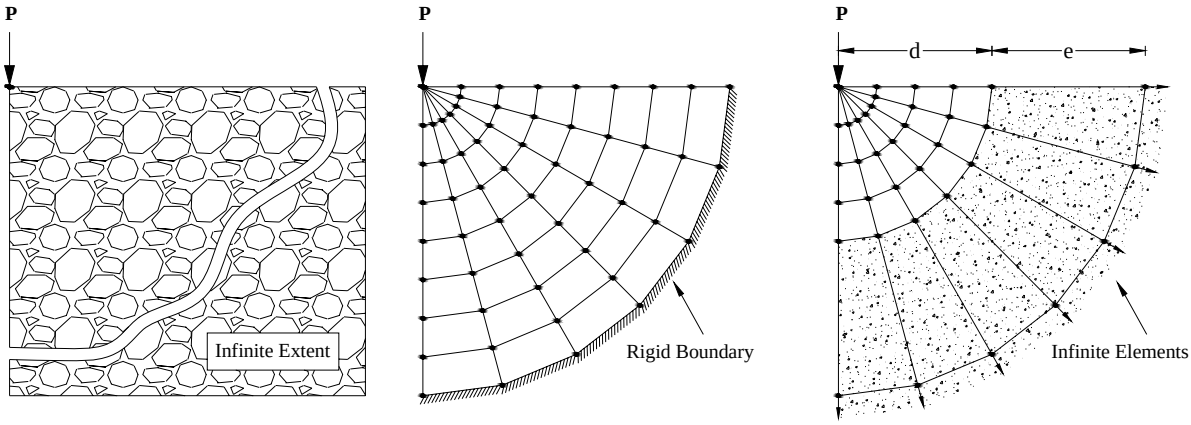

(a) Real Domain (b) Bounded Domain (c) Unbounded Domain

Figure 3.1. (a) Load P on axially symmetric body of infinite extent, (b) Large mesh of conventional finite elements, (c) Smaller mesh bounded by infinite elements

In static stress analysis, infinite elements are analogous to elastic foundations in the sense that they provide approximately correct support conditions for the domain of interest that is modeled by conventional finite elements. Infinite elastic elements based on the standard total potential energy principle have been constructed with two alternate techniques as follows:

3.1. Mapped Infinite Elements

Mapped infinite elements use completely different shape functions in the infinite direction. This type of infinite element almost always involves a mapping, if only to obtain a numerical integration formula. Sometimes two mappings are needed, one for the shape function and one for the integration formula. For conciseness these methods will all be called mapped infinite elements. Many of the infinite elements proposed have used the idea of mapping, or can be cast in that form. (Bettess, 1992)

Mapping of the element from finite to infinite domain is performed. Standard shape functions are used for the field variables and growth shape functions are used for the geometry. The latter grow without bound as a natural coordinate approaches a certain value.

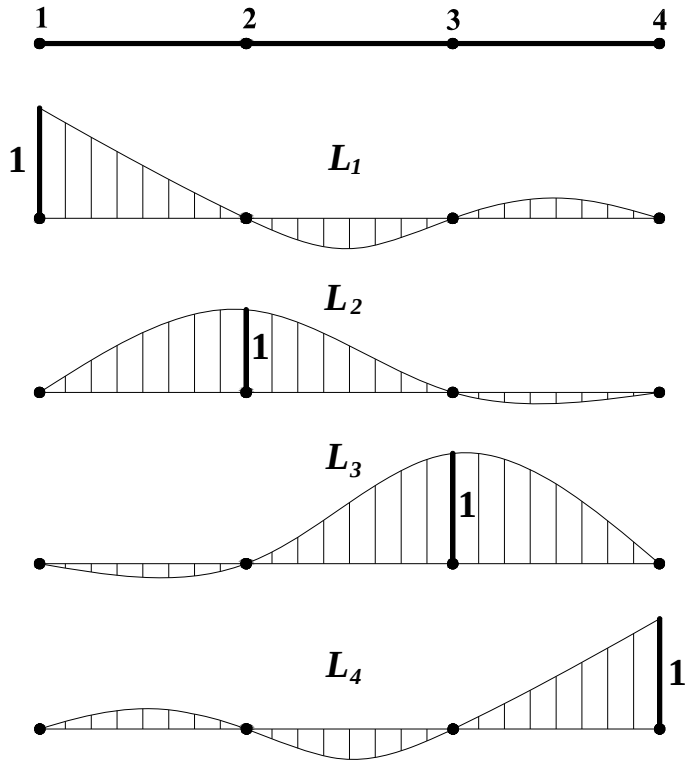

Figure 3.2. Standard shape functions of four-node line element for field variables

In order to illustrate field variable interpolation of four-node line element, standard shape functions are sketched in Figure 3.2. Growth shape functions are pictured to demonstrate geometry interpolation of four-node line element in Figure 3.3.

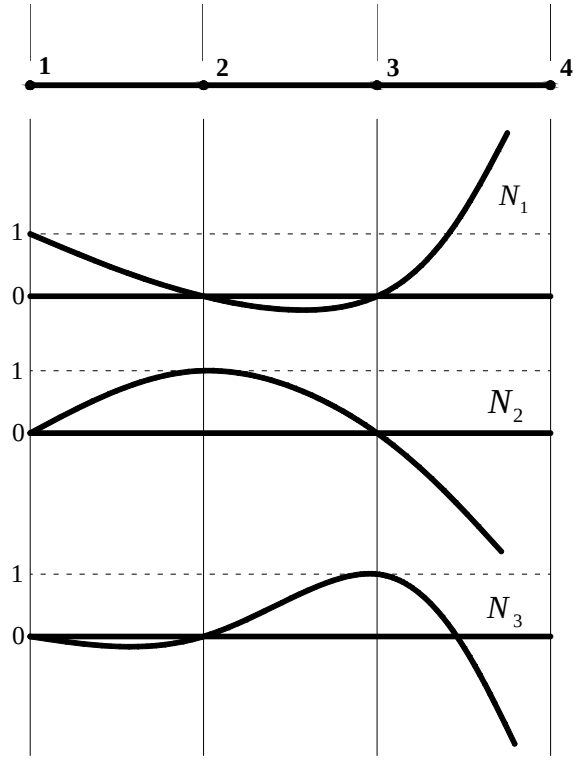

Figure 3.3. Growth shape functions of four-node line element for the geometry

3.2. Decay Function Infinite Elements

In the last decades, many special elements have been introduced to extend the scope of the finite element method to infinite elements. The main idea of the decay function infinite element approach is that the finite element shape function is multiplied by a decay function. The finite shape functions will not be appropriate to describe the behavior of the field variables, towards infinity, and so decay functions are introduced, which modify the finite element shape functions. Decay function ensures that the behavior of the element at infinity is a reasonable reflection of the problem. This usually means that the field variable must tend monotonically to its far field value. If the parent finite element shape function is written as $P_i = (\xi, \eta)$ where ξ and η are local coordinates and the decay function is $f_i = (\xi, \eta)$, where the subscript denotes the node number then:

$$N_i(\xi,\eta) = P_i(\xi,\eta)\, f_i(\xi,\eta) \tag{3.1}$$

(no summation on *i*)

The decay function $f_i(\xi,\eta)$ must be unity at its own node, that is:

$$f_i(\xi_i,\eta_i)=1 \tag{3.2}$$

In addition N_i must tend to the far field value at infinity. There is no requirement that the decay function takes any special value at other nodes. Whatever f is, the required derivatives of the element shape function can easily be established using the chain rule:

$$\frac{\partial N_i}{\partial \xi}=\frac{\partial P_i}{\partial \xi}f_i+P_i\frac{\partial f_i}{\partial \xi} \qquad \text{and} \qquad \frac{\partial N_i}{\partial \eta}=\frac{\partial P_i}{\partial \eta}f_i \tag{3.3}$$

for decay only in the ξ direction, and

$$\frac{\partial N_i}{\partial \xi}=\frac{\partial P_i}{\partial \xi}f_i+P_i\frac{\partial f_i}{\partial \xi} \qquad \text{and} \qquad \frac{\partial N_i}{\partial \eta}=\frac{\partial P_i}{\partial \eta}f_i+P_i\frac{\partial f_i}{\partial \eta} \tag{3.4}$$

for decay in both ξ and η directions. Similar considerations apply in three dimensions. Second derivatives can also be found if required. The ξ coordinate would normally be in the radial direction, away from the domain of interest, and is usually simply a constant multiplied by *r*, the radial coordinate. It is therefore simple to match ξ to $1/r$ or other known forms of decay.

3.2.1. Exponential Decay Functions

An obvious choice for the decay function, and the first to be used, is the function *exp(-x)*. This has the advantage that it decays to zero faster than any polynomial and so dominates the polynomial behavior as *x* is large and ensures convergence towards zero as *x* increases. It is also almost as easy to manipulate mathematically as a polynomial. The more precise expression for the decay function is:

$$N_i(\xi)=\exp\left[(\xi_i-\xi)/L\right] \qquad (\xi>\xi_i) \tag{3.5}$$

for decay only in the positive ξ direction. The inclusion of ξ_i ensures that equation (3.2) holds. For decay in both ξ and η directions the equation (3.5) becomes:

$$N_i(\xi,\eta) = \exp\left[\left(\xi_i + \eta_i - \xi - \eta\right)/L\right] \tag{3.6}$$

Here *L* is a length which determines the severity of the decay. It is also possible to set *L* to unity and to set the severity of the decay by the distance between the nodes. It is a trivial matter, if required, to cause the decay to be in the negative ξ direction, in which case equation (3.5) becomes:

$$N_i(\xi) = \exp\left[\left(\xi - \xi_i\right)/L\right] \qquad \left(\xi < \xi_i\right) \tag{3.7}$$

It is also possible to define the exponential decay in the global co-ordinates of the problem. In this case the dominant part of the decay function is $\exp(-r/L)$, where *L* is again decay length and *r* is the radius from some origin.

For instance, a set of shape functions based on Lagrange polynomials multiplied by exponential decay terms may be written using the equation (3.8). The shape functions for $n=3$ and $L=1$ are sketched in Figure 3.4. How the shape functions decay at infinity is seen easily.

$$N_i = e^{(x_i - x)/L} L_i = e^{(x_i - x)/L} \prod_{\substack{j=1 \\ j \neq i}}^{n-1} \left(\frac{x_j - x}{x_j - x_i} \right) \tag{3.8}$$

Please note $e^{(x_i - x)}$ is present only when $x > x_i$.

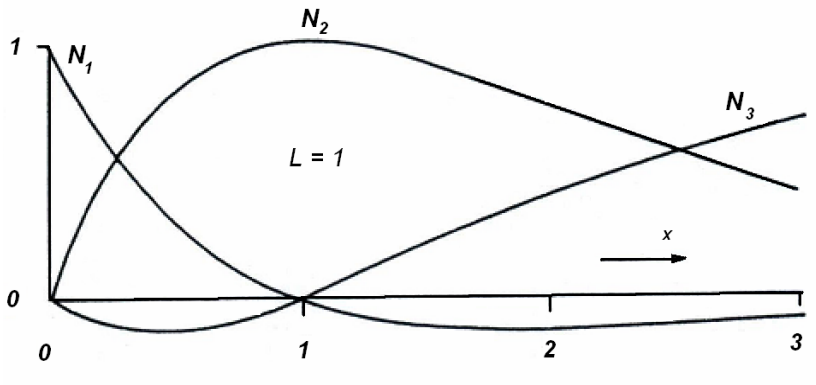

Figure 3.4. Typical decay shape functions (Bettess, 1977)

3.2.2. Reciprocal Decay Functions

The procedure is simple. A reciprocal decay function is taken of the form:

$$N_i(\xi) = \left(\frac{\xi_i - \xi_0}{\xi - \xi_0} \right)^n \tag{3.9}$$

where ξ_0 is some origin point. This point must be outside the infinite element, i.e. it will be on the opposite side to that which extends to infinity. Usually, if the decay is in the positive ξ direction then $\xi_0 < -1$. This avoids a singularity within the infinite element and n is selected to be greater than the highest power of ξ encountered in P_i. This ensures that as ξ tends to infinity the shape function, N_i, tends to 0. There is no necessity for *n* to be an integer. For instance, if 3 points are considered, the first two points having finite co-ordinates and the 3rd point being infinitely distant, shape function for the 2nd node may be sketched in Figure 3.5.

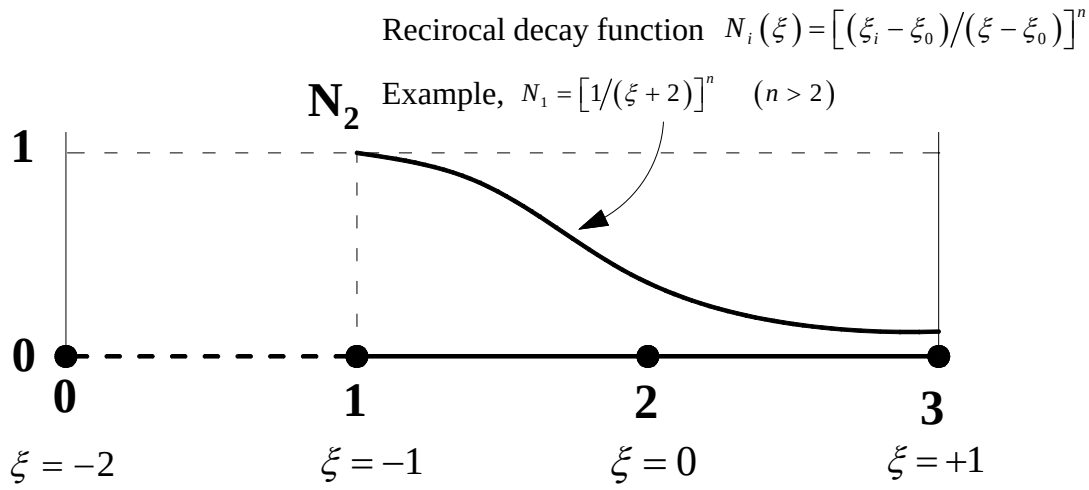

Figure 3.5. Reciprocal shape function for the 2nd node

As in the case of exponential decay, the decay function can be generalized to two directions, for example:

$$N_i(\xi,\eta)=\left(\frac{\xi_i-\xi_0}{\xi-\xi_0}\right)^l\left(\frac{\eta_i-\eta_0}{\eta-\eta_0}\right)^m \tag{3.10}$$

Decay in the negative ξ direction can also be dealt with

$$N_i(\xi)=\left(\frac{\xi_0-\xi_i}{\xi_0-\xi}\right)^n \tag{3.11}$$

where now ξ_0 must be > 1. It is also possible to have a decay in the global coordinate. This makes little difference to the theory. The decay function is written as

$$N_i(\xi)=\left(\frac{\xi_i-\xi_0}{\xi-\xi_0}\right)^n\left(\frac{r_i}{r}\right) \tag{3.12}$$

where the last term dictates the decay in global coordinates.

4. UNI-DIMENSIONAL INFINITE ELEMENTS

The theoretical derivations for uni-dimensional infinite elements will be discussed in this chapter.

4.1. Uni-dimensional Two-node Mapped Infinite Element

As shown in Figure 4.1, a uni-dimensional two-node mapped infinite element will be studied. For geometry interpolation, the mapping function for a linear uni-dimensional element is

$$N_1 = \frac{2}{1-\xi} \tag{4.1}$$

The satisfactory performance of this mapping function can be easily shown. Let the co-ordinate of the left hand of the infinite element be x_1. Then the geometry interpolant can be written as seen in equation (4.2).

$$x = x_1 N_1 \tag{4.2}$$

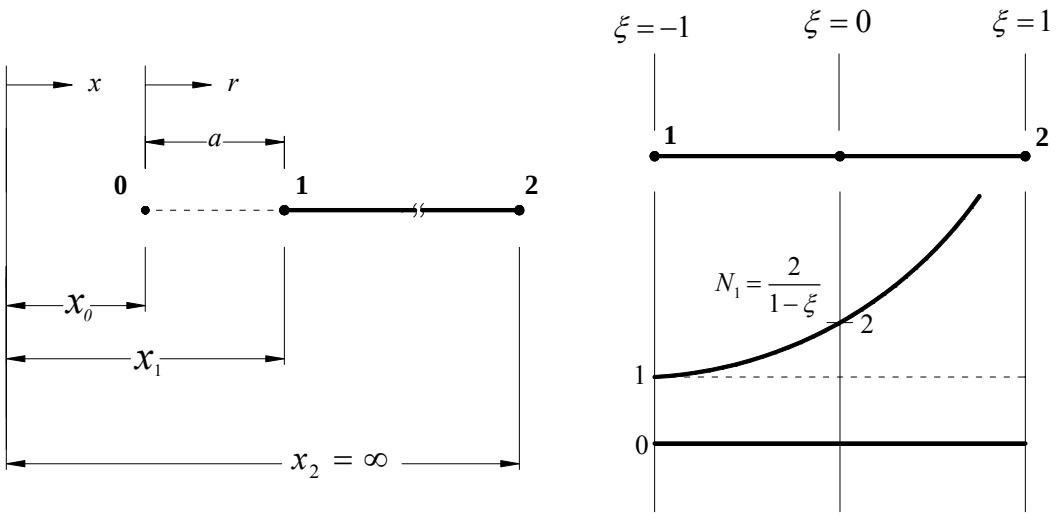

(a) Physical space (b) Natural coordinate space

Figure 4.1. Uni-dimensional two-node mapped infinite element

The shape functions for field variables, $u(x) \equiv u(\xi)$, can be written by the use of Lagrange functions for the element as following and can be seen in Figure 4.2.

$$\{u\} = \{L_1 \quad L_2\} \begin{Bmatrix} d_1 \\ d_2 \end{Bmatrix} \tag{4.3}$$

$$L_1 = \frac{1}{2}(1-\xi) \tag{4.4}$$

$$L_2 = \frac{1}{2}(1+\xi) \tag{4.5}$$

In general coordinates, using $\xi_i = -1$ at node 1, and $\xi_i = +1$ at node 2 the shape function L_i becomes;

$$L_i = \frac{1}{2}(1+\xi\xi_i) \tag{4.6}$$

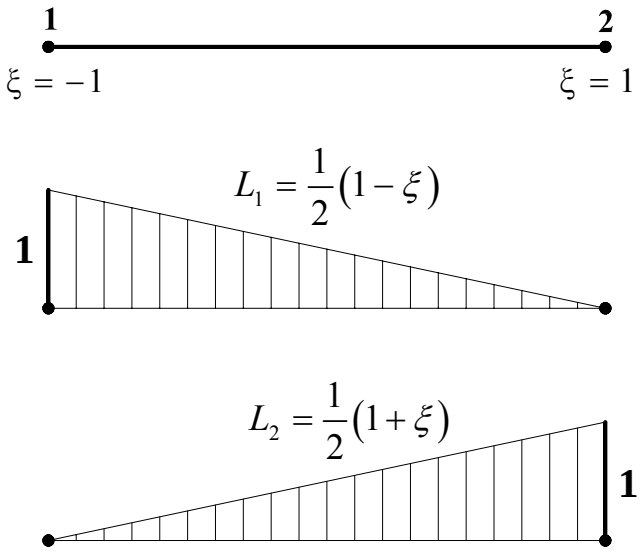

Figure 4.2. Shape functions of two-node line element for field variables

As an example of axially loaded two-node line element, let *u* be axial displacement and let node 2 be fixed. The generic displacement vector of the element:

$$\{u\} = \begin{Bmatrix} \frac{1-\xi}{2} & \frac{1+\xi}{2} \end{Bmatrix} \begin{Bmatrix} d_1 \\ 0 \end{Bmatrix} \tag{4.7}$$

The strain component of the element can be written as

$$\{\varepsilon_x\} = \begin{Bmatrix} \frac{du}{dx} \end{Bmatrix} = \frac{d}{dx} \{L_1 \quad L_2\} \begin{Bmatrix} d_1 \\ 0 \end{Bmatrix} = \frac{d}{dx} \begin{Bmatrix} \frac{1-\xi}{2} & \frac{1+\xi}{2} \end{Bmatrix} \begin{Bmatrix} d_1 \\ 0 \end{Bmatrix} \tag{4.8}$$

From Figure 4.1, it is seen that, $x_1 = a$ and derivative of L_1 with respect to x

$$\frac{dL_1}{dx} = \frac{dL_1}{d\xi}\frac{d\xi}{dx} = \left(\frac{dL_1}{d\xi}\right)\frac{1}{\frac{dx}{d\xi}} = \left(-\frac{1}{2}\right)\frac{1}{\frac{2a}{(1-\xi)^2}} = -\frac{1}{2}\frac{(1-\xi)^2}{2a} \tag{4.9}$$

Derivative of L_2 can be obtain in the same fashion but it is not needed here. The axial strain is

$$\{\varepsilon_x\} = \begin{Bmatrix} \frac{dL}{dx} \end{Bmatrix} \begin{Bmatrix} d_1 \\ 0 \end{Bmatrix} = -\frac{d_1}{2a}\frac{(1-\xi)^2}{2} \tag{4.10}$$

We see that for a two-node line element of physical length *2a* between nodes 1 and 2, axial strain decays parabolically from $\varepsilon_x = -d_1/a$ at end $\xi = -1$ to $\varepsilon_x = 0$ at end $\xi = +1$, rather than being constant value $\varepsilon_x = -d_1/2a$ throughout as would be the case for a standard two node element of length 2a.

4.2. Zienkiewicz Uni-dimensional Three-node Mapped Infinite Element

Zienkiewicz uni-dimensional three-node mapped infinite element will be defined. The element extends from point x_1 through x_2 to x_3, which is at infinity as seen in Figure 4.3. This element is mapped onto the finite domain $-1 < \xi < 1$ by the mapping expression

$$x = x_0 N_0 + x_2 N_2 \tag{4.11}$$

where

$$N_0 = \frac{-\xi}{1-\xi} \qquad N_2 = \frac{1}{1-\xi} \tag{4.12}$$

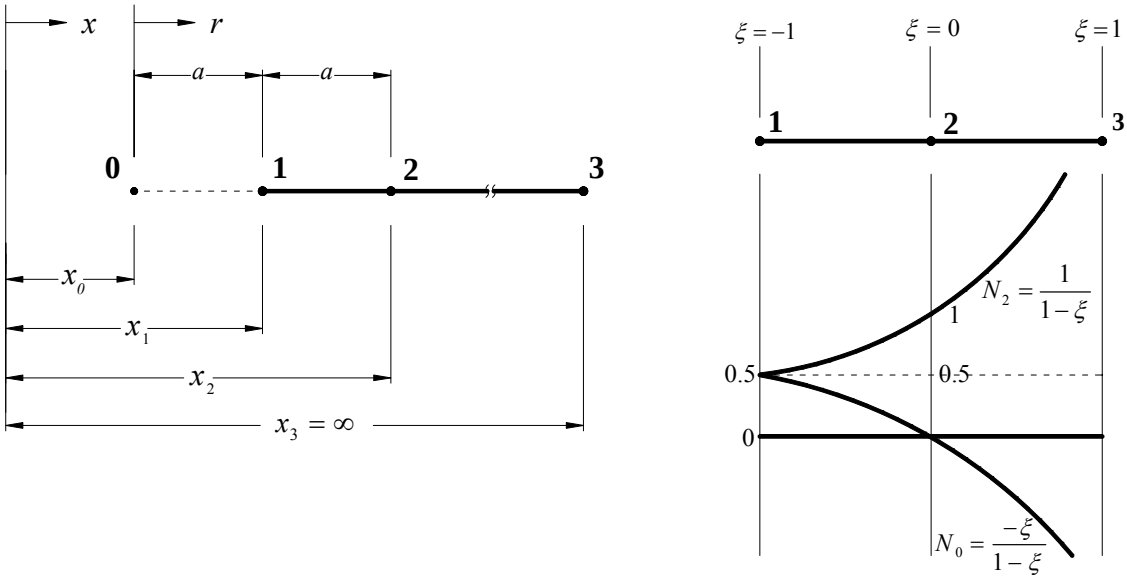

(a) physical space (b) natural coordinate space

Figure 4.3. Zienkiewicz uni-dimensional three-node mapped infinite element

$$\text{At } \xi = -1 \qquad x = x_0 0.5 + x_2 0.5 = x_1 \tag{4.13}$$

$$\text{At } \xi = 0 \qquad x = x_0 0 + x_2 1 = x_2 \tag{4.14}$$

$$\text{At } \xi = 1 \qquad x = x_0 \infty + x_2 \infty = \infty \tag{4.15}$$

Although, the point at $\xi = -1$ is the mid-point between x_0 and x_2, it is possible to chose x_1 anywhere in the interval x_0 to x_2 by writing:

$$x_1 = \gamma x_2 + (1-\gamma) x_0 \tag{4.16}$$

The theory is worked out here for the case $\gamma = 1/2$.

An important feature of this mapping is the condition that

$$N_0 + N_2 = 1 \tag{4.17}$$

Otherwise the mapping will be affected by any change in the origin of the coordinate system. Thus a shift in the origin by Δx leads to the new coordinates

$$x_0' = x_0 + \Delta x \tag{4.18}$$

$$x_2' = x_2 + \Delta x \tag{4.19}$$

If these values are inserted in the equation (4.11) then:

$$x + \Delta x = (x_0 + \Delta x)N_0 + (x_2 + \Delta x)N_2 \tag{4.20}$$

$$\Delta x = \Delta x(N_0 + N_2) \tag{4.21}$$

This is only true if equation (4.17) is satisfied. The next step is to see what form polynomials in the finite, ξ, domain are transformed into in the unbounded x domain. Consider a polynomial P,

$$P = \alpha_0 + \alpha_1\xi + \alpha_2\xi^2 + \alpha_3\xi^3 + \ldots \tag{4.22}$$

which is typical of those used in finite element methods. The ξ to x mapping already obtained is

$$x = x_0 + \frac{2a}{1-\xi} \tag{4.23}$$

and its inverse is

$$\xi = 1 - \frac{2a}{x - x_0} \tag{4.24}$$

And where $r = x - x_0$, these can be written as

$$r = \frac{2a}{1-\xi} \qquad \text{and} \qquad \xi = 1 - \frac{2a}{r} \tag{4.25}$$

On substitution into the general polynomial, *P*, a new polynomial in inverse powers of *r* is obtained.

$$P = \beta_0 + \frac{\beta_1 \xi}{r} + \frac{\beta_2 \xi^2}{r^2} + \frac{\beta_3 \xi^3}{r^3} + \ldots \tag{4.26}$$

where the β_i can be determined from the α's and *a*. If the polynomial is required to decay to zero at infinity then $\beta_0 = 0$ (Zienkiewicz et al., 1983).

A generic field variable is interpolated over the infinite element by the standard shape functions of the 3-node line element.

$$\{u\} = \{L_1 \quad L_2 \quad L_3\} \begin{Bmatrix} d_1 \\ d_2 \\ d_3 \end{Bmatrix} \tag{4.27}$$

where

$$L_1 = -\frac{1}{2}\xi(1-\xi), \quad L_2 = 1 - \xi^2, \quad L_3 = \frac{1}{2}\xi(1+\xi). \tag{4.28}$$

and they are shown in Figure 4.4.

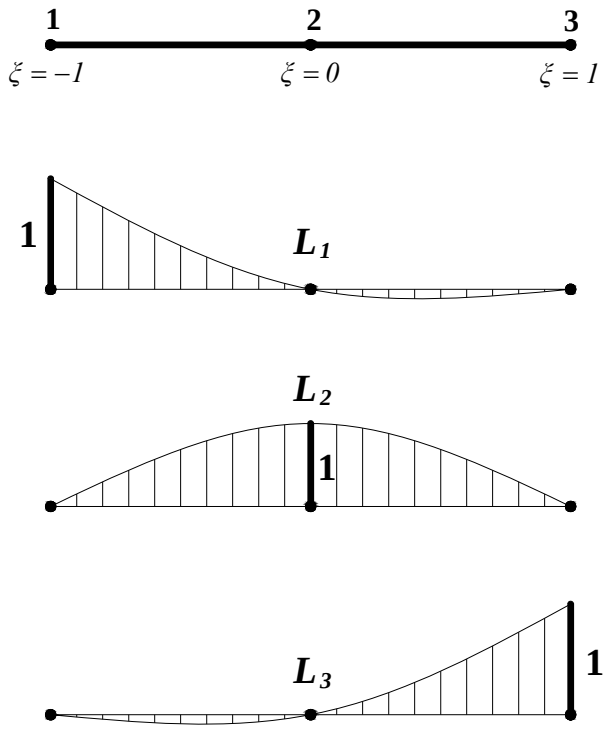

Figure 4.4. Shape functions of three-node line element for field variables

4.3. Uni-dimensional Three-node Mapped Infinite Element

In order to illustrate the concepts and procedures, a uni-dimensional three-node mapped infinite element will be studied as shown in Figure 4.5. The distance *a* between nodes 1 and 2 may be considered a characteristic length of the element. Figure 4.5 also shows a point labeled 0 at a distance *a* from 1. This point is not a node but a pole, whose significance is explained subsequently.

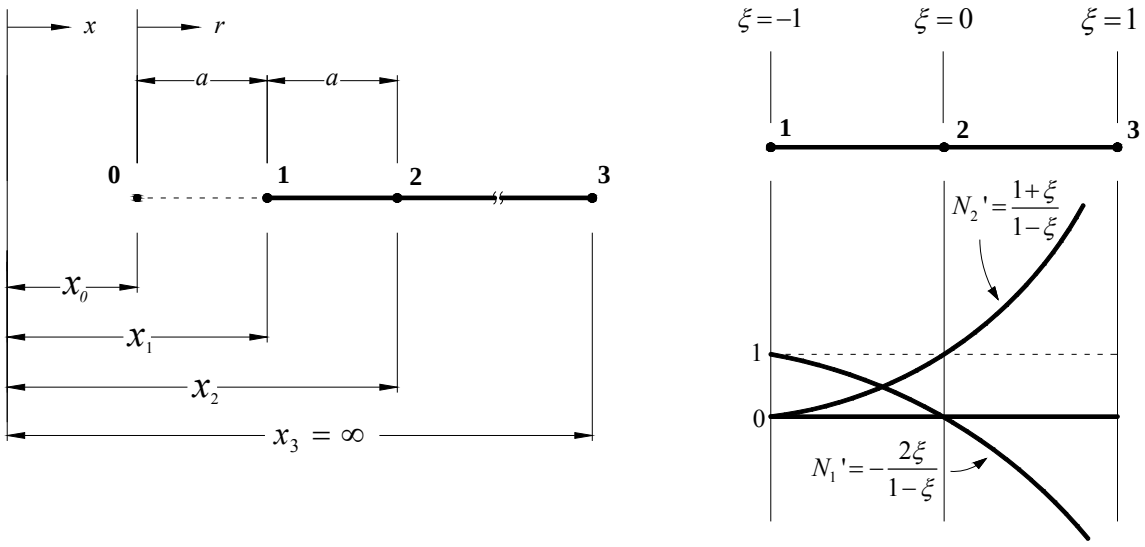

(a) Physical space (b) Natural coordinate space

Figure 4.5. Uni-dimensional three-node mapped infinite element

4.3.1. Geometry Interpolation

The element geometry is interpolated according to two mapping functions, N_1 and, N_2 which are rational in the natural coordinate ξ :

$$\{x\} = \{N_1 \quad N_2\} \begin{Bmatrix} x_1 \\ x_2 \end{Bmatrix} \tag{4.29}$$

in which,

$$N_1 = -\frac{2\xi}{1-\xi}, \qquad N_2 = \frac{1+\xi}{1-\xi}. \tag{4.30}$$

Note that $x = x_1$ and $x = x_2$ for $\xi = -1$ and $\xi = 0$, respectively. However, $x \to \infty$, for $\xi = 1$. Thus, the mapping in equation (4.29) automatically places the node 3 at infinity; consequently the node 3 need not be explicitly present in the geometry interpolant as seen in equation (4.31).

$$x_3 = \lim_{\xi \to 1} \frac{-2\xi x_1 + (1+\xi)x_2}{1-\xi} = \infty \tag{4.31}$$

Consider the set of natural co-ordinates ξ, η and a corresponding set of global co-ordinates *x, y*. By the usual rules of partial differentiation, the ξ derivative can be written as

$$\frac{\partial N_i}{\partial \xi} = \frac{\partial N_i}{\partial x}\frac{\partial x}{\partial \xi} + \frac{\partial N_i}{\partial y}\frac{\partial y}{\partial \xi} \tag{4.32}$$

Performing the same differentiation with respect to the other natural coordinate η and writing in the matrix form:

$$\begin{Bmatrix} \frac{\partial N_i}{\partial \xi} \\ \frac{\partial N_i}{\partial \eta} \end{Bmatrix} = \begin{bmatrix} \frac{\partial x}{\partial \xi} & \frac{\partial y}{\partial \xi} \\ \frac{\partial x}{\partial \eta} & \frac{\partial y}{\partial \eta} \end{bmatrix} \begin{Bmatrix} \frac{\partial N_i}{\partial x} \\ \frac{\partial N_i}{\partial y} \end{Bmatrix} = [J] \begin{Bmatrix} \frac{\partial N_i}{\partial x} \\ \frac{\partial N_i}{\partial y} \end{Bmatrix} \tag{4.33}$$

In the above, the left-hand side can be evaluated as the functions N_i are specified in natural co-ordinates. Further as *x, y* are explicitly given, the matrix $[J]$, can be found explicitly in terms of the natural co-ordinates. The matrix is known as the Jacobian matrix.

To find now the global derivatives, $[J]$ is inverted:

$$\begin{Bmatrix} \frac{\partial N_i}{\partial x} \\ \frac{\partial N_i}{\partial y} \end{Bmatrix} = [J]^{-1} \begin{Bmatrix} \frac{\partial N_i}{\partial \xi} \\ \frac{\partial N_i}{\partial \eta} \end{Bmatrix} = \frac{1}{Det|J|} \begin{bmatrix} \frac{\partial y}{\partial \eta} & -\frac{\partial y}{\partial \xi} \\ -\frac{\partial x}{\partial \eta} & \frac{\partial x}{\partial \xi} \end{bmatrix} \begin{Bmatrix} \frac{\partial N_i}{\partial \xi} \\ \frac{\partial N_i}{\partial \eta} \end{Bmatrix} \tag{4.34}$$

The global derivative for a one-dimensional problem becomes:

$$\frac{\partial N_i}{\partial x} = J^{-1}\frac{\partial N_i}{\partial \xi} \tag{4.35}$$

The Jacobian matrix for this uni-dimensional infinite element (same as its determinant because it is a scalar) is

$$J = \frac{dx}{d\xi} = x_1 \frac{dN_1}{d\xi} + x_2 \frac{dN_2}{d\xi} \tag{4.36}$$

It is seen from Figure 4.5 that $x_1 = a$, $x_2 = 2a$ and the derivatives of the shape functions N_1 and N_2 are as follows:

$$\frac{dN_1}{d\xi} = -\frac{2}{(1-\xi)^2} \tag{4.37}$$

$$\frac{dN_2}{d\xi} = \frac{2}{(1-\xi)^2} \tag{4.38}$$

The Jacobian for this element may then be written as

$$J = \frac{dx}{d\xi} = x_1 \frac{dN_1}{d\xi} + x_2 \frac{dN_2}{d\xi} = \frac{2a}{(1-\xi)^2} \tag{4.39}$$

and goes to $+\infty$ as $\xi \rightarrow 1$.

4.3.2. Interpolation of Field Variables

A generic field variable is interpolated over the infinite element by the standard shape functions of the 3-node line element.

$$\{u\} = \{L_1 \quad L_2 \quad L_3\} \begin{Bmatrix} d_1 \\ d_2 \\ d_3 \end{Bmatrix} \tag{4.40}$$

where

$$L_1 = -\frac{1}{2}\xi(1-\xi), \quad L_2 = 1-\xi^2, \quad L_3 = \frac{1}{2}\xi(1+\xi). \tag{4.41}$$

and they are shown Figure 4.4. The above expressions have been written in accordance with Lagrangian Shape Functions for the 3-node line element. In fact,

$$N(x) = \prod_{\substack{j=1 \\ (i \neq j)}}^{j=n} \frac{(\xi - \xi_j)}{(\xi_i - \xi_j)} \tag{4.42}$$

In static analysis d_3 is typically set to a prescribed value, usually zero as a boundary condition. The x derivative of u is obtained in the usual fashion as ε_x:

$$\{\varepsilon_x\} = \frac{du}{dx} = \begin{Bmatrix} \frac{dL_1}{dx} & \frac{dL_2}{dx} & \frac{dL_3}{dx} \end{Bmatrix} \begin{Bmatrix} d_1 \\ d_2 \\ d_3 \end{Bmatrix} \tag{4.43}$$

Since the shape functions are dependent on the natural coordinates ζ and η, differentiation of them with respect to x and y will be obtained through the Jacobi transformation. If the shape functions are differentiated, following equations can be written:

$$\frac{dL_1}{dx} = J^{-1}\frac{dL_1}{d\xi} = J^{-1}(-1/2 + \xi) \tag{4.44}$$

$$\frac{dL_2}{dx} = J^{-1}\frac{dL_2}{d\xi} = J^{-1}(-2\xi) \tag{4.45}$$

$$\frac{dL_3}{dx} = J^{-1}\frac{dL_3}{d\xi} = J^{-1}(1/2 + \xi) \tag{4.46}$$

where $J^{-1} = \frac{(1-\xi)^2}{2a}$. When equations (4.44), (4.45) and (4.46) are substituted in equation (4.43), equation (4.47) is obtained.

$$\{\varepsilon_x\} = [\Delta]\{u\} = [\Delta]\{L\}\{d\} = [G]\{d\} = J^{-1}\{(-1/2+\xi) \quad (-2\xi) \quad (1/2+\xi)\} \begin{Bmatrix} d_1 \\ d_2 \\ d_3 \end{Bmatrix} \quad (4.47)$$

here, the strain matrix $[G]$ of the element can be written as

$$[G] = \frac{(1-\xi^2)}{2a}\{(-1/2+\xi) \quad (-2\xi) \quad (1/2+\xi)\} \quad (4.48)$$

The stress component of the element is formulated obtaining stress matrix $[S]$

$$\{\sigma\} = [D]\{\varepsilon\} = E\{\varepsilon\} = E[G]\{d\} = [S]\{d\} \quad (4.49)$$

where $[D]$ is the material matrix which is Elastic Modulus of the element here.

Variation of $\{u\}$ by ξ can be written by the help of equations (4.40) and (4.41) as:

$$\{u\} = \{-\tfrac{1}{2}\xi(1-\xi) \quad (1-\xi^2) \quad \tfrac{1}{2}\xi(1+\xi)\} \begin{Bmatrix} d_1 \\ d_2 \\ d_3 \end{Bmatrix} \quad (4.50)$$

To show the representation of u in terms of the physical coordinates *x*, let us solve for ξ from the geometry interpolant. The equation (4.29) is rewritten as equation (4.51) as follows:

$$\{x\} = \begin{Bmatrix} -\frac{2\xi}{1-\xi} & \frac{1+\xi}{1-\xi} \end{Bmatrix} \begin{Bmatrix} x_1 \\ x_2 \end{Bmatrix} \quad (4.51)$$

If equation (4.51) is solved for ξ and $x_1 = x_0 + a$, $x_2 = x_0 + 2a$, and $r = x - x_0$ relations are substituted, equation (4.52) is obtained.

$$\xi = \frac{x - x_2}{x + x_2 - 2x_1} = 1 - \frac{2a}{r} \tag{4.52}$$

If equation (4.52) is substituted in equation (4.50), equation (4.53) is obtained.

$$u = d_3 + \left(-d_1 + 4d_2 - 3d_3\right)\frac{a}{r} + 2\left(d_1 - 2d_2 + d_3\right)\frac{a^2}{r^2} \tag{4.53}$$

It is seen that as $r \to \infty$, $u \to d_3$ which is set to zero ($d_3 = 0$) as a boundary condition. If $d_1 = d_2 = d_3 = C$, the constant value $u = C$ prevails, rigid body movement as expected. Linear variations of *u* with *r* are not represented. In general, the two parenthetic expressions in equation (4.53) do not vanish, so *u* becomes infinite at point 0 because *r = 0* at point *0*. Point *0* is therefore a pole or singular point about which field quantity *u* decays. This suggests that in a problem such as that of Figure 3.1 (c), in which there is indeed a singularity at *r = 0*, one should use *d = e*. The presence of the decay functions is noted.

$$\frac{1}{r}, \quad \frac{1}{r^2} \tag{4.54}$$

The coefficients of these terms are generally nonzero. It is also seen that as $r \to a$, $u \to d_1$ and $r \to 2a$, $u \to d_2$ as it is expected ($d_3 = 0$ for static analysis). Strain component can be obtained by differentiating equation (4.53) with respect to *x*:

$$\frac{du}{dx} = \frac{du}{dr}\frac{dr}{dx} = \left(d_1 - 4d_2 + 3d_3\right)\frac{a}{r^2} - 4\left(d_1 - 2d_2 + d_3\right)\frac{a}{r^3} \tag{4.55}$$

in which $\frac{dr}{dx} = 1$.

The stiffness matrix of the infinite element can be given by the usual expression

$$[K] = \int_V [G]^T [D][G] dV \tag{4.56}$$

where $[D] = E$ and $dV = Adx = AJd\xi$

$$[K] = \int_{-1}^{+1} EA[G]^T [G] Jd\xi \tag{4.57}$$

$$[K] = EA \int_{-1}^{+1} \frac{(1-\xi^2)}{2a} \begin{Bmatrix} (-1/2+\xi) \\ (-2\xi) \\ (1/2+\xi) \end{Bmatrix} \frac{(1-\xi^2)}{2a} \{(-1/2+\xi) \quad (-2\xi) \quad (1/2+\xi)\} Jd\xi \tag{4.58}$$

After the integration, the stiffness matrix of an infinite bar element as shown in Figure 4.5 (a) is obtained as

$$[K] = \frac{EA}{2a} \begin{bmatrix} 46/15 & -52/15 & 2/5 \\ -52/15 & 64/15 & -4/5 \\ 2/5 & -4/5 & 2/5 \end{bmatrix} \tag{4.59}$$

4.4. Uni-dimensional Four-node Mapped Infinite Element

The element geometry is interpolated according to three mapping functions, N_1, N_2 and, N_3 which are rational in the natural coordinate ξ :

$$\{x\} = \{N_1 \quad N_2 \quad N_3\} \begin{Bmatrix} x_1 \\ x_2 \\ x_3 \end{Bmatrix} \tag{4.60}$$

where,

$$N_1 = \frac{-1+9\xi^2}{4(1-\xi)} \qquad N_2 = \frac{4-8\xi-12\xi^2}{4(1-\xi)} \qquad N_3 = \frac{1+4\xi+3\xi^2}{4(1-\xi)} \tag{4.61}$$

The element and the mapping functions can be seen in Figure 4.6.

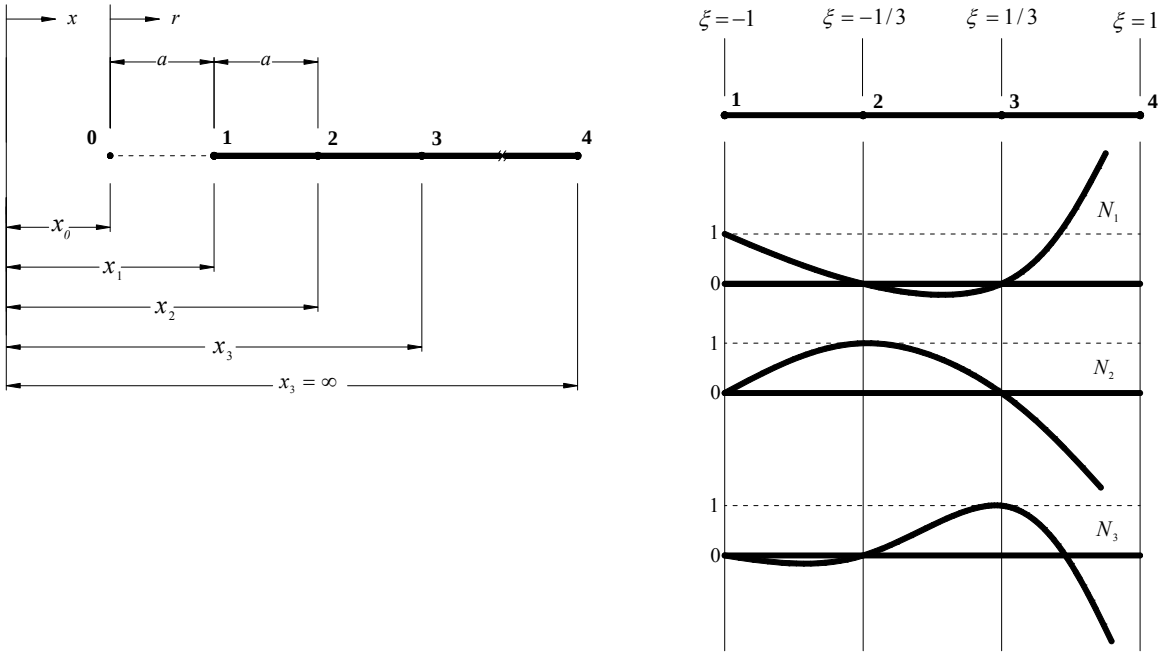

(a) Physical space (b) Natural coordinate space

Figure 4.6. Uni-dimensional four-node mapped infinite element

Lagrange shape functions for field variable interpolation over the element are used for four-node line element.

$$\{u\} = \{L_1 \quad L_2 \quad L_3 \quad L_4\} \begin{Bmatrix} d_1 \\ d_2 \\ d_3 \\ d_4 \end{Bmatrix} \tag{4.62}$$

where

$$L_1 = \frac{9}{16}\left(-\frac{1}{9}+\frac{\xi}{9}+\xi^2-\xi^3\right) \tag{4.63}$$

$$L_2 = \frac{9}{16}\left(1 - 3\xi - \xi^2 + 3\xi^3\right) \tag{4.64}$$

$$L_3 = \frac{9}{16}\left(1 + 3\xi - \xi^2 - 3\xi^3\right) \tag{4.65}$$

$$L_4 = \frac{9}{16}\left(-\frac{1}{9} - \frac{\xi}{9} + \xi^2 + \xi^3\right) \tag{4.66}$$

and can be seen in Figure 4.7.

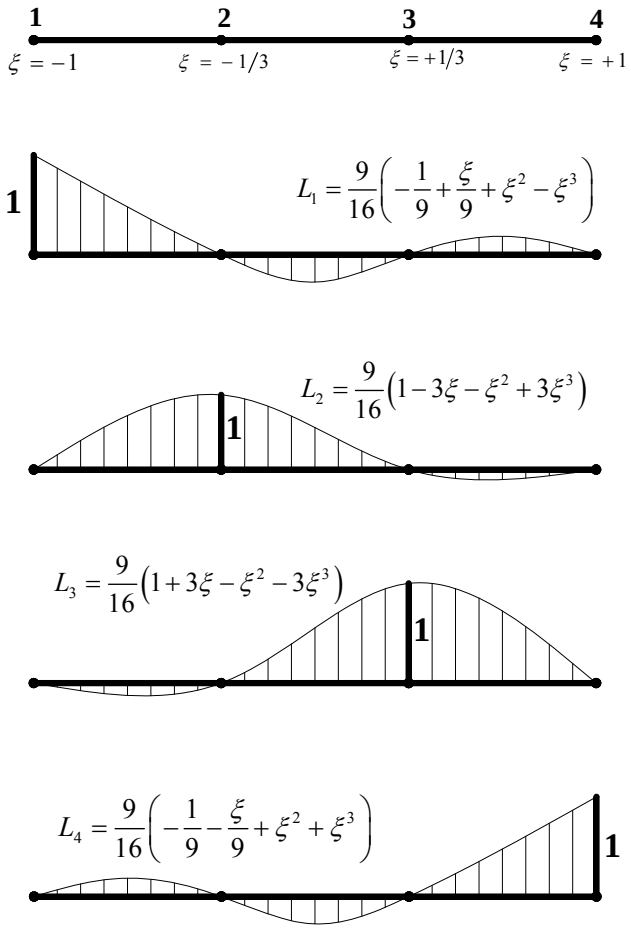

Figure 4.7. Shape functions of four-node line element for field variables

4.5. Uni-dimensional Two-node Decay Infinite Element

Dynamic axi-symmetric infinite elements are developed for the soil structure interaction problems, whose domains extend to infinity. Element can include additional wave components in its shape functions by introducing nodeless variables. The additional shape functions corresponding to the nodeless variables are constructed by considering the conditions under which the shape functions have zero values at other nodes.

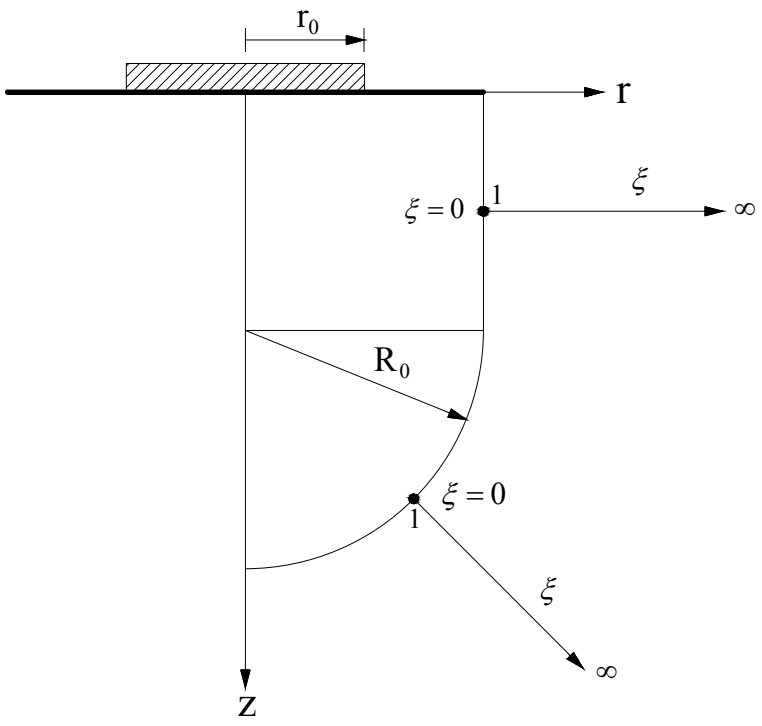

Figure 4.8. Global and local co-ordinate system of uni-dimensional two-node decay infinite element

The element can be seen in Figure 4.8 and the geometrical mapping of the infinite elements from the local coordinates (ξ,η) to the global coordinates (r,z) can be defined as:

$$r = \sum_{j=1}^{1} M(\xi) L_j(\eta) r_j = M(\xi) R_0 \tag{4.67}$$

where $M(\xi)$ is the mapping function for the infinite direction seen in Figure 4.9 and defined as

$$M(\xi) = (1+\xi) \qquad (0 \le \xi \le \infty) \tag{4.68}$$

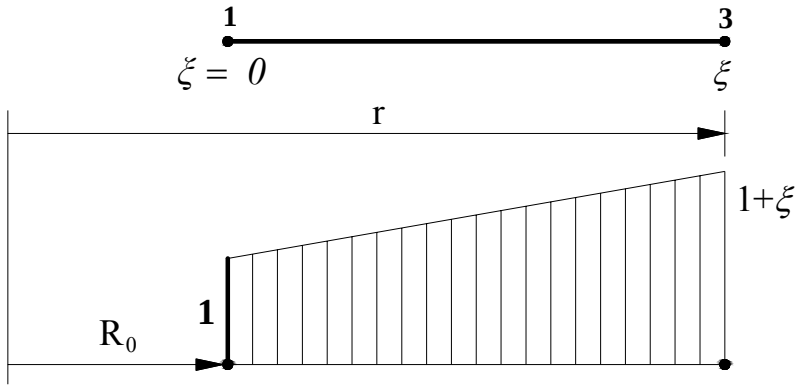

Figure 4.9. Mapping function of a bar element

The elastodynamic problems often produce displacement fields in which wave components propagate. In such problems, a typical displacement component may be expressed for the uni-dimensional two-node decay infinite element as

$$u = [N_1]\{d_1\} = e^{-(\alpha+ikR_0)\xi} d_1 \tag{4.69}$$

where α is a positive constant $(\alpha \to 0)$, d is the element nodal point co-ordinate, and k_L is the wave propagation number, defined as

$$k_L = \frac{\omega}{V_L} \tag{4.70}$$

such that ω and V_L are the vibration frequency and propagation velocity, respectively, of the wave traveling through the element. (Yong and Yun, 1992)

4.6. Solution of a Differential Equation Using Decay Shape Functions of Uni-dimensional Three-node Decay Infinite Element

In choosing shape function for an element which extends to infinity there are two requirements to satisfy. Firstly, the shape function should be realistic, secondly, it should lead to integrations over the element which are finite.

A set of shape functions based on Lagrange polynomials multiplied by exponential decay terms is used in order to model an element extending from $x=1$ to infinity. A set of shape functions N_i is defined for $i=1$ to $n-1$.

$$N_i = e^{(x_i - x)/L} \prod_{\substack{j=1 \\ j \neq i}}^{n-1} \left(\frac{x_j - x}{x_j - x_i} \right) \tag{4.71}$$

L is an arbitrary distance giving a measure of the severity of the exponential decay. Consider the differential equation

$$\frac{d^2u}{dx^2} = \frac{2}{x^3} \tag{4.72}$$

subjected to the boundary conditions that $u(1)=1$, and $u(0)=\infty$. The analytical solution is easily seen to be $u=1/x$. The variational form of the equation can be presented using the functional

$$\int_1^\infty F \, dx = \int_1^\infty \left[\left(\frac{du}{dx} \right)^2 + \frac{4u}{x^3} \right] dx \tag{4.73}$$

The Euler-Lagrange equation obtained by varying u is

$$\frac{\partial F}{\partial u} - \frac{d}{dx} \left\{ \frac{\partial F}{\partial u'} \right\} = 0 \tag{4.74}$$

which can be written

$$\frac{4}{x^3} - \frac{d}{dx}\left\{\frac{2du}{dx}\right\} = 0 \tag{4.75}$$

and hence

$$\frac{d^2u}{dx^2} = \frac{2}{x^3} \tag{4.76}$$

the same as equation (4.72). This equation is modeled using an element extending from $x = 1$ to infinity and having one internal node at $x = 2$ and one variable associated with that node. Take

$$u = N_1 + N_2 u_2 \tag{4.77}$$

where u_2 is the value of u at $x = 2$, and

$$N_1 = \left(\frac{x_2 - x}{x_2 - x_1}\right) e^{(x_1 - x)/L} = (2 - x) e^{(1-x)/L} \tag{4.78}$$

$$N_2 = \left(\frac{x_1 - x}{x_1 - x_2}\right) e^{(x_2 - x)/L} = (x - 1) e^{(2-x)/L} \tag{4.79}$$

It can be seen that the equation (4.77) satisfies the boundary conditions for any value of u_2. dN_1/dx and dN_2/dx can easily be found, and the equation (4.73) for the functional can be evaluated. A variation of the functional with respect to u_2 yields an equation with one unknown

$$\int_1^{\infty} \frac{dN_1}{dx}\frac{dN_2}{dx}dx + u_2\int_1^{\infty}\left(\frac{dN_2}{dx}\right)^2 dx + \int_1^{\infty}\frac{2N_2}{x^3}dx = 0 \tag{4.80}$$

This can be solved for u_2. The analytical value of for u_2 is $1/2$. The numerical value obtained in this method depends on the choice of L. $u_2 = 0.49$ for $L = 2$ and $u_2 = 0.59$ for $L = 2$. The results show that the method reasonably effective in solving problems of this nature. The form of the element solution depends on the value of the exponential decay length, L. (Bettess, 1977)

5. TWO-DIMENSIONAL INFINITE ELEMENTS

5.1. Shape Functions of 2-D Infinite Elements

Based on direction of infinity, type being mapped of decay, two-dimensional infinite elements are presented in a summary chart in Table 5.1. Then; geometrical configuration, coordinate mapping, and field variable mapping functions of two-dimensional infinite elements are one by one presented in a tabular and explicit manner in Tables 5.2 through 5.14.

In order to describe the infinite elements in Chapters 5 and 6, information to keys of the code for infinite element is given in Figure 5.1.

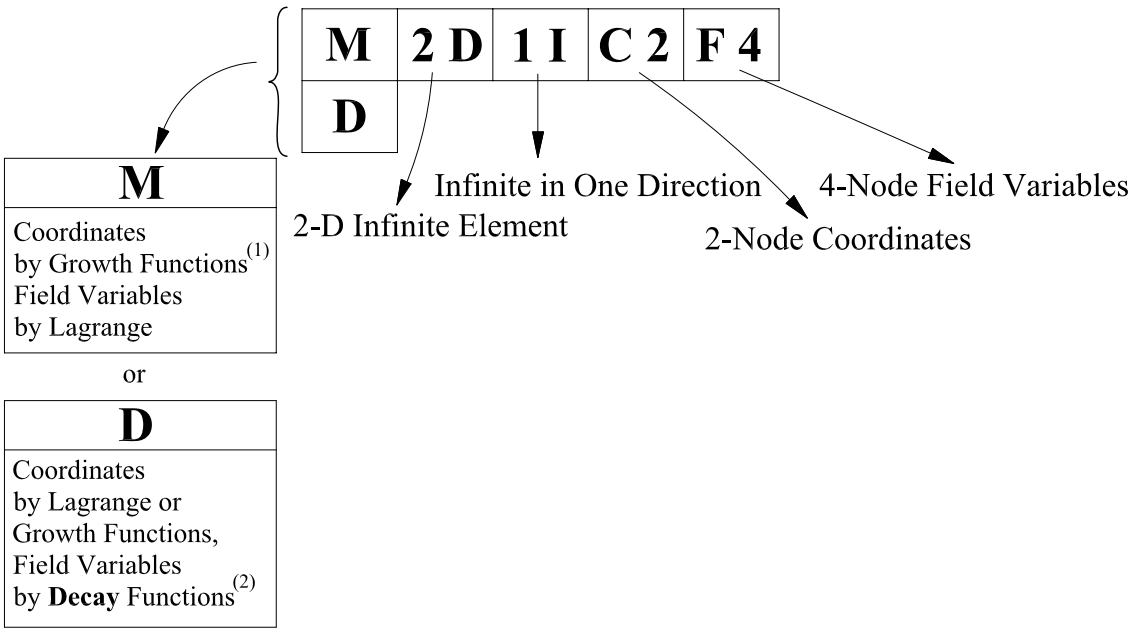

Figure 5.1. Information to keys of the code for infinite elements

(1) For growth functions seeTable 5.12.

(2) For exponential and reciprocal decay functions see Article 3.1.

Table 5.1. Two-dimensional infinite elements summary chart

Infinite Direction	***Type***	***Code***	***Description***	***Reference***
1	Mapped	M2D-1I/C2-F4	Mapped, 2-dimensional, 1-infinite direction, 4-node, infinite element	Bettess, P., 1977
1	Mapped	M2D-1I/C4-F6	Mapped, 2-dimensional, 1-infinite direction, 6-node, infinite element	Cook, R. D., D. S. Malkus, and M. E. Plesha, 1989
1	Mapped	M2D-1I/C5-F8	Mapped, 2-dimensional, 1-infinite direction, 8-node, infinite element	Bettess, P., 1977
1	Mapped	M2D-1I/C6-F8	Mapped, 2-dimensional, 1-infinite direction, 8-node, infinite element	Beer, G. and J. L. Meek, 1981
1	Mapped	M2D-1I/C6-F9	Mapped, 2-dimensional, 1-infinite direction, 9-node, infinite element	Bettess, P., 1977
1	Mapped	M2D-1I/C6-F9	Mapped, 2-dimensional, 1-infinite direction, 9-node, infinite element	Zienkiewicz, O. C., C. Emson and P. Bettess, 1983
1	Decay	D2D-1I/C5-F3	Decay, 2-dimensional, 1-infinite direction, 7-node, infinite element	Chuhan Z. and Z. Chongbin, 1987
1	Decay	D2D-1I/C6-F9	Decay, 2-dimensional, 1-infinite direction, 5-node, infinite element	Yang, S. C., and C. B. Yun, 1992
1	Decay	D2D-1I/C-F4	Decay, 2-dimensional, 1-infinite direction, 6-node, infinite element	Chow Y. K., and I. M. Smith, 1981
2	Mapped	M2D-2I/C1-F3	Mapped, 2-dimensional, 2-infinite direction, 3-node, infinite element	Bettess, P., 1977
2	Mapped	M2D-2I/C3-F5	Mapped, 2-dimensional, 2-infinite direction, 5-node, infinite element	Bettess, P., 1977
2	Mapped	M2D-2I/C4-F6	Mapped, 2-dimensional, 2-infinite direction, 6-node, infinite element	Bettess, P., 1977
2	Decay	D2D-2I/C4-F6	Decay, 2-dimensional, 2-infinite direction, 6-node, infinite element	Chow Y. K., and I. M. Smith, 1981

Table 5.2. Mapped, 2-dimensional, 1-infinite direction, 4-node, infinite element

Mapped, 2-Dimensional, 1-infinite direction, 4-node, Infinite Element	
Geometrical Configuration	**M2D-1I/C2-F4**

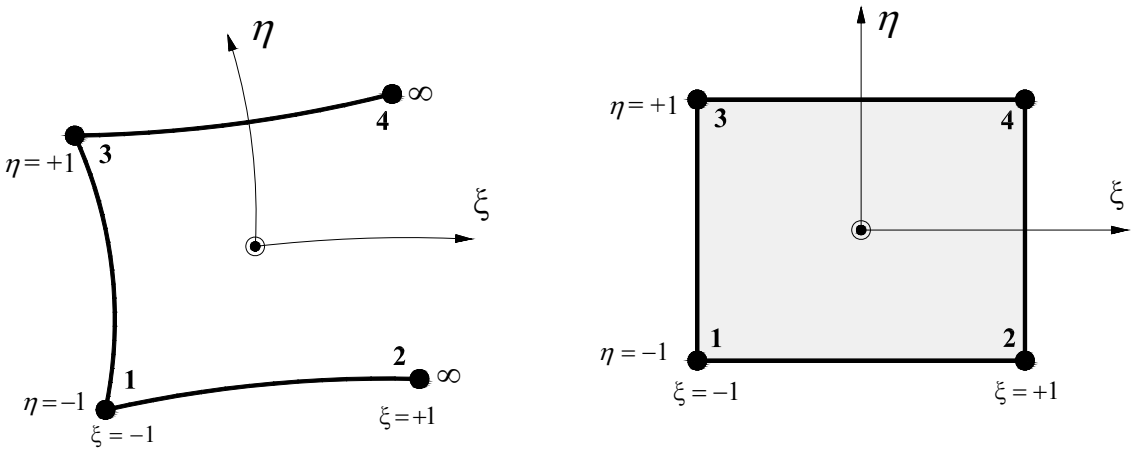

Coordinate Mapping

$$\{x\} = [M_i]\{x_i\}$$

$$M_i = (G_j)(L_k)$$

$$M_1 = \frac{2}{1-\xi}\,\frac{1}{2}(1-\eta)$$

$$M_3 = \frac{2}{1-\xi}\,\frac{1}{2}(1+\eta)$$

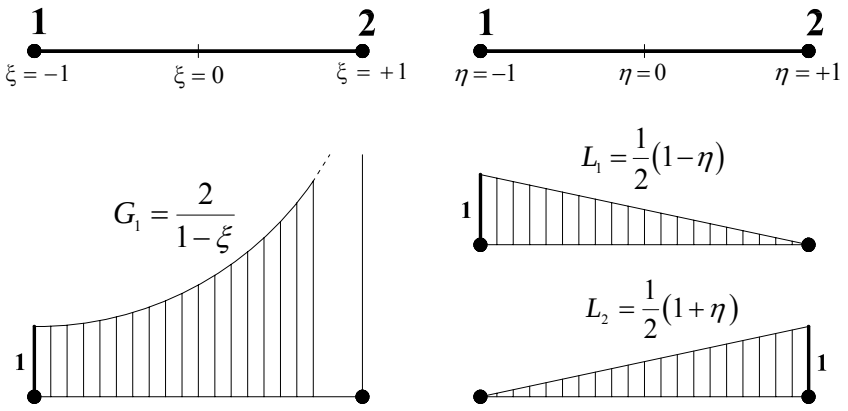

Table 5.2 (Contd)

Mapped, 2-Dimensional, 1-infinite direction, 4-node, Infinite Element
(contd)

Field Variable Mapping	**M2D-1I/C2-F4**

$$\{u\} = [N_i]\{d_i\}$$

$$N_i = (L_{j\xi})(L_{k\eta})$$

$$N_1 = \frac{1}{2}(1-\xi)\frac{1}{2}(1-\eta)$$

$$N_2 = \frac{1}{2}(1+\xi)\frac{1}{2}(1-\eta)$$

$$N_3 = \frac{1}{2}(1-\xi)\frac{1}{2}(1+\eta)$$

$$N_4 = \frac{1}{2}(1+\xi)\frac{1}{2}(1+\eta)$$

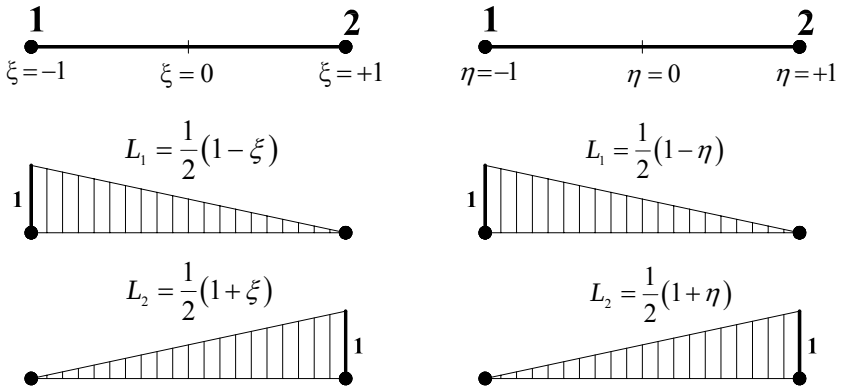

Table 5.3. Mapped, 2-dimensional, 1-infinite direction, 6-node, infinite element

Mapped, 2-Dimensional, 1-infinite direction, 6-node, Infinite Element

Geometrical Configuration	**M2D-1I/C4-F6**

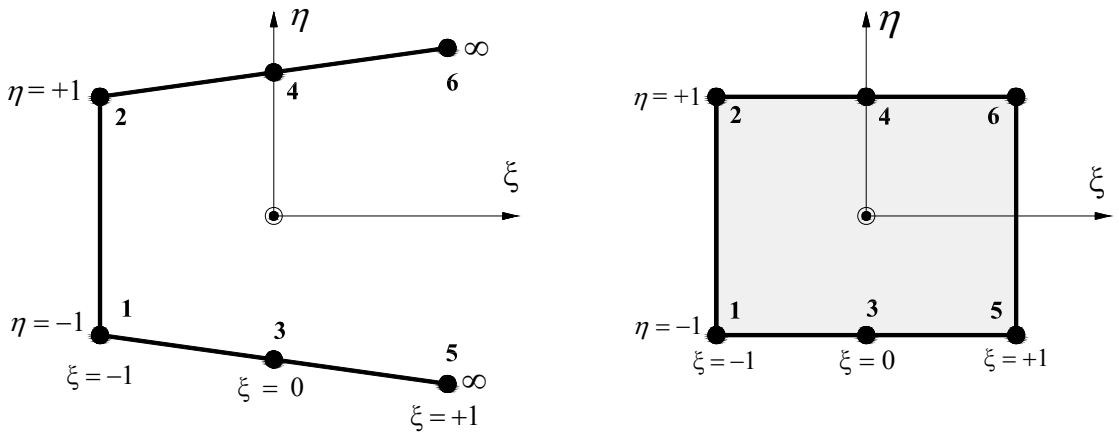

Coordinate Mapping

$$\{x\} = [M_i]\{x_i\}$$

$$M_i = (G_j)(L_k)$$

$$M_1 = \frac{-2\xi}{1-\xi}\,\frac{1}{2}(1-\eta)$$

$$M_2 = \frac{-2\xi}{1-\xi}\,\frac{1}{2}(1+\eta)$$

$$M_3 = \frac{1+\xi}{1-\xi}\,\frac{1}{2}(1-\eta)$$

$$M_4 = \frac{1+\xi}{1-\xi}\,\frac{1}{2}(1+\eta)$$

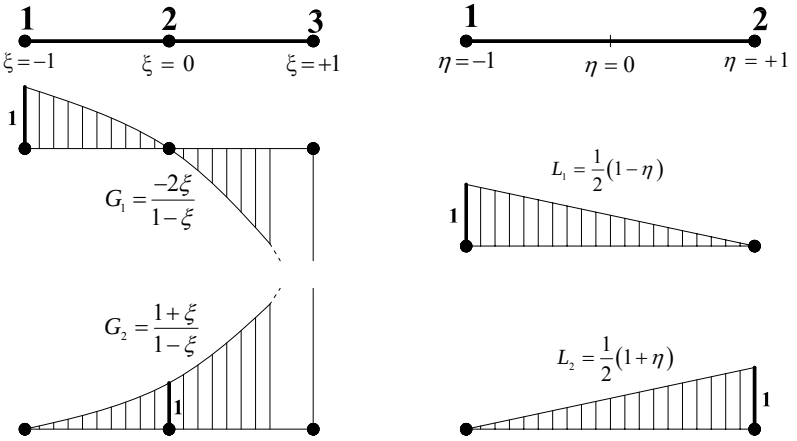

Table 5.3 (Contd)

Mapped, 2-Dimensional, 1-infinite direction, 6-node, Infinite Element
(contd)

Field Variable Mapping	**M2D-1I/C4-F6**

$$\{u\} = \lceil N_i \rceil \{d_i\}$$

$$N_i = \left(L_{j\xi}\right)\left(L_{k\eta}\right)$$

$$N_1 = -\frac{1}{2}\xi(1-\xi)\,\frac{1}{2}(1-\eta)$$

$$N_2 = -\frac{1}{2}\xi(1-\xi)\,\frac{1}{2}(1+\eta)$$

$$N_3 = \left(1-\xi^2\right)\frac{1}{2}(1-\eta)$$

$$N_4 = \left(1-\xi^2\right)\frac{1}{2}(1+\eta)$$

$$N_5 = \frac{1}{2}\xi(1+\xi)\,\frac{1}{2}(1-\eta)$$

$$N_6 = \frac{1}{2}\xi(1+\xi)\,\frac{1}{2}(1+\eta)$$

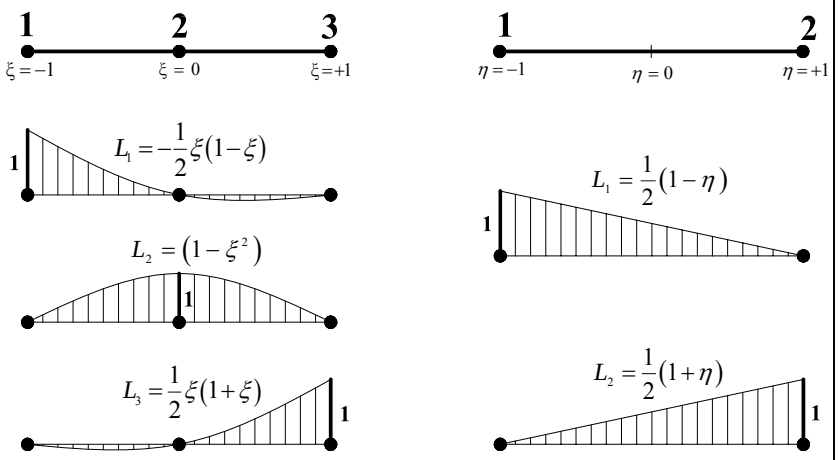

Table 5.4. Mapped, 2-dimensional, 1-infinite direction, 8-node, infinite element

Mapped, 2-Dimensional, 1-infinite direction, 8-node, Infinite Element

Geometrical Configuration	**M2D-1I/C5-F8**

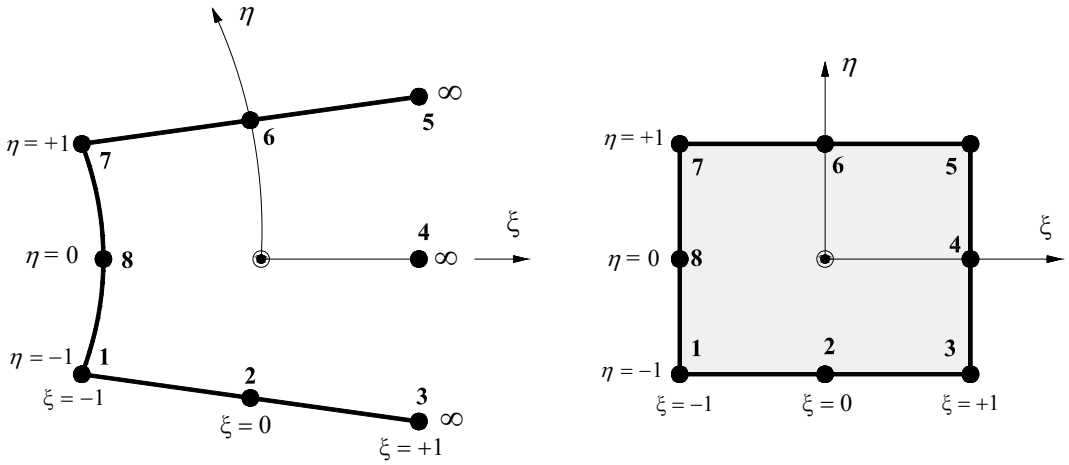

Coordinate Mapping *(serendipity)*

$$\{x\} = [M_i]\{x_i\}$$

$$M_i = (G_j)(L_k)$$

$$M_1 = \frac{(-1-\xi+\xi\eta+\eta^2)}{(1-\xi)}$$

$$M_2 = \left(\frac{1+\xi}{1-\xi}\right)\frac{1}{2}(1-\eta)$$

$$M_6 = \left(\frac{1+\xi}{1-\xi}\right)\frac{1}{2}(1+\eta)$$

$$M_7 = \frac{(-1-\xi-\xi\eta+\eta^2)}{(1-\xi)}$$

$$M_8 = \left(\frac{2}{1-\xi}\right)(1-\eta^2)$$

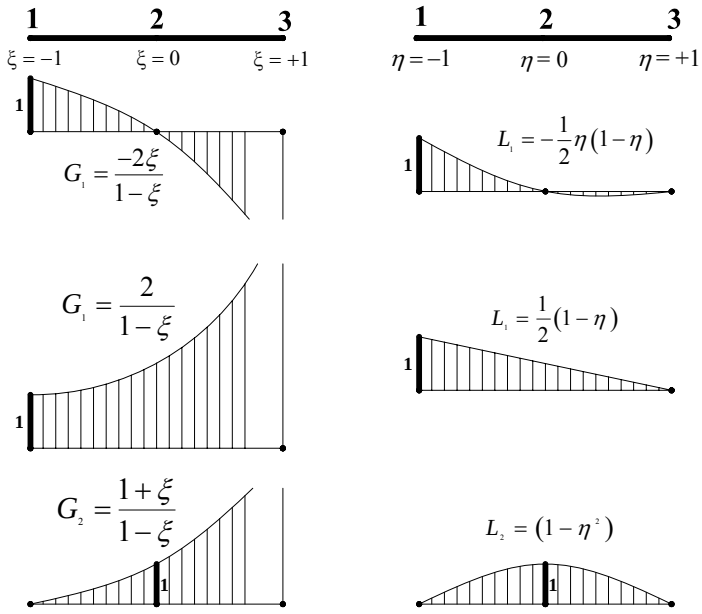

Table 5.4 (Contd)

Mapped, 2-Dimensional, 1-infinite direction, 8-node, Infinite Element
(contd)

Field Variable Mapping	**M2D-1I/C5-F8**

$$\{u\} = [N_i]\{d_i\}$$

$$N_i = \left(L_{j\xi}\right)\left(L_{k\eta}\right)$$

$$N_1 = -\frac{1}{2}\xi(1-\xi)\left(-\frac{1}{2}\right)\eta(1-\eta)$$

$$N_2 = \left(1-\xi^2\right)\frac{1}{2}(1-\eta)$$

$$N_3 = \frac{1}{2}\xi(1+\xi)\left(-\frac{1}{2}\right)\eta(1-\eta)$$

$$N_4 = \frac{1}{2}(1+\xi)\left(1-\eta^2\right)$$

$$N_5 = \frac{1}{2}\xi(1+\xi)\frac{1}{2}\eta(1+\eta)$$

$$N_6 = \left(1-\xi^2\right)\frac{1}{2}(1+\eta)$$

$$N_7 = -\frac{1}{2}\xi(1-\xi)\frac{1}{2}\eta(1+\eta)$$

$$N_8 = \frac{1}{2}(1-\xi)\left(1-\eta^2\right)$$

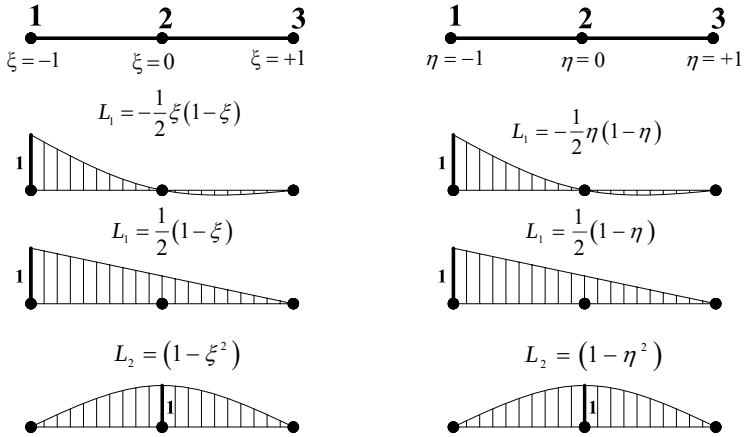

Table 5.5. Mapped, 2-dimensional, 1-infinite direction, 8-node, infinite element

Mapped, 2-Dimensional, 1-infinite direction, 8-node, Infinite Element

Geometrical Configuration	**M2D-1I/C6-F8**

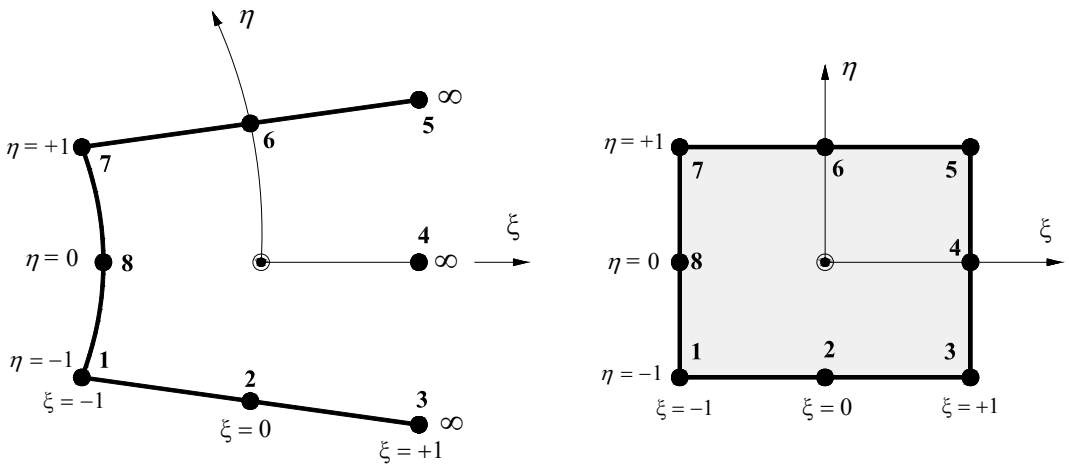

Coordinate Mapping *(serendipity)*

$$\{x\} = [M_i]\{x_i\}$$

$$M_i = (G_j)(L_k)$$

$$G_j = 1 + \xi_j + (1 + 2\xi_j)\xi$$

for $\xi \le 0$

and

$$G_j = 1 + \xi_j + \frac{(1 + 2\xi_j)\xi}{1 - \xi}$$

for $\xi \ge 0$

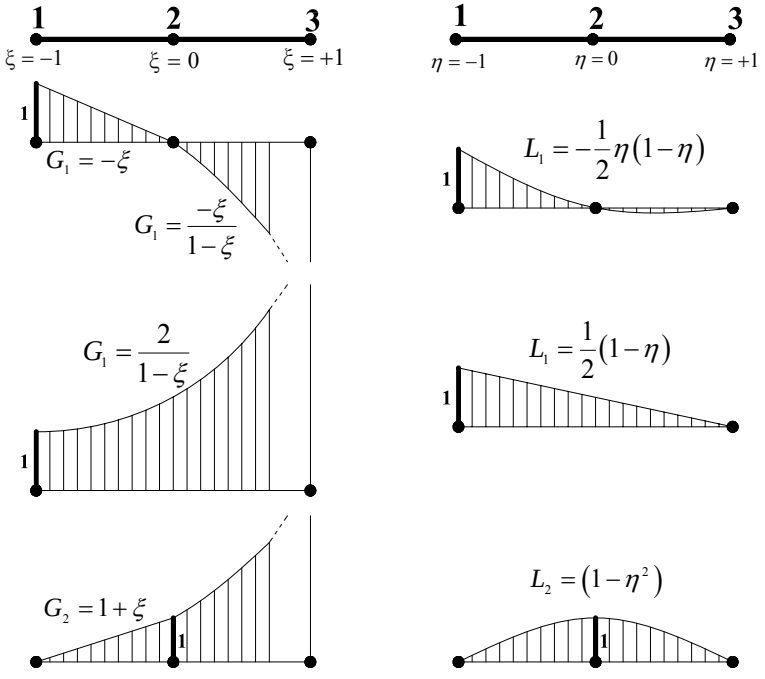

Table 5.5 (Contd)

Mapped, 2-Dimensional, 1-infinite direction, 8-node, Infinite Element
(contd)

Field Variable Mapping	**M2D-1I/C6-F8**

$$\{u\} = [N_i]\{d_i\}$$

$$N_i = \left(L_{j\xi}\right)\left(L_{k\eta}\right)$$

$$N_1 = F\left(\frac{r_1}{r}\right)\left(-\frac{1}{2}\right)\eta(1-\eta)$$

$$N_2 = F\left(\frac{r_1}{r}\right)\frac{1}{2}(1-\eta)$$

$$N_3 = F\left(\frac{r_1}{r}\right)\left(-\frac{1}{2}\right)\eta(1-\eta)$$

$$N_4 = F\left(\frac{r_1}{r}\right)\left(1-\eta^2\right)$$

$$N_5 = F\left(\frac{r_1}{r}\right)\frac{1}{2}\eta(1+\eta)$$

$$N_6 = F\left(\frac{r_1}{r}\right)\frac{1}{2}(1+\eta)$$

$$N_7 = F\left(\frac{r_1}{r}\right)\frac{1}{2}\eta(1+\eta)$$

$$N_8 = F\left(\frac{r_1}{r}\right)\left(1-\eta^2\right)$$

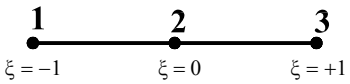

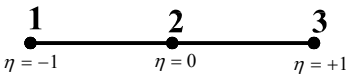

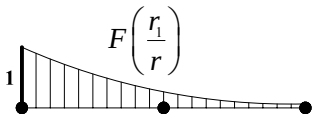

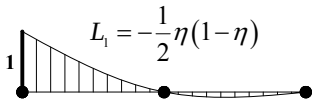

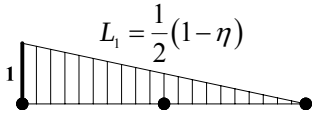

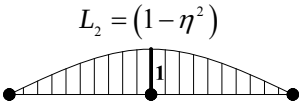

Table 5.6. Mapped, 2-dimensional, 1-infinite direction, 9-node, infinite element

Mapped, 2-Dimensional, 1-infinite direction, 9-node, Infinite Element

Geometrical Configuration	**M2D-1I/C6-F9**

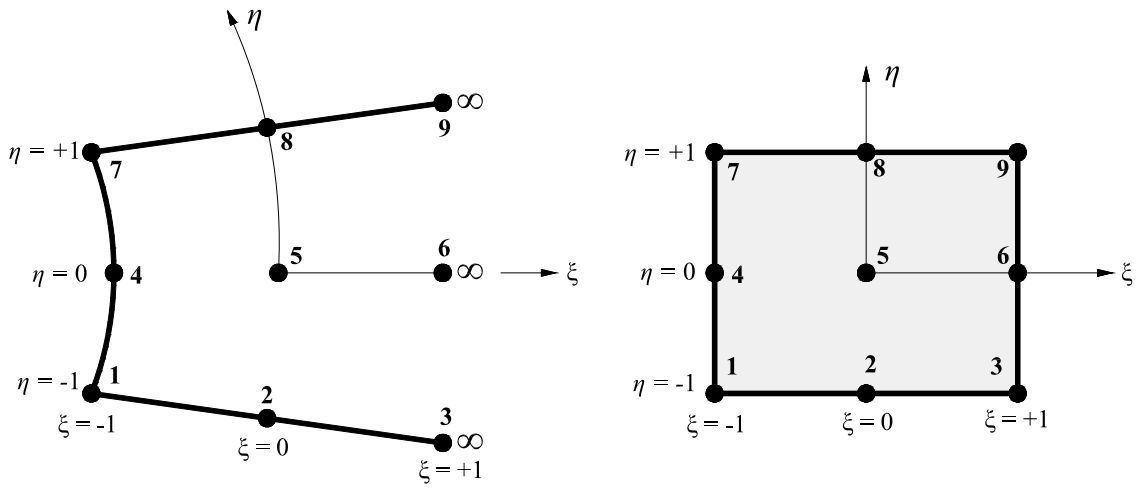

Coordinate Mapping

$$\{x\} = [M_i]\{x_i\}$$

$$M_i = (G_j)(L_k)$$

$$M_1 = -\frac{2\xi}{1-\xi}\left(-\frac{1}{2}\right)\eta(1-\eta)$$

$$M_2 = -\frac{1+\xi}{1-\xi}\left(-\frac{1}{2}\right)\eta(1-\eta)$$

$$M_4 = -\frac{2\xi}{1-\xi}\left(1-\eta^2\right)$$

$$M_5 = \frac{1+\xi}{1-\xi}\left(1-\eta^2\right)$$

$$M_7 = -\frac{2\xi}{1-\xi}\frac{1}{2}\eta(1+\eta)$$

$$M_8 = \frac{1+\xi}{1-\xi}\frac{1}{2}\eta(1+\eta)$$

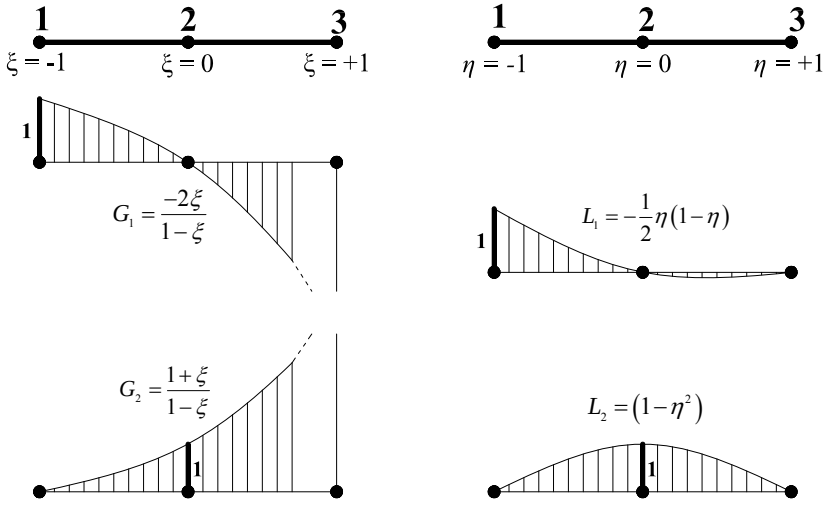

Table 5.6 (Contd)

Mapped, 2-Dimensional, 1-infinite direction, 9-node, Infinite Element
(contd)

Field Variable Mapping	**M2D-1I/C6-F9**

$$\{u\} = [N_i]\{d_i\}$$

$$N_i = \left(L_{j\xi}\right)\left(L_{k\eta}\right)$$

$$N_1 = -\frac{1}{2}\xi(1-\xi)\left(-\frac{1}{2}\right)\eta(1-\eta)$$

$$N_2 = \left(1-\xi^2\right)\left(-\frac{1}{2}\right)\eta(1-\eta)$$

$$N_3 = \frac{1}{2}\xi(1+\xi)\left(-\frac{1}{2}\right)\eta(1-\eta)$$

$$N_4 = -\frac{1}{2}\xi(1-\xi)\left(1-\eta^2\right)$$

$$N_5 = \left(1-\xi^2\right)\left(1-\eta^2\right)$$

$$N_6 = \frac{1}{2}\xi(1+\xi)\left(1-\eta^2\right)$$

$$N_7 = -\frac{1}{2}\xi(1-\xi)\frac{1}{2}\eta(1+\eta)$$

$$N_8 = \left(1-\xi^2\right)\frac{1}{2}\eta(1+\eta)$$

$$N_9 = \frac{1}{2}\xi(1+\xi)\frac{1}{2}\eta(1+\eta)$$

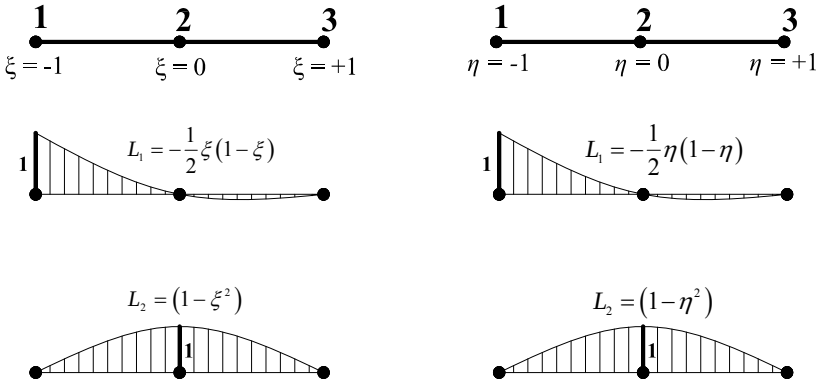

Table 5.7. Mapped, 2-dimensional, 1-infinite direction, 9-node, infinite element

Mapped, 2-Dimensional, 1-infinite direction, 9-node, Infinite Element

Geometrical Configuration	**M2D-1I/C6-F9**

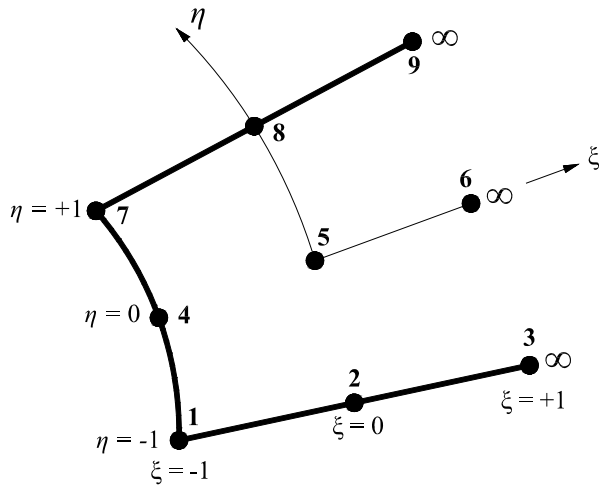

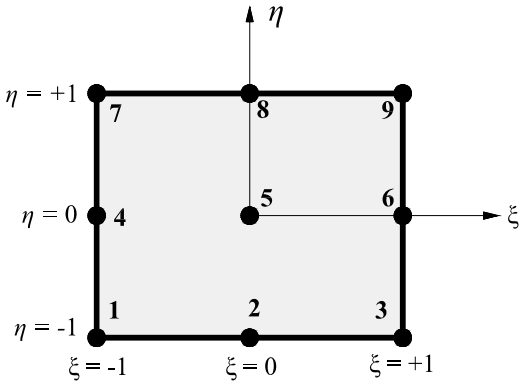

Coordinate Mapping

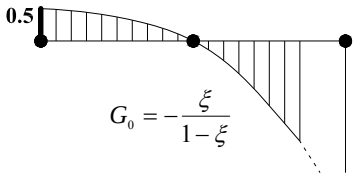

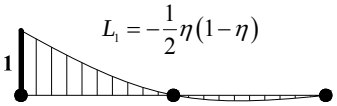

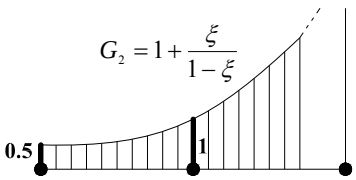

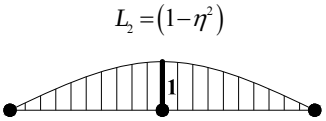

$$\{x\} = \begin{bmatrix} L_1G_0 & L_1G_2 & L_2G_0 & L_2G_2 & L_3G_0 & L_3G_2 \end{bmatrix} \begin{Bmatrix} 2x_1 - x_2 \\ x_2 \\ 2x_3 - x_4 \\ x_4 \\ 2x_5 - x_6 \\ x_6 \end{Bmatrix}$$

$$\{y\} = \begin{bmatrix} L_1G_0 & L_1G_2 & L_2G_0 & L_2G_2 & L_3G_0 & L_3G_2 \end{bmatrix} \begin{Bmatrix} 2y_1 - y_2 \\ y_2 \\ 2y_3 - y_4 \\ y_4 \\ 2y_5 - y_6 \\ y_6 \end{Bmatrix}$$

Table 5.7 (Contd)

Mapped, 2-Dimensional, 1-infinite direction, 9-node, Infinite Element *(contd)*

Field Variable Mapping	**M2D-1I/C6-F9**

$$\{u\} = [N_i]\{d_i\}$$

$$N_i = \left(L_{j\xi}\right)\left(L_{k\eta}\right)$$

$$N_1 = -\frac{1}{2}\xi(1-\xi)\left(-\frac{1}{2}\right)\eta(1-\eta)$$

$$N_2 = \left(1-\xi^2\right)\left(-\frac{1}{2}\right)\eta(1-\eta)$$

$$N_3 = \frac{1}{2}\xi(1+\xi)\left(-\frac{1}{2}\right)\eta(1-\eta)$$

$$N_4 = -\frac{1}{2}\xi(1-\xi)\left(1-\eta^2\right)$$

$$N_5 = \left(1-\xi^2\right)\left(1-\eta^2\right)$$

$$N_6 = \frac{1}{2}\xi(1+\xi)\left(1-\eta^2\right)$$

$$N_7 = -\frac{1}{2}\xi(1-\xi)\,\frac{1}{2}\eta(1+\eta)$$

$$N_8 = \left(1-\xi^2\right)\frac{1}{2}\eta(1+\eta)$$

$$N_9 = \frac{1}{2}\xi(1+\xi)\,\frac{1}{2}\eta(1+\eta)$$

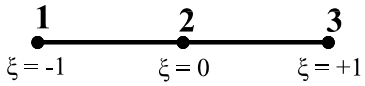

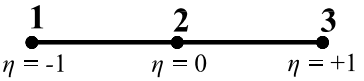

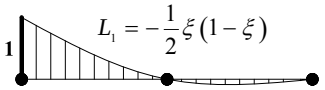

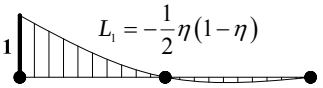

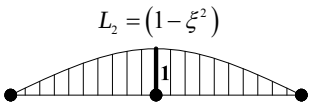

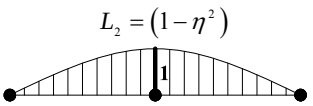

Table 5.8. Decay, 2-dimensional, 1-infinite direction, 7-node, infinite element

Decay, 2-Dimensional, 1-infinite direction, 7-node, Infinite Element

Geometrical Configuration	**D2D-1I/C5-F3**

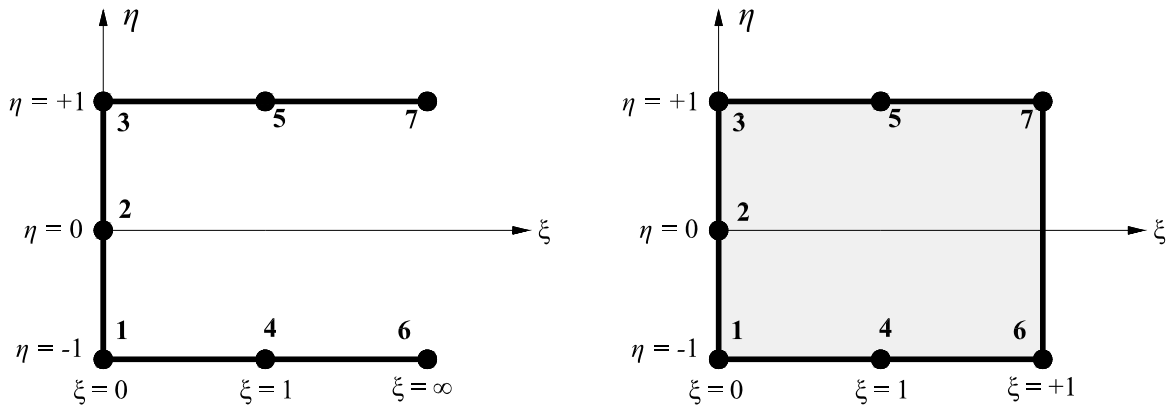

Coordinate Mapping

$$\{x\} = [M_i]\{x_i\}$$

$$M_i = \left(L_{j\xi}\right)\left(L_{k\eta}\right)$$

$$M_1 = (1-\xi)\,\frac{1}{2}(1-\eta)$$

$$M_2 \equiv 0$$

$$M_3 = (1-\xi)\,\frac{1}{2}(1+\eta)$$

$$M_4 = \xi\,\frac{1}{2}(1-\eta)$$

$$M_5 = \xi\,\frac{1}{2}(1+\eta)$$

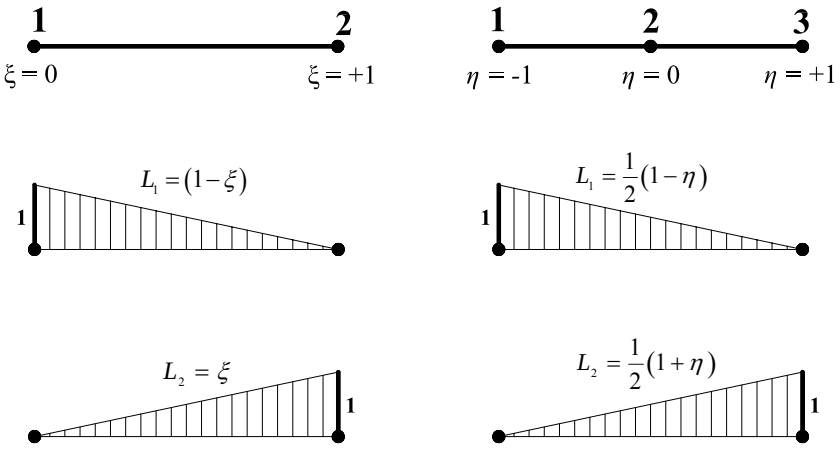

Table 5.8 (Contd)

Decay, 2-Dimensional, 1-infinite direction, 7-node, Infinite Element *(contd)*

Field Variable Mapping	**D2D-1I/C5-F3**

$$\{u\} = [N_i]\{d_i\}$$

$$N_i = \left(L_{k\eta}\right)\left(D_{j\xi}\right)$$

$$N_1 = -\frac{1}{2}\eta(1-\eta)\, e^{-\left(\alpha + iR_0\frac{w}{v}\right)\xi}$$

$$N_2 = \left(1-\eta^2\right) e^{-\left(\alpha + iR_0\frac{w}{v}\right)\xi}$$

$$N_3 = \frac{1}{2}\eta(1+\eta)\, e^{-\left(\alpha + iR_0\frac{w}{v}\right)\xi}$$

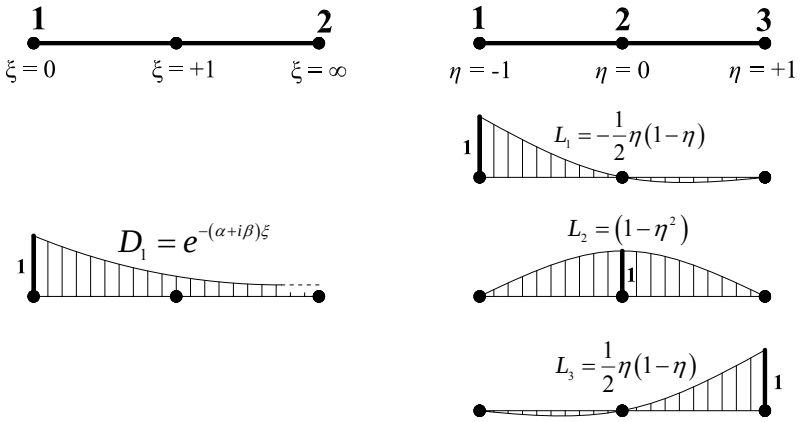

Table 5.9. Decay, 2-dimensional, 1-infinite direction, 5-node, infinite element

Decay, 2-Dimensional, 1-infinite direction, 5-node, Infinite Element

Geometrical Configuration | **D2D-1I/C6-F9**

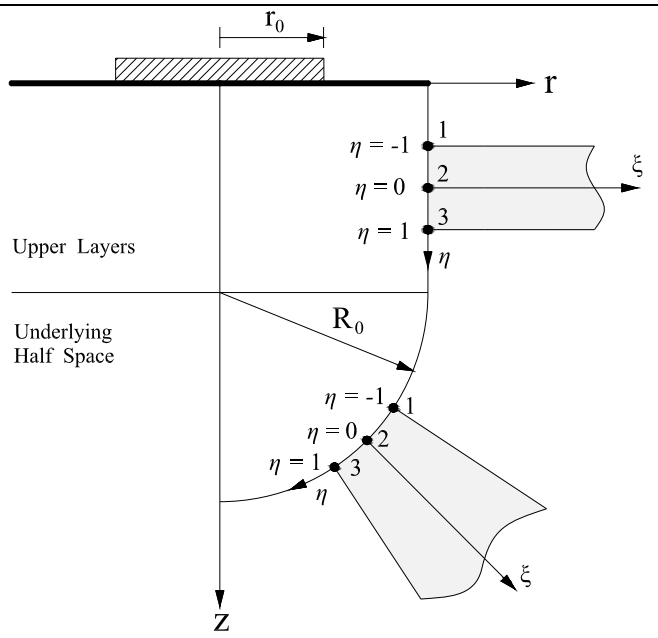

Coordinate Mapping

For horizontal infinite elements

$$r = \sum_{j=1}^{3} M(\xi)\, L_j(\eta)\, r_j$$

$$z = \sum_{j=1}^{3} L_j(\eta)\, z_j$$

For radiational infinite elements

$$r = \sum_{j=1}^{3} M(\xi)\, L_j(\eta)\, r_j$$

$$z = \sum_{j=1}^{3} M(\xi)\, L_j(\eta)\, z_j$$

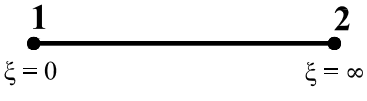

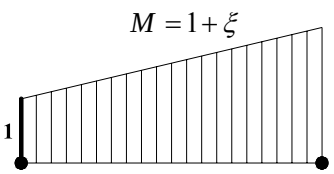

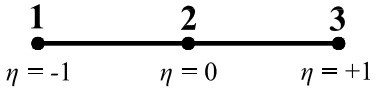

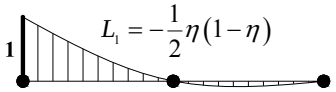

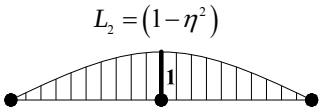

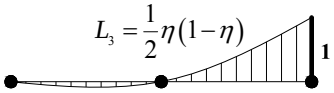

Table 5.9 (Contd)

Decay, 2-Dimensional, 1-infinite direction, 7-node, Infinite Element *(contd)*

Field Variable Mapping	**D2D-1I/C6-F9**

$$u(r) = \sum_{j=1}^{3} L_j(\eta)\, F(r)$$

$$F(r) = e^{-(\alpha + i\, k\, R_0)\xi}$$

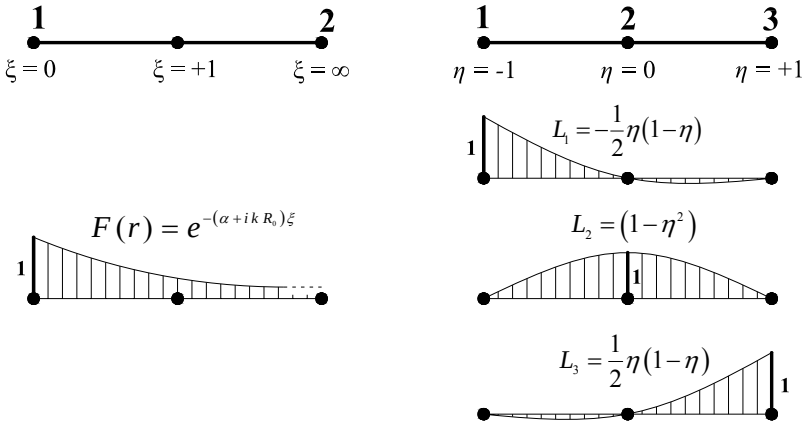

Table 5.10. Decay, 2-dimensional, 1-infinite direction, 6-node, infinite element

Decay, 2-Dimensional, 1-infinite direction, 6-node, Infinite Element

Geometrical Configuration	**D2D-1I/C4-F4**

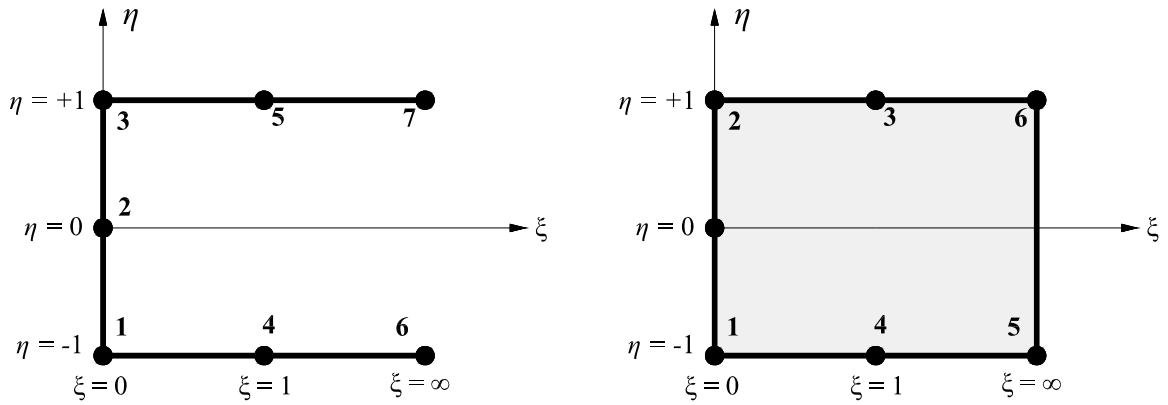

Coordinate Mapping	
$\{x\} = [M_i]\{x_i\}$	
$M_i = (L_j)(L_k)$	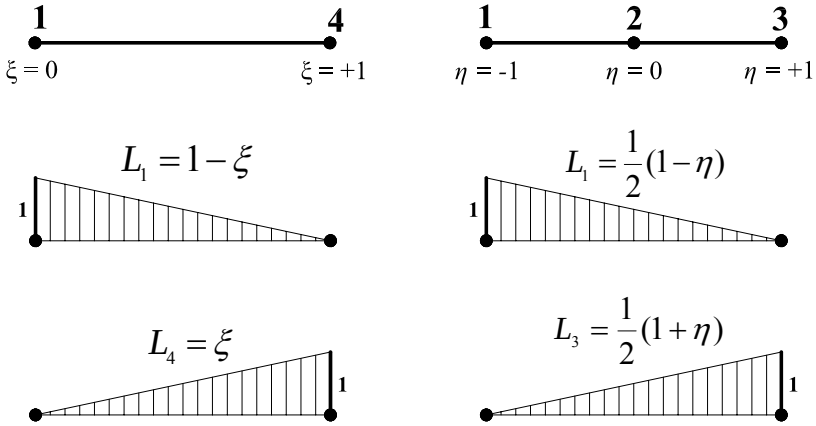
$M_1 = (1-\xi)\frac{1}{2}(1-\eta)$	
$M_2 = 0$	
$M_3 = (1-\xi)\frac{1}{2}(1+\eta)$	
$M_4 = \xi\frac{1}{2}(1-\eta)$	

Table 5.10 (Contd)

Decay, 2-Dimensional, 1-infinite direction, 6-node, Infinite Element *(contd)*

Field Variable Mapping	**D2D-1I/C4-F4**

$$\{u\} = [N_i]\{d_i\}$$

$$N_i = (L_{j\xi})(L_{k\eta})(D_{z\xi})$$

$$N_1 = (1-\xi)\frac{1}{2}(1-\eta)\, e^{\frac{1-\xi}{L}}$$

$$N_2 = 0$$

$$N_3 = (1-\xi)\frac{1}{2}(1+\eta)\, e^{\frac{1-\xi}{L}}$$

$$N_4 = (\xi)\frac{1}{2}(1-\eta)\, e^{\frac{1-\xi}{L}}$$

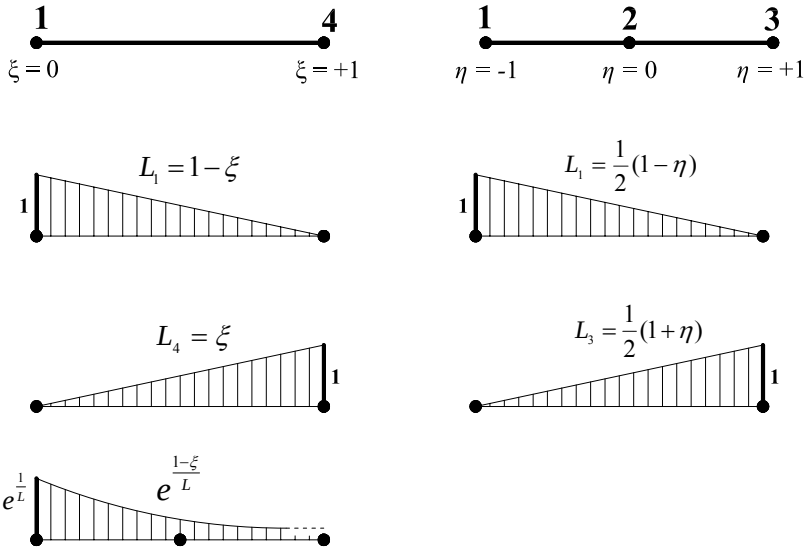

Table 5.11. Mapped, 2-dimensional, 2-infinite direction, 3-node, infinite element

Mapped, 2-Dimensional, 2-infinite direction, 3-node, Infinite Element

Geometrical Configuration	**M2D-2I/C1-F3**

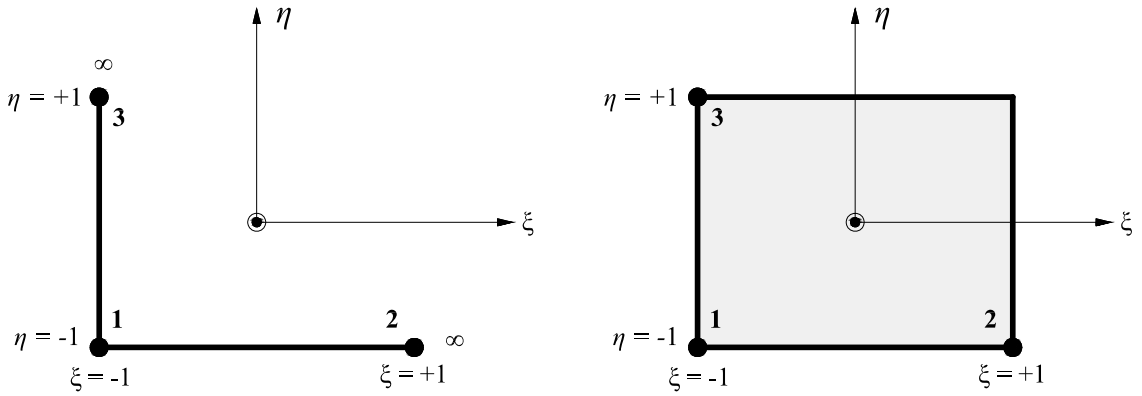

Coordinate Mapping	
$\{x\} = [M_i]\{x_i\}$	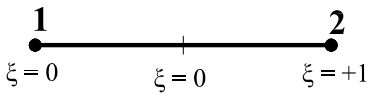
$M_i = (G_j)(G_k)$	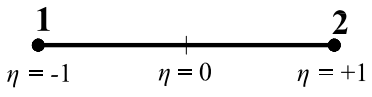
$M_1 = \frac{2}{1-\xi}\frac{2}{1-\eta}$	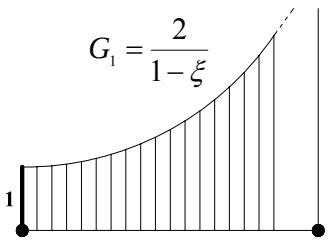 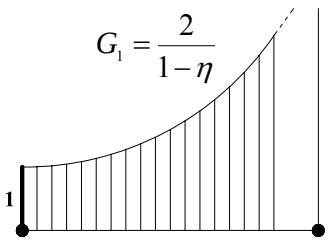

Table 5.11 (Contd)

Mapped, 2-Dimensional, 2-infinite direction, 3-node, Infinite Element
(contd)

Field Variable Mapping	**M2D-2I/C1-F3**

$$\{u\} = [N_i]\{d_i\}$$

$$N_i = (L_{j\xi})(L_{k\eta})$$

$$N_1 = \frac{1}{2}(1-\xi)\frac{1}{2}(1-\eta)$$

$$N_2 = \frac{1}{2}(1+\xi)\frac{1}{2}(1-\eta)$$

$$N_3 = \frac{1}{2}(1-\xi)\frac{1}{2}(1+\eta)$$

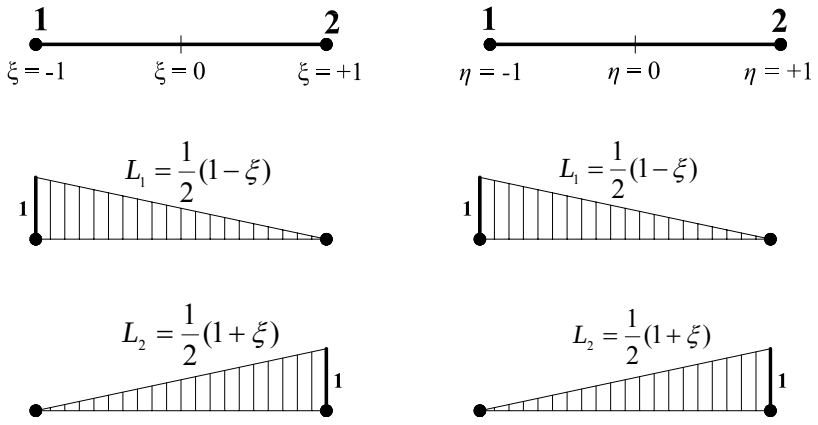

Table 5.12. Mapped, 2-dimensional, 2-infinite direction, 5-node, infinite element

Mapped, 2-Dimensional, 2-infinite direction, 5-node, Infinite Element

Geometrical Configuration	**M2D-2I/C3-F5**

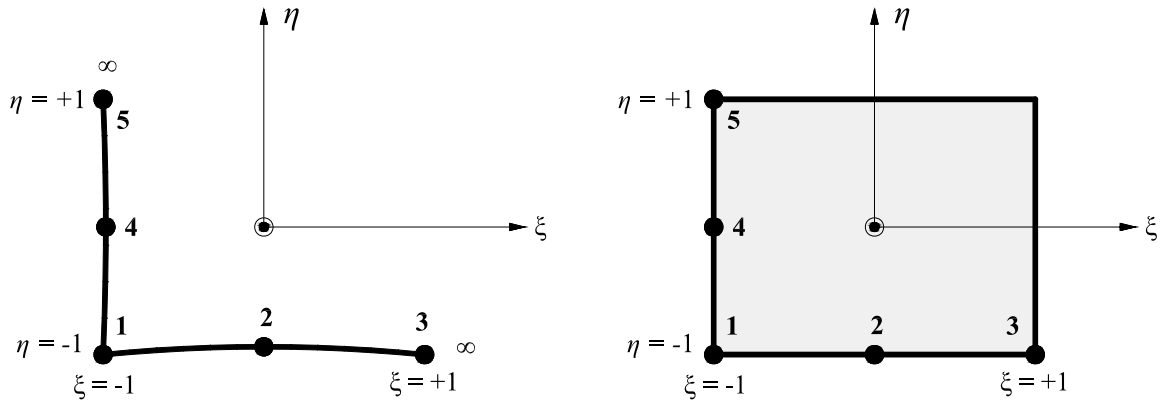

Coordinate Mapping *(serendipity)*

$$\{x\} = [M_i]\{x_i\}$$

$$M_i = (G_j)(G_k)$$

$$M_1 = \frac{-4(1+\xi+\eta)}{(1-\xi)(1-\eta)}$$

$$M_2 = \left(\frac{1+\xi}{1-\xi}\right)\left(\frac{2}{1-\eta}\right)$$

$$M_4 = \left(\frac{2}{1-\xi}\right)\left(\frac{1+\eta}{1-\eta}\right)$$

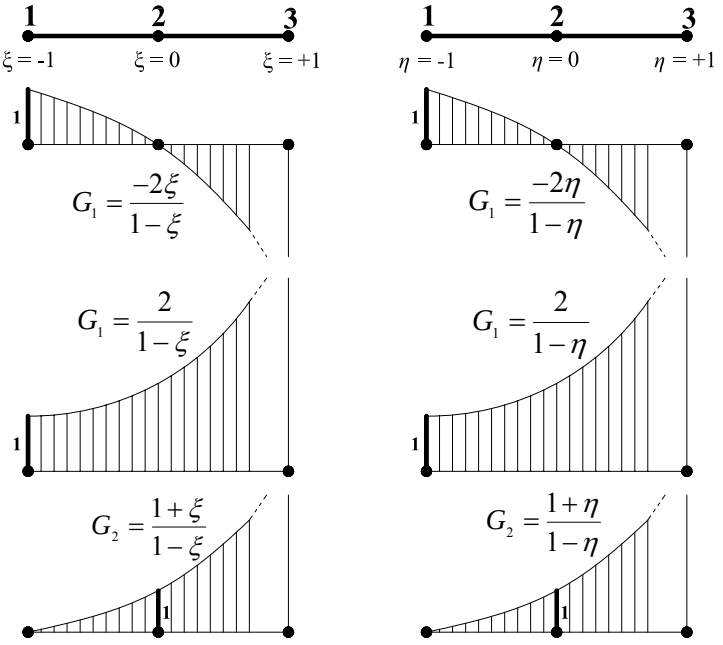

Table 5.12 (Contd)

Mapped, 2-Dimensional, 2-infinite direction, 5-node, Infinite Element
(contd)

Field Variable Mapping	**M2D-2I/C3-F5**

$$\{u\} = [N_i]\{d_i\}$$

$$N_i = \left(L_{j\xi}\right)\left(L_{k\eta}\right)$$

$$N_1 = -\frac{1}{2}\xi(1-\xi)\left(-\frac{1}{2}\right)\eta(1-\eta)$$

$$N_2 = \left(1-\xi^2\right)\frac{1}{2}(1-\eta)$$

$$N_3 = \frac{1}{2}\xi(1+\xi)\frac{1}{2}(1-\eta)$$

$$N_4 = \frac{1}{2}(1-\xi)\left(1-\eta^2\right)$$

$$N_5 = \frac{1}{2}\xi(1+\xi)\frac{1}{2}(1-\eta)$$

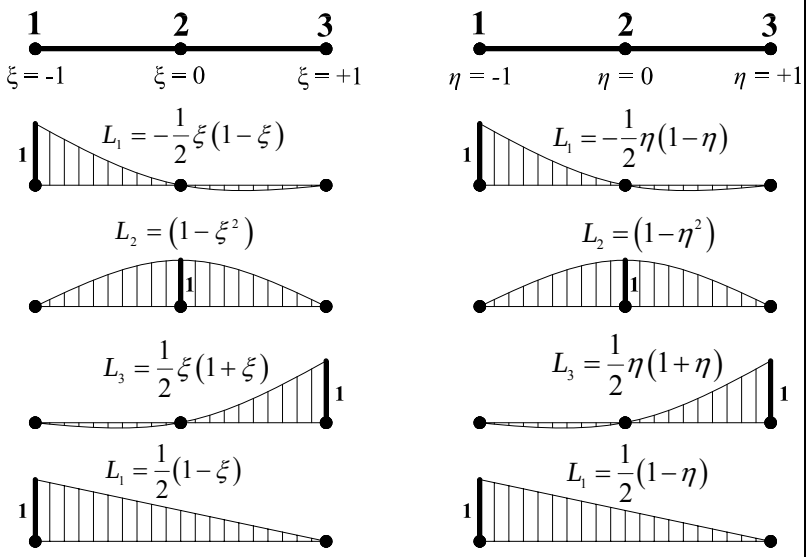

Table 5.13. Mapped, 2-dimensional, 2-infinite direction, 6-node, infinite element

Mapped, 2-Dimensional, 2-infinite direction, 6-node, Infinite Element

Geometrical Configuration | **M2D-2I/C4-F6**

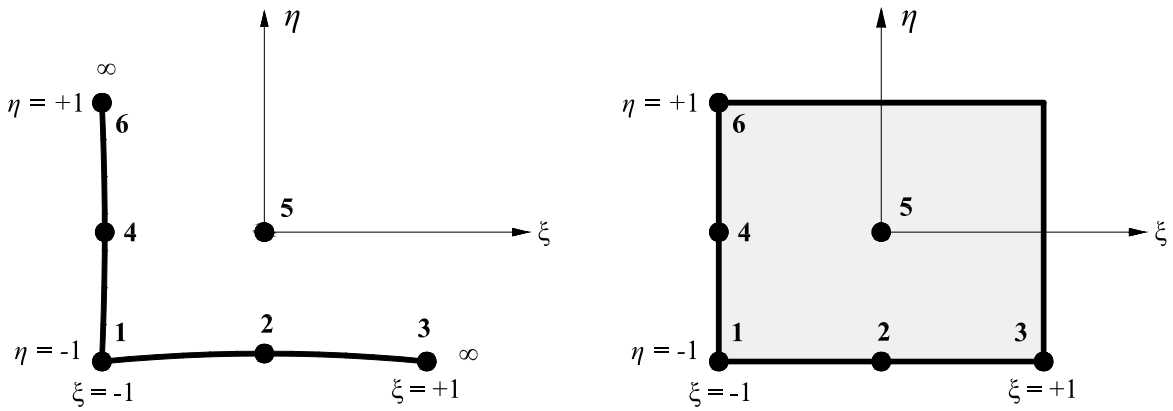

Coordinate Mapping *(serendipity)*

$$\{x\} = [M_i]\{x_i\}$$

$$M_i = (G_j)(G_k)$$

$$M_1 = \left(\frac{-2\xi}{1-\xi}\right)\left(\frac{-2\eta}{1-\eta}\right)$$

$$M_2 = \left(\frac{1+\xi}{1-\xi}\right)\left(\frac{-2\eta}{1-\eta}\right)$$

$$M_4 = \left(\frac{-2\xi}{1-\xi}\right)\left(\frac{1+\eta}{1-\eta}\right)$$

$$M_5 = \left(\frac{1+\xi}{1-\xi}\right)\left(\frac{1+\eta}{1-\eta}\right)$$

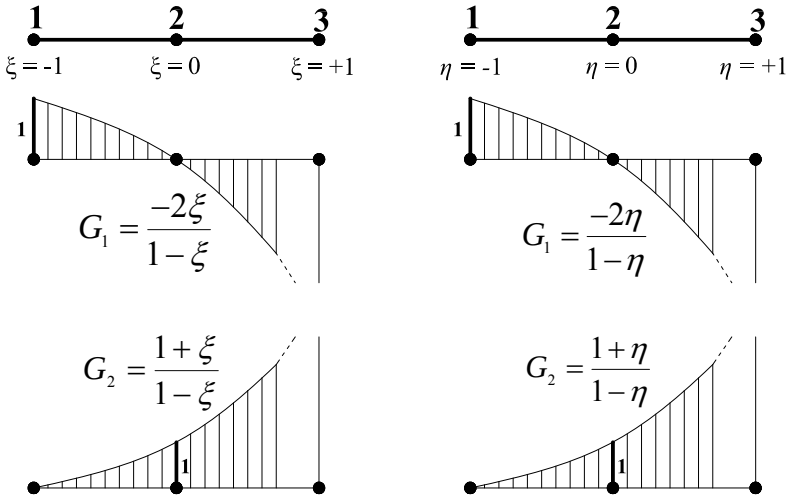

Table 5.13 (Contd)

Mapped, 2-Dimensional, 2-infinite direction, 6-node, Infinite Element
(contd)

Field Variable Mapping	**M2D-2I/C4-F6**

$$\{u\} = [N_i]\{d_i\}$$

$$N_i = \left(L_{j\xi}\right)\left(L_{k\eta}\right)$$

$$N_1 = -\frac{1}{2}\xi(1-\xi)\left(-\frac{1}{2}\right)\eta(1-\eta)$$

$$N_2 = \left(1-\xi^2\right)\left(-\frac{1}{2}\right)\eta(1-\eta)$$

$$N_3 = \frac{1}{2}\xi(1+\xi)\,\frac{1}{2}(1-\eta)$$

$$N_4 = -\frac{1}{2}\xi(1-\xi)\left(1-\eta^2\right)$$

$$N_5 = \left(1-\xi^2\right)\left(1-\eta^2\right)$$

$$N_6 = \frac{1}{2}(1-\xi)\,\frac{1}{2}\eta(1+\eta)$$

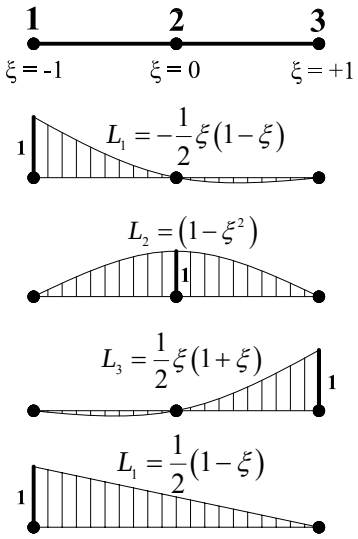

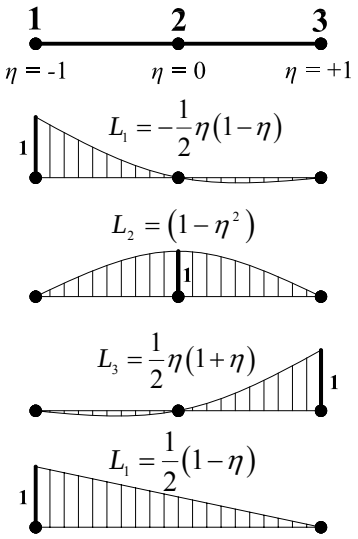

Table 5.14. Decay, 2-dimensional, 2-infinite direction, 6-node, infinite element

Decay, 2-Dimensional, 2-infinite direction, 6-node, Infinite Element

Geometrical Configuration	**D2D-2I/C4-F6**

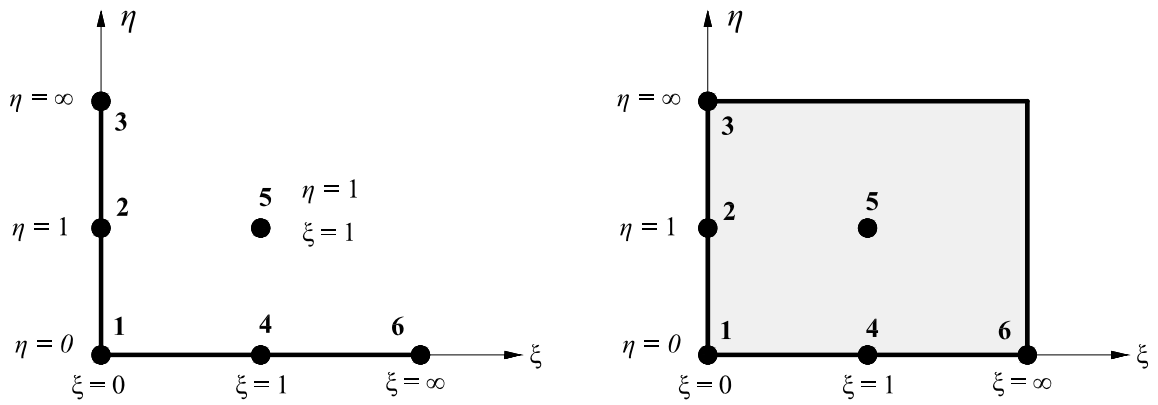

Coordinate Mapping

$$\{x\} = [M_i]\{x_i\}$$

$$M_i = \left(L_{j\xi}\right)\left(L_{k\eta}\right)$$

$$M_1 = (1-\xi)(1-\eta)$$

$$M_2 = (1-\xi)\eta$$

$$M_4 = \xi(1-\eta)$$

$$M_5 = \xi\,\eta$$

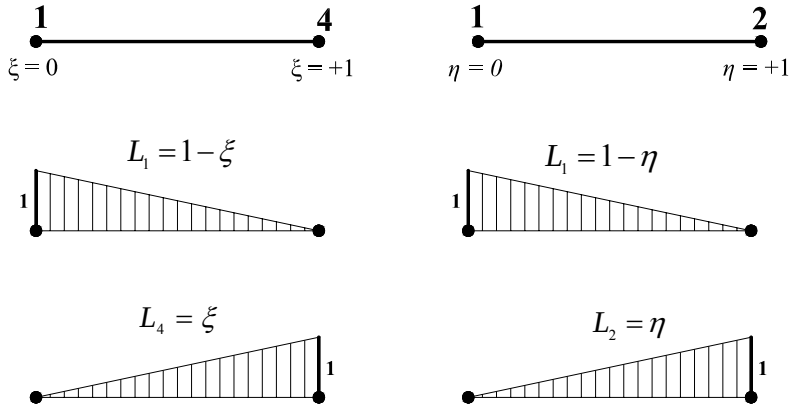

Table 5.14 (Contd)

Decay, 2-Dimensional, 2-infinite direction, 6-node, Infinite Element *(contd)*

Field Variable Mapping	**D2D-2I/C4-F6**

$$\{u\} = [N_i]\{d_i\}$$

$$N_i = \left(L_{j\xi}\right)\left(L_{k\eta}\right)\left(D_{z\xi}\right)$$

$$N_1 = (1-\xi)(1-\eta)\, e^{\frac{1-\xi}{L_1}}\, e^{\frac{1-\eta}{L_2}}$$

$$N_2 = (1-\xi)\,\eta\, e^{\frac{1-\xi}{L_1}}\, e^{\frac{1-\eta}{L_2}}$$

$$N_4 = \xi\,(1-\eta)\, e^{\frac{1-\xi}{L_1}}\, e^{\frac{1-\eta}{L_2}}$$

$$N_5 = \xi\,\eta\, e^{\frac{1-\xi}{L_1}}\, e^{\frac{1-\eta}{L_2}}$$

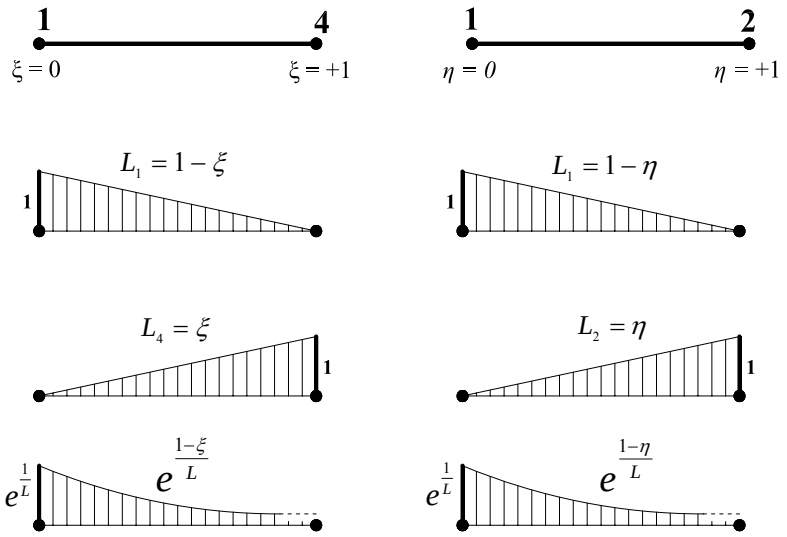

5.2. Derivation of Properties of Infinite Elements

The equilibrium equation of a finite element is expressed as

$$[M]\{\ddot{d}\}+[C]\{\dot{d}\}+[K]\{d\}=\{P\}-\sum\left[\{f\}_X+\{f\}_S+\{f\}_{\varepsilon_0}+\{f\}_{\sigma_0}+\{f\}_T+\{f\}_0\right] \quad (5.1)$$

where; $\{d\}$ = nodal displacements, $[M]$ = consistent mass matrix, $[C]$ = consistent damping matrix, $[K]$ = stiffness matrix, $\{P\}$ = nodal loads, $\{f\}_X$ = body forces at nodes, $\{f\}_S$ = edge loads at nodes, $\{f\}_{\varepsilon_0}$ = nodal loads due to initial strains, $\{f\}_{\sigma_0}$ = nodal loads due to initial stresses, $\{f\}_T$ = temperature change loads, $\{f\}_0$ = known displacement loads.

$$[M]=\rho\int_V [N]^T[N]dV \quad (5.2)$$

$$[C]=c_0\int_V [N]^T[N]dV \quad (5.3)$$

$$[K]=\int_V [G]^T[D][G]dV \quad (5.4)$$

$$\{f\}_X=-\int_V [N]^T\begin{Bmatrix}X_x\\X_y\\X_z\end{Bmatrix}dV \quad (5.5)$$

$$\{f\}_S=-\int_S [N]^T\begin{Bmatrix}p_x\\p_y\\p_z\end{Bmatrix}_S ds \quad (5.6)$$

$$\{f\}_{\varepsilon_0} = -\left(\int_v [G]^T dV\right)[D]\{\varepsilon\}_0 \tag{5.7}$$

$$\{f\}_{\sigma_0} = \left(\int_V [G]^T dV\right)\{\sigma\}_0 \tag{5.8}$$

$$\{f\}_T = -\alpha_T \Delta T\left(\int_v [G]^T dV\right)\{D\}_T \tag{5.9}$$

$$\{f\}_0 = [K]\{d\}_{known} \tag{5.10}$$

and generic displacements, strains and $[\underline{\Delta}][\mathrm{N}]$ can be expressed as:

$$\{u\} = [N]\{d\} \qquad \{\varepsilon\} = [\underline{\Delta}]\{u\} \qquad [\underline{\Delta}][N] = [G] \tag{5.11}$$

in which, $[\underline{\Delta}]$ is the operator matrix to differentiate the shape function matrix $[N]$ and,

$$\{\varepsilon\} = [\mathrm{G}]\{\mathrm{d}\} \qquad \{\sigma\} = \underbrace{[\mathrm{D}][\mathrm{G}]}_{[\mathrm{S}]}\{\mathrm{d}\} \tag{5.12}$$

in which $[\mathrm{G}]$, $[\mathrm{D}]$ and $[\mathrm{S}]$ are the strain matrix, elasticity matrix and stress matrix, respectively. Interpolation for geometry and field variables for infinite elements may be written in the compact matrix form as follows:

$$\{x\} = \begin{Bmatrix} x \\ y \end{Bmatrix} = \begin{bmatrix} x_1 & x_2 & x_3 & x_4 \\ y_1 & y_2 & y_3 & y_4 \end{bmatrix} \begin{Bmatrix} M_1 \\ M_2 \\ M_3 \\ M_4 \end{Bmatrix} \quad \{u\} = \begin{Bmatrix} u \\ v \end{Bmatrix} = \begin{bmatrix} d_1 & d_2 & d_3 & d_4 \\ d_5 & d_6 & d_7 & d_8 \end{bmatrix} \begin{Bmatrix} N_1 \\ N_2 \\ N_3 \\ N_4 \end{Bmatrix} \tag{5.13}$$

In order the obtain the derivatives of shape functions with respect to global coordinates, Jacobi transformation is needed

$$\begin{Bmatrix} N_{1,x} \\ N_{1,y} \end{Bmatrix} = \left[J\right]^{-1} \begin{Bmatrix} N_{1,\xi} \\ N_{1,\eta} \end{Bmatrix} \tag{5.14}$$

where,

$$\left[J\right]^{-1} = \frac{1}{\left|J\right|}\begin{bmatrix} y_{,\eta} & -y_{,\xi} \\ -x_{,\eta} & x_{,\xi} \end{bmatrix} \qquad Det\left|J\right| = x_{,\xi}\ y_{,\eta} - y_{,\xi}\ x_{,\eta} \tag{5.15}$$

For the numerical integration, dV is converted and Gaussian Quadrature integration scheme or Gaussian-Laguerre Quadrature integration scheme is used.

$$dV = t\,dA = t\left|J\right| d_{\xi} d_{\eta} \tag{5.16}$$

$$\left[M\right] = \rho t \int_{-1}^{+1}\int_{-1}^{+1} \left[N\right]^{T}\left[N\right]\left|J\right| d\xi\, d\eta = \int_{-1}^{+1}\int_{-1}^{+1} f\left(\xi,\eta\right) d\xi\, d\eta = \sum_{i=1}^{n}\sum_{j=1}^{m} A_i A_j\, f\left(\xi_i,\eta_i\right) \tag{5.17}$$

$$\left[C\right] = \rho_0 t \int_{-1}^{+1}\int_{-1}^{+1} \left[N\right]^{T}\left[N\right]\left|J\right| d\xi\, d\eta = \int_{-1}^{+1}\int_{-1}^{+1} f\left(\xi,\eta\right) d\xi\, d\eta = \sum_{i=1}^{n}\sum_{j=1}^{m} A_i A_j\, f\left(\xi_i,\eta_i\right) \tag{5.18}$$

$$\left[K\right] = t \int_{-1}^{+1}\int_{-1}^{+1} \left[G\right]^{T}\left[D\right]\left[G\right]\left|J\right| d\xi\, d\eta = \int_{-1}^{+1}\int_{-1}^{+1} f\left(\xi,\eta\right) d\xi\, d\eta = \sum_{i=1}^{n}\sum_{j=1}^{m} A_i A_j\, f\left(\xi_i,\eta_i\right) \tag{5.19}$$

$$\int_{0}^{\infty}\int_{0}^{\infty} x^{\alpha} e^{-x} f\left(\xi,\eta\right) d\xi\, d\eta = \sum_{i=1}^{n}\sum_{j=1}^{m} A_i A_j\, f\left(\xi_i,\eta_i\right) \tag{5.20}$$

6. THREE-DIMENSIONAL INFINITE ELEMENTS

A brief summary of a three-dimensional, 6-node triangular prism infinite element as introduced by Ungless and Anderson (1973) is presented herein.

6.1. Six-node Triangular Prism Infinite Element

Instead of dealing with an imposed rigid or free boundary, a flexible boundary formed by the infinite elements has been introduced. The element model as introduced by Ungless and Anderson is shown in Figure 6.1. The geometry of the element and the two right hand cartesian coordinate systems; global (X, Y, Z) and local (x, y, z) can be seen.

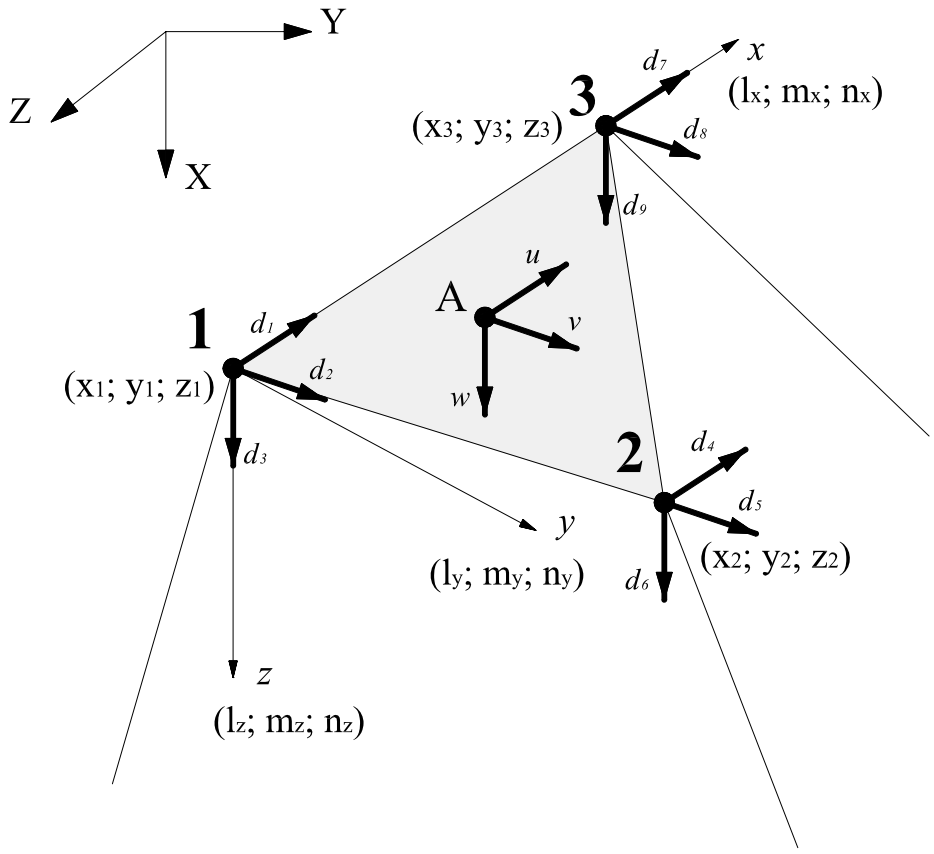

Figure 6.1. A three dimensional infinite element by Ungless and Anderson

Direction cosines of z-axis are found by the cross product of side 1-3 (v_{1-3}) and side 1-2 (v_{1-2}):

$$\left(\vec{v}_x = \vec{v}_{1-3}\right) \times \left(\vec{v}_{1-2}\right) = \vec{v}_z \tag{6.1}$$

$$L_{1-3} = \sqrt{\left(x_3 - x_1\right)^2 + \left(y_3 - y_1\right)^2 + \left(z_3 - z_1\right)^2} \tag{6.2}$$

$$l_x = \left(x_3 - x_1\right)/L_{1-3}\,, \quad m_x = \left(y_3 - y_1\right)/L_{1-3}\,, \quad n_x = \left(z_3 - z_1\right)/L_{1-3} \tag{6.3}$$

$$L_{1-2} = \sqrt{\left(x_2 - x_1\right)^2 + \left(y_2 - y_1\right)^2 + \left(z_2 - z_1\right)^2} \tag{6.4}$$

$$l_{1-2} = \left(x_2 - x_1\right)/L_{1-2}\,,\ m_{1-2} = \left(y_2 - y_1\right)/L_{1-2}\,,\ n_{1-2} = \left(z_2 - z_1\right)/L_{1-2} \tag{6.5}$$

$$\left(\vec{v}_{1-3}\right) \times \left(\vec{v}_{1-2}\right) = \begin{pmatrix} l_{1-3} & m_{1-3} & n_{1-3} \\ l_{1-2} & m_{1-2} & n_{1-2} \end{pmatrix} = l_z\vec{i} + m_z\vec{j} + n_z\vec{k} \tag{6.6}$$

Direction cosines of y axis are obtained by:

$$\left(\vec{v}_z\right) \times \left(\vec{v}_x\right) = \begin{pmatrix} l_z & m_z & n_z \\ l_x & m_x & n_x \end{pmatrix} = l_y\vec{i} + m_y\vec{j} + n_y\vec{k} \tag{6.7}$$

Decaying shape functions of the infinite element by Ungless and Anderson is seen in Figure 6.2 and also the decay function of this element is in equation (6.8).

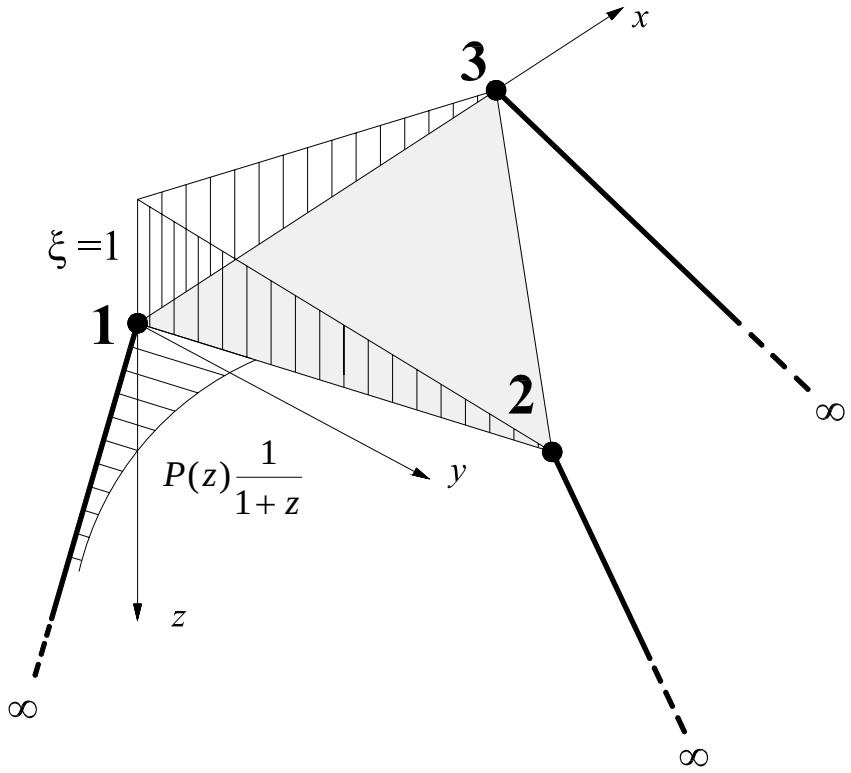

Figure 6.2. Decaying shape functions

$$N = L_i P(z) \tag{6.8}$$

where

$$P(z) = \frac{1}{1+z} \tag{6.9}$$

and

$$L_1 = \xi, \quad L_2 = \eta, \quad L_3 = \zeta \tag{6.10}$$

The displacement vector can be expressed as following:

$$\{U\}=\begin{Bmatrix}u\\v\\w\end{Bmatrix}=[N]\{d\}=\frac{1}{1+z}\begin{bmatrix}\xi&0&0&\eta&0&0&\zeta&0&0\\0&\xi&0&0&\eta&0&0&\zeta&0\\0&0&\xi&0&0&\eta&0&0&\zeta\end{bmatrix}\begin{Bmatrix}d_1\\d_2\\d_3\\d_4\\d_5\\d_6\\d_7\\d_8\\d_9\end{Bmatrix} \tag{6.11}$$

In order to obtain strains, strain matrix $[G]$ should be obtained:

$$\{\varepsilon\}=[\Delta]\{U\}=[\Delta][N]\{d\}=[G]\{d\} \tag{6.12}$$

$$\begin{Bmatrix}\varepsilon_x\\\varepsilon_z\\\varepsilon_x\\\gamma_{xz}\\\gamma_{yz}\\\gamma_{xy}\end{Bmatrix}=\begin{bmatrix}\frac{\partial}{\partial x}&0&0\\0&\frac{\partial}{\partial y}&0\\0&0&\frac{\partial}{\partial z}\\\frac{\partial}{\partial y}&\frac{\partial}{\partial x}&0\\\frac{\partial}{\partial z}&0&\frac{\partial}{\partial x}\\0&\frac{\partial}{\partial z}&\frac{\partial}{\partial y}\end{bmatrix}\begin{Bmatrix}u\\v\\w\end{Bmatrix} \tag{6.13}$$

Derivatives of ξ, η, and ζ with respect to *x*, *y*, and *z* are as follows:

$$\frac{\partial\xi}{\partial x}=\frac{b_1}{2A},\quad \frac{\partial\eta}{\partial x}=\frac{b_2}{2A},\quad \frac{\partial\zeta}{\partial x}=\frac{b_3}{2A} \tag{6.13}$$

$$\frac{\partial\xi}{\partial y}=\frac{a_1}{2A},\quad \frac{\partial\eta}{\partial y}=\frac{a_2}{2A},\quad \frac{\partial\zeta}{\partial y}=\frac{a_3}{2A} \tag{6.14}$$

where A is the area of triangle, $a_1 = x_1,\ a_2 = x_2,\ a_3 = x_3$ and $b_1 = y_1,\ b_2 = y_2,\ b_3 = y_3$.

When $[\Delta]$and $[N]$matrices are multiplied, $[G]$matrix is obtained as follows with the multiplier of $h = \left(\frac{1}{1+z}\right)\left(\frac{1}{2A}\right)$.

$$[G] = \begin{bmatrix} b_1 & 0 & 0 & b_2 & 0 & 0 & b_3 & 0 & 0 \\ 0 & a_1 & 0 & 0 & a_2 & 0 & 0 & a_3 & 0 \\ 0 & 0 & \frac{-2A\xi}{1+z} & 0 & 0 & \frac{-2A\eta}{1+z} & 0 & 0 & \frac{-2A\zeta}{1+z} \\ a_1 & b_1 & 0 & a_2 & b_2 & 0 & a_3 & b_3 & 0 \\ \frac{-2A\xi}{1+z} & 0 & b_1 & \frac{-2A\eta}{1+z} & 0 & b_2 & \frac{-2A\zeta}{1+z} & 0 & b_3 \\ 0 & \frac{-2A\xi}{1+z} & a_1 & 0 & \frac{-2A\eta}{1+z} & a_2 & 0 & \frac{-2A\zeta}{1+z} & a_3 \end{bmatrix} h \quad (6.15)$$

Material matrix is:

$$[D] = \frac{E(1-\mu)}{(1+\mu)(1-2\mu)} \begin{bmatrix} 1 & \frac{\mu}{1-\mu} & \frac{\mu}{1-\mu} & 0 & 0 & 0 \\ \frac{\mu}{1-\mu} & 1 & \frac{\mu}{1-\mu} & 0 & 0 & 0 \\ \frac{\mu}{1-\mu} & \frac{\mu}{1-\mu} & 1 & 0 & 0 & 0 \\ 0 & 0 & 0 & \frac{1-2\mu}{2(1-\mu)} & 0 & 0 \\ 0 & 0 & 0 & 0 & \frac{1-2\mu}{2(1-\mu)} & 0 \\ 0 & 0 & 0 & 0 & 0 & \frac{1-2\mu}{2(1-\mu)} \end{bmatrix} \quad (6.16)$$

Stiffness matrix is obtained as

$$[k] = \int_V [G]^T [D][G] dV \tag{6.17}$$

Direction cosines matrix of the *xyz*-axes can be written as

$$[t] = \begin{bmatrix} l_x & m_x & n_x \\ l_y & m_y & n_y \\ l_z & m_z & n_z \end{bmatrix} \tag{6.18}$$

Stiffness matrix in global directions is obtained through a congruent transformation;

$$[k]_{XYZ} = [T]^T [k][T] \tag{6.19}$$

As a numerical example, semi-infinite solid loaded with a point load perpendicular to the free surface is selected. The quarter surface of the hemispherical bowl on which the point load is acting forms the base plane for the infinite elements. This surface is subdivided into a mesh as seen in Figure 6.3.

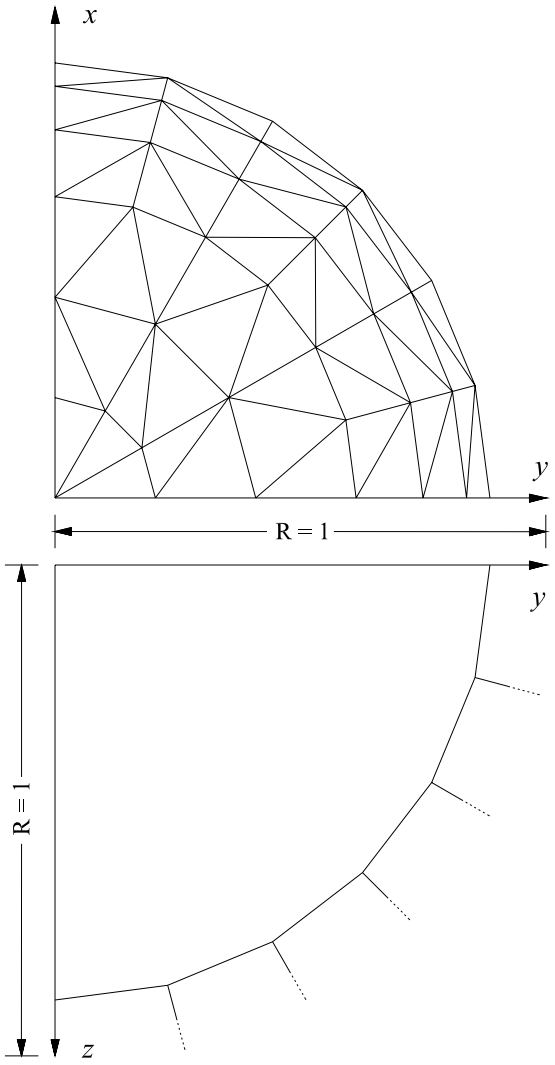

Figure 6.3. Finite element mesh of hemispherical bowl with one quarter symmetry

Figure 6.4 compares the results obtained from the infinite finite element analysis with the exact elasticity solution. The infinite element results are found to vary by 4% on the average from the exact solution. Directly beneath the load, agreement within 2% is achieved.

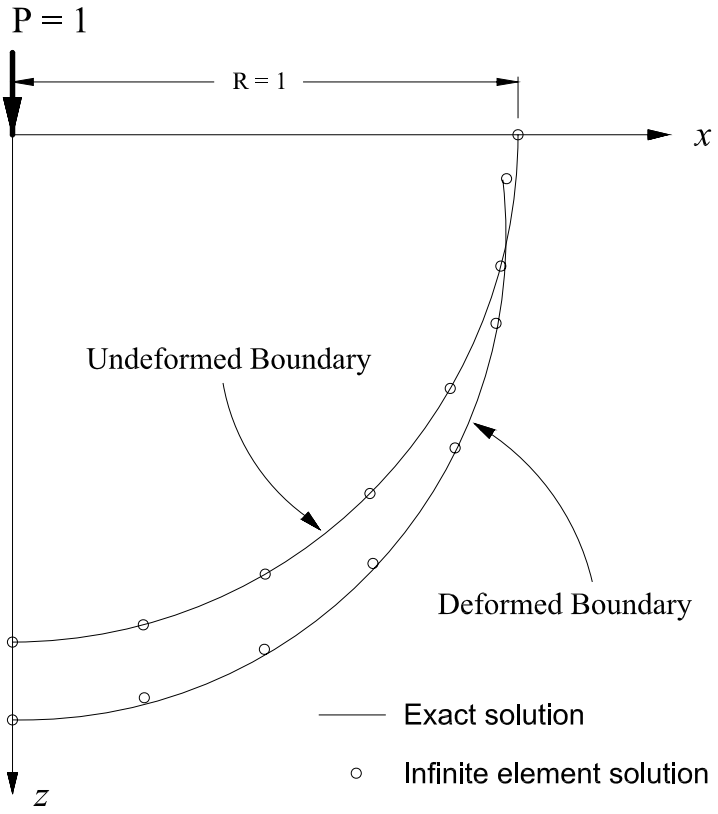

Figure 6.4. Deflections of hemispherical boundary loaded perpendicular to surface

6.2. Three-dimensional Infinite Element Geometrical Configurations

Based on direction of infinity, type of infinite element being mapped or decay, three-dimensional infinite elements are summarized in Table 6.1. Geometrical configuration, coordinate mapping, and field variable mapping functions of three-dimensional infinite elements are presented in a tabular manner in Tables 6.2 through 6.6.

Table 6.1. Three-dimensional infinite element summary chart

Infinite Direction	***Type***	***Code***	***Description***	***Reference***
1	Mapped	M3D-1I/C4-F8	Mapped, 3-Dimensional, 1-infinite direction, 8-node, infinite element	Bettess, P., 1977
1	Mapped	M3D-1I/C10-F6	Mapped, 3-Dimensional, 1-infinite direction, 10-node, infinite element	Beer, G. and J. L. Meek, 1981
1	Mapped	M3D-1I/C8-F8	Mapped, 3-Dimensional, 1-infinite direction, 8-node, infinite element	Zienkiewicz, O. C., C. Emson and P. Bettess, 1983
2	Mapped	M3D-2I/C2-F8	Mapped, 3-Dimensional, 2-infinite direction, 6-node, infinite element	Bettess, P., 1977
3	Mapped	M3D-3I/C1-F8	Mapped, 3-Dimensional, 3-infinite direction, 4-node, infinite element	Bettess, P., 1977

Table 6.2. Mapped, 3-Dimensional, 1-infinite direction, 8-node, infinite element

Mapped, 3-Dimensional, 1-infinite direction, 8-node, Infinite Element

Geometrical Configuration	**M3D-1I/C4-F8**

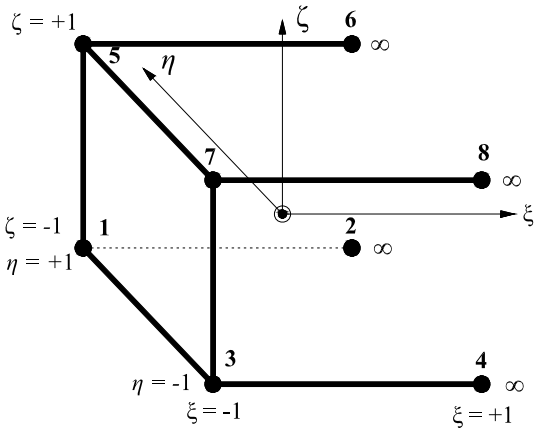

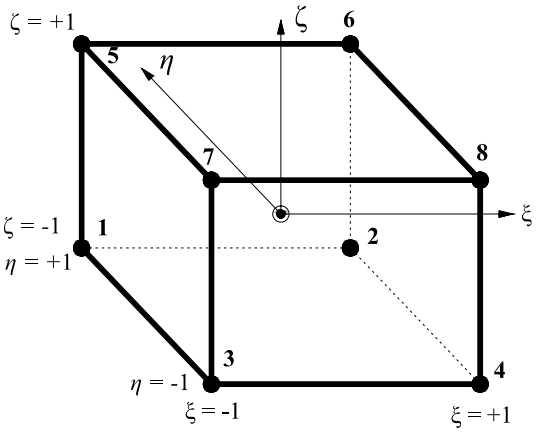

Coordinate Mapping

$$\{x\} = [M_i]\{x_i\}$$

$$M_i = (G_j)(L_k)(L_z)$$

$$M_1 = \left(\frac{2}{1-\xi}\right)\frac{1}{2}(1+\eta)\,\frac{1}{2}(1-\varsigma)$$

$$M_3 = \left(\frac{2}{1-\xi}\right)\frac{1}{2}(1-\eta)\,\frac{1}{2}(1-\varsigma)$$

$$M_5 = \left(\frac{2}{1-\xi}\right)\frac{1}{2}(1+\eta)\,\frac{1}{2}(1+\varsigma)$$

$$M_7 = \left(\frac{2}{1-\xi}\right)\frac{1}{2}(1-\eta)\,\frac{1}{2}(1+\varsigma)$$

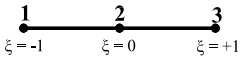

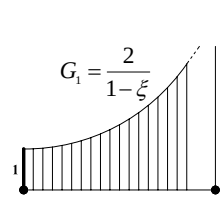

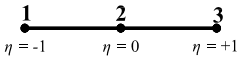

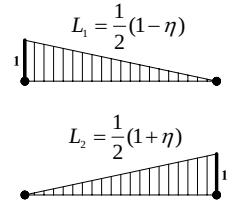

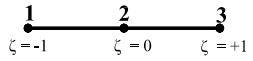

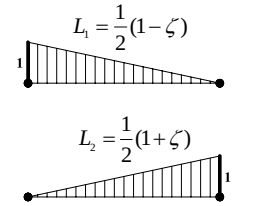

Table 6.2 (Contd)

Mapped, 3-Dimensional, 1-infinite direction, 8-node, Infinite Element

(contd)

Field Variable Mapping	**M3D-1I/C4-F8**

$$\{u\} = [N_i]\{d_i\}$$

$$N_i = \left(L_{j\xi}\right)\left(L_{k\eta}\right)\left(L_{z\varsigma}\right)$$

$$N_1 = \frac{1}{2}(1-\xi)\,\frac{1}{2}(1+\eta)\,\frac{1}{2}(1-\varsigma)$$

$$N_2 = \frac{1}{2}(1+\xi)\,\frac{1}{2}(1+\eta)\,\frac{1}{2}(1-\varsigma)$$

$$N_3 = \frac{1}{2}(1-\xi)\,\frac{1}{2}(1-\eta)\,\frac{1}{2}(1-\varsigma)$$

$$N_4 = \frac{1}{2}(1+\xi)\,\frac{1}{2}(1-\eta)\,\frac{1}{2}(1-\varsigma)$$

$$N_5 = \frac{1}{2}(1-\xi)\,\frac{1}{2}(1+\eta)\,\frac{1}{2}(1+\varsigma)$$

$$N_6 = \frac{1}{2}(1+\xi)\,\frac{1}{2}(1+\eta)\,\frac{1}{2}(1+\varsigma)$$

$$N_7 = \frac{1}{2}(1-\xi)\,\frac{1}{2}(1-\eta)\,\frac{1}{2}(1+\varsigma)$$

$$N_8 = \frac{1}{2}(1+\xi)\,\frac{1}{2}(1-\eta)\,\frac{1}{2}(1+\varsigma)$$

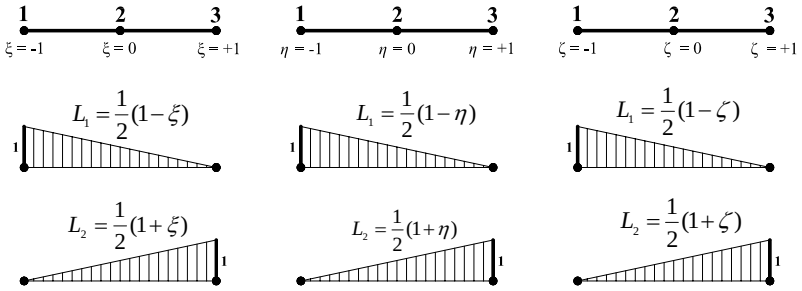

Table 6.3. Mapped, 3-Dimensional, 1-infinite direction, 10-node, infinite element

Mapped, 3-Dimensional, 1-infinite direction, 10-node, Infinite Element

Geometrical Configuration	**M3D-1I/C10-F6**

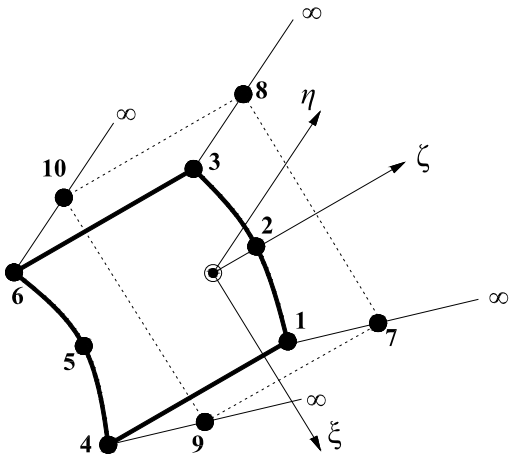

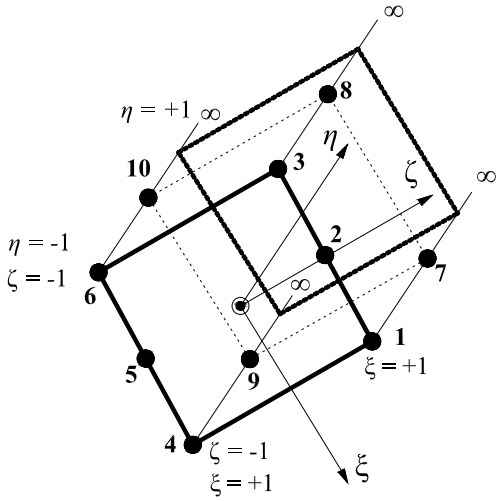

Coordinate Mapping *(serendipity)*

$$\{x\} = [M_i]\{x_i\}$$

$$M_i = (L_j)(G_k)(L_z)$$

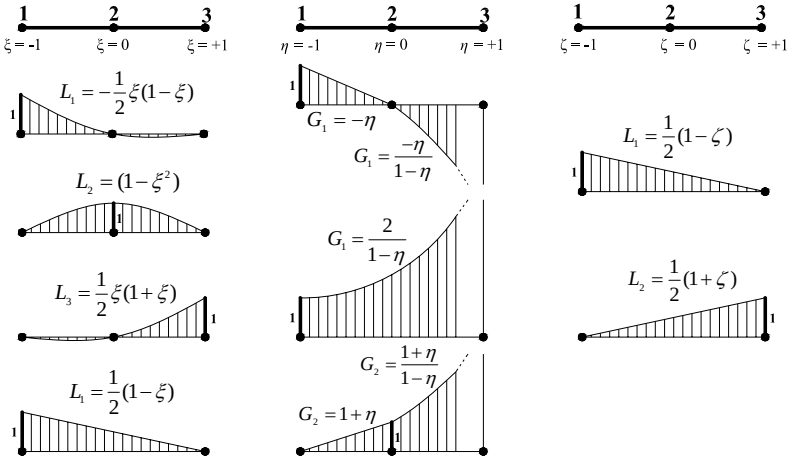

Table 6.3 (Contd)

Mapped, 2-Dimensional, 1-infinite direction, 8-node, Infinite Element
(contd)

Field Variable Mapping	**M3D-1I/C10-F6**

$$\{u\} = [N_i]\{d_i\}$$

$$N_i = \left(L_{j\xi}\right) F\left(\frac{r_1}{r}\right)\left(L_{k\zeta}\right)$$

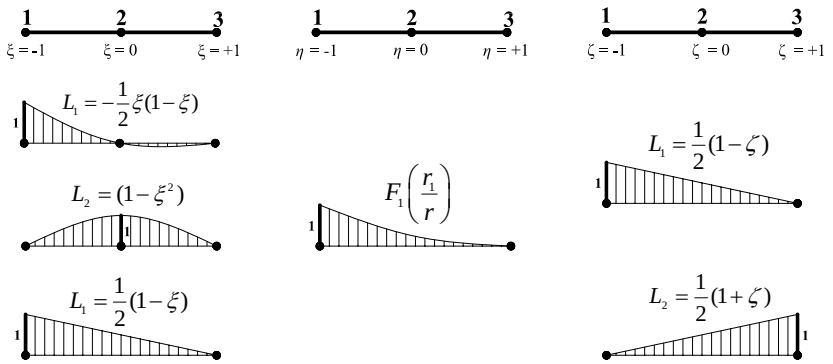

Table 6.4. Mapped, 3-Dimensional, 1-infinite direction, 8-node, infinite element

Mapped, 3-Dimensional, 1-infinite direction, 8-node, Infinite Element

Geometrical Configuration	**M3D-1I/C4-F8**

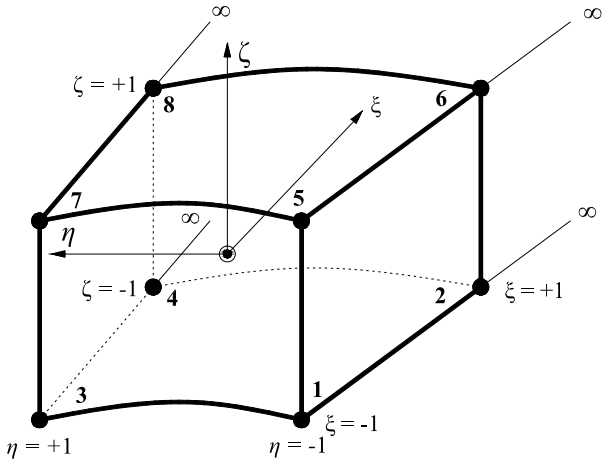

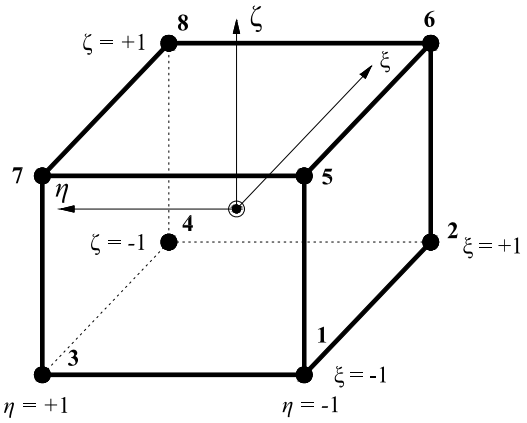

Coordinate Mapping

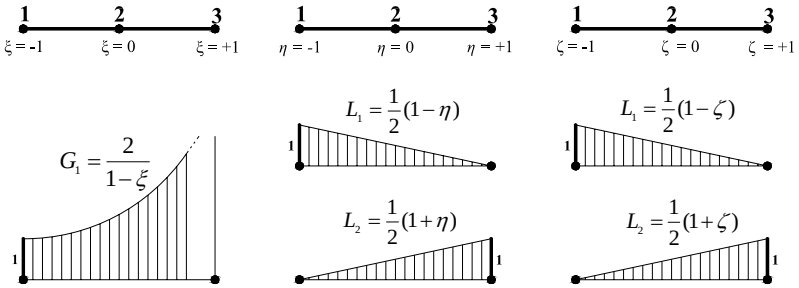

$$\{x\} = \begin{bmatrix} L_{1\eta}L_{1\xi}G_0 & L_{1\eta}L_{1\xi}G_2 & L_{2\eta}L_{1\xi}G_0 & L_{2\eta}L_{1\xi}G_2 & L_{2\eta}L_{2\xi}G_0 & L_{2\eta}L_{2\xi}G_2 & L_{1\eta}L_{2\xi}G_0 & L_{1\eta}L_{2\xi}G_2 \end{bmatrix} \begin{Bmatrix} 2x_1 - x_2 \\ x_2 \\ 2x_3 - x_4 \\ x_4 \\ 2x_7 - x_8 \\ x_8 \\ 2x_5 - x_6 \\ x_6 \end{Bmatrix}$$

$\{y\}$ and $\{z\}$ can be obtained similarly

Table 6.4 (Contd)

Mapped, 3-Dimensional, 1-infinite direction, 8-node, Infinite Element *(contd)*

Field Variable Mapping	**M3D-1I/C4-F8**
$\{u\} = [N_i]\{d_i\}$	
$N_i = (L_{j\xi})(L_{k\eta})(L_{z\varsigma})$	
$N_1 = \frac{1}{2}(1-\xi)\frac{1}{2}(1+\eta)\frac{1}{2}(1-\varsigma)$	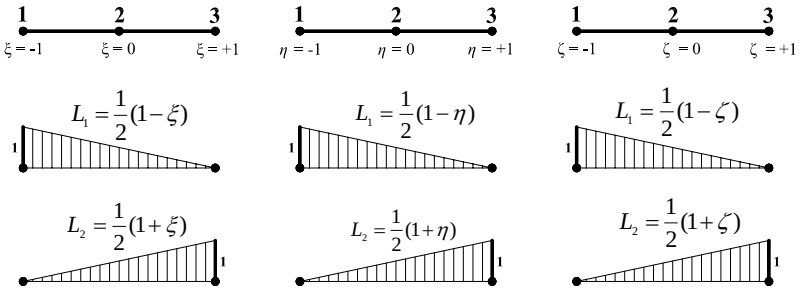
$N_2 = \frac{1}{2}(1+\xi)\frac{1}{2}(1+\eta)\frac{1}{2}(1-\varsigma)$	
$N_3 = \frac{1}{2}(1-\xi)\frac{1}{2}(1-\eta)\frac{1}{2}(1-\varsigma)$	
$N_4 = \frac{1}{2}(1+\xi)\frac{1}{2}(1-\eta)\frac{1}{2}(1-\varsigma)$	
$N_5 = \frac{1}{2}(1-\xi)\frac{1}{2}(1+\eta)\frac{1}{2}(1+\varsigma)$	
$N_6 = \frac{1}{2}(1+\xi)\frac{1}{2}(1+\eta)\frac{1}{2}(1+\varsigma)$	
$N_7 = \frac{1}{2}(1-\xi)\frac{1}{2}(1-\eta)\frac{1}{2}(1+\varsigma)$	
$N_8 = \frac{1}{2}(1+\xi)\frac{1}{2}(1-\eta)\frac{1}{2}(1+\varsigma)$	

Table 6.5. Mapped, 3-Dimensional, 2-infinite direction, 6-node, infinite element

Mapped, 3-Dimensional, 2-infinite direction, 6-node, Infinite Element

Geometrical Configuration	**M3D-2I/C2-F8**

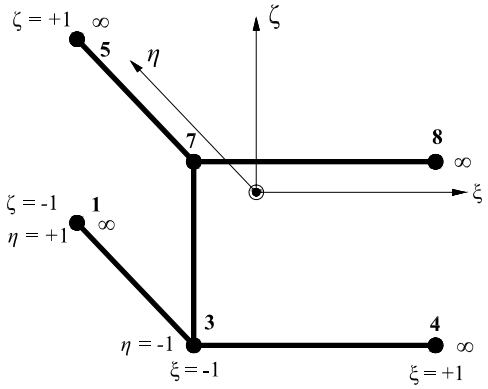

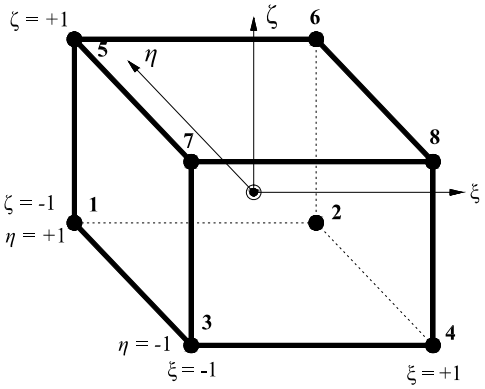

Coordinate Mapping

$$\{x\} = [M_i]\{x_i\}$$

$$M_i = (G_j)(G_k)(L_z)$$

$$M_3 = \left(\frac{2}{1-\xi}\right)\left(\frac{2}{1-\eta}\right)\frac{1}{2}(1-\varsigma)$$

$$M_7 = \left(\frac{2}{1-\xi}\right)\left(\frac{2}{1-\eta}\right)\frac{1}{2}(1+\varsigma)$$

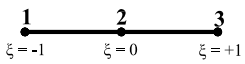

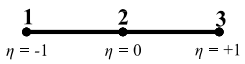

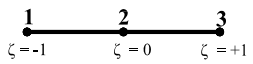

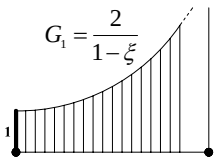

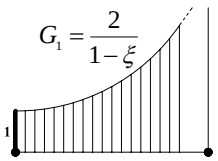

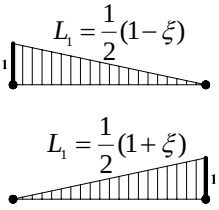

Table 6.5 (Contd)

Mapped, 3-Dimensional, 2-infinite direction, 6-node, Infinite Element
(contd)

Field Variable Mapping	**M3D-2I/C2-F8**

$$\{u\} = [N_i]\{d_i\}$$

$$N_i = (L_{j\xi})(L_{k\eta})(L_{z\varsigma})$$

$$N_1 = \frac{1}{2}(1-\xi)\frac{1}{2}(1+\eta)\frac{1}{2}(1-\varsigma)$$

$$N_2 = \frac{1}{2}(1+\xi)\frac{1}{2}(1+\eta)\frac{1}{2}(1-\varsigma)$$

$$N_3 = \frac{1}{2}(1-\xi)\frac{1}{2}(1-\eta)\frac{1}{2}(1-\varsigma)$$

$$N_4 = \frac{1}{2}(1+\xi)\frac{1}{2}(1-\eta)\frac{1}{2}(1-\varsigma)$$

$$N_5 = \frac{1}{2}(1-\xi)\frac{1}{2}(1+\eta)\frac{1}{2}(1+\varsigma)$$

$$N_6 = \frac{1}{2}(1+\xi)\frac{1}{2}(1+\eta)\frac{1}{2}(1+\varsigma)$$

$$N_7 = \frac{1}{2}(1-\xi)\frac{1}{2}(1-\eta)\frac{1}{2}(1+\varsigma)$$

$$N_8 = \frac{1}{2}(1+\xi)\frac{1}{2}(1-\eta)\frac{1}{2}(1+\varsigma)$$

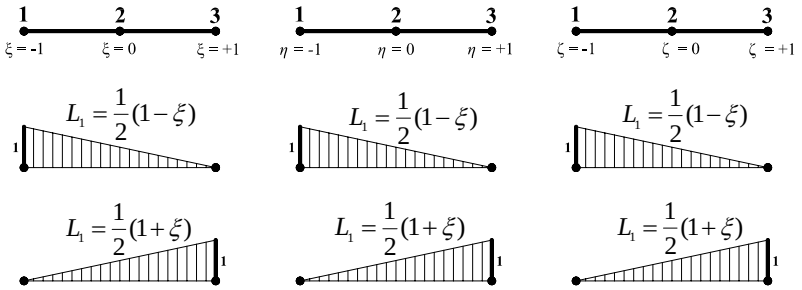

Table 6.6. Mapped, 3-Dimensional, 3-infinite direction, 4-node, infinite element

Mapped, 3-Dimensional, 3-infinite direction, 4-node, Infinite Element

Geometrical Configuration	**M3D-3I/C1-F8**

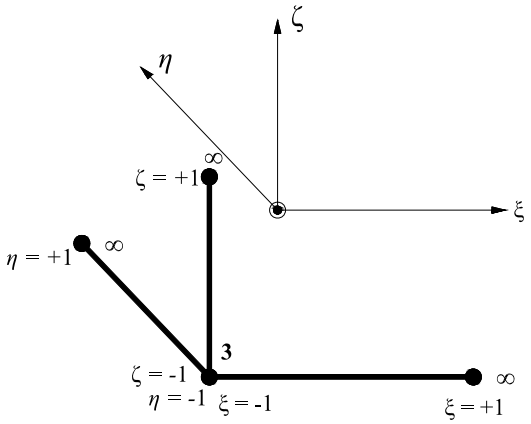

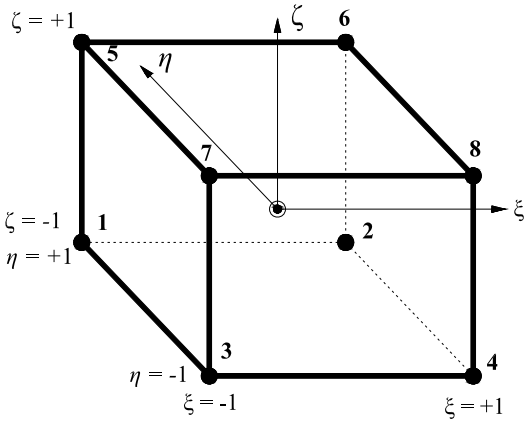

Coordinate Mapping

$$\{x\} = [M_i]\{x_i\}$$

$$M_i = (G_j)(G_k)(G_z)$$

$$M_3 = \left(\frac{2}{1-\xi}\right)\left(\frac{2}{1-\xi}\right)\left(\frac{2}{1-\xi}\right)$$

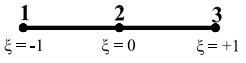

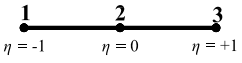

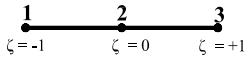

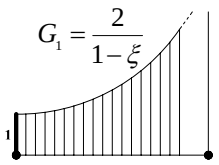

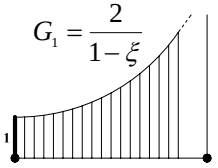

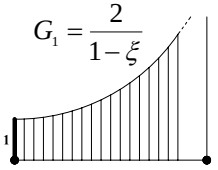

Table 6.6 (Contd)

Mapped, 3-Dimensional, 3-infinite direction, 4-node, Infinite Element
(contd)

Field Variable Mapping	**M3D-3I/C1-F8**

$$\{u\} = [N_i]\{d_i\}$$

$$N_i = \left(L_{j\xi}\right)\left(L_{k\eta}\right)\left(L_{z\varsigma}\right)$$

$$N_1 = \frac{1}{2}(1-\xi)\,\frac{1}{2}(1+\eta)\,\frac{1}{2}(1-\varsigma)$$

$$N_2 = \frac{1}{2}(1+\xi)\,\frac{1}{2}(1+\eta)\,\frac{1}{2}(1-\varsigma)$$

$$N_3 = \frac{1}{2}(1-\xi)\,\frac{1}{2}(1-\eta)\,\frac{1}{2}(1-\varsigma)$$

$$N_4 = \frac{1}{2}(1+\xi)\,\frac{1}{2}(1-\eta)\,\frac{1}{2}(1-\varsigma)$$

$$N_5 = \frac{1}{2}(1-\xi)\,\frac{1}{2}(1+\eta)\,\frac{1}{2}(1+\varsigma)$$

$$N_6 = \frac{1}{2}(1+\xi)\,\frac{1}{2}(1+\eta)\,\frac{1}{2}(1+\varsigma)$$

$$N_7 = \frac{1}{2}(1-\xi)\,\frac{1}{2}(1-\eta)\,\frac{1}{2}(1+\varsigma)$$

$$N_8 = \frac{1}{2}(1+\xi)\,\frac{1}{2}(1-\eta)\,\frac{1}{2}(1+\varsigma)$$

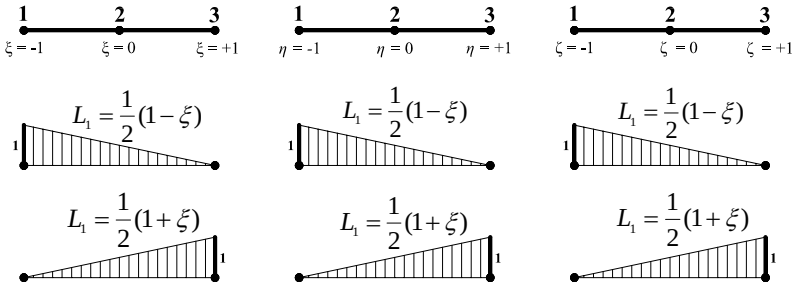

6.3. A Dynamic Infinite Element for 3-D Infinite Domain Wave Problems

6.3.1. Introduction

P-waves, S-waves and R-waves in the foundation can be simulated simultaneously in the present infinite element domain. The good accuracy is obtained using the present infinite element and finite element coupling model to simulate foundation wave problems has been proven by comparing the current numerical results with previous analytical results.

The simulation of the infinite medium in the numerical method is a very important topic in dynamic soil-structure interaction problems. This topic arose from numerous practical problems such as the numerical simulation of building structure foundations, offshore structure foundations, dam foundations, nuclear power station foundations and so forth. The study of this topic becomes more important when the structure is large and the effects of earthquakes are considered. Due to the importance of the problem, much work has been done by researchers in the past. The general method for treating this problem is to divide the infinite medium into the near field, which includes the geometric irregularity as well as the non-homogeneity of the foundation, and the far field, which is simplified as an isotropic homogeneous elastic medium. The near field is modeled using finite elements and the far field is treated by adding some special artificial boundaries or connecting some special elements on the truncated boundary, which is a part of the representation of the finite elements. It has been proven that these special artificial boundaries work well for the wave radiation problems in which the vibration source acts on the interior region of the near field. However, for seismic structural analysis, which, in fact, is a typical wave scattering problem in the near field, these artificial boundaries are not satisfactory due to the earthquake wave which is incident from the far field. In such a case, some special elements known as infinite elements and boundary elements can still handle this problem even when an incident earthquake wave is presented. Although the boundary element method is a very effective way to simulate wave scattering problems in the homogeneous medium due to the great reduction in the number of degrees of freedom of the system, the infinite element is better for simulating wave scattering problems in the non-homogeneous

medium due to the banded and symmetrical nature of the global stiffness and mass matrices (Zhao and Valliappan, 1993).

The concept of infinite elements was presented by Bettess and Ungless in the 1970s. Further work has been done by some other authors to apply the infinite elements to the solution of static problems in engineering practice. The fundamental idea to construct a static infinite element is to derive a special element displacement shape function, which is the product of the Lagrange interpolation function and the so-called decay function, or to use some special mapping techniques to map the infinite element into a finite one. The same ideas have also been employed to develop the dynamic infinite elements. However, owing to the quite complicated mechanism of wave propagation in the infinite medium, the decay function in the static infinite element was replaced by the wave propagation function in its dynamic counterparts. For the dynamic infinite elements used in solid media, Chow and Smith (1981), Medina (1983) as well as Zhao et al. (1987) have presented the corresponding element models which differ from the selection of the wave propagation function in the dynamic infinite elements.

Different type of waves such as R-wave, SH-wave, SV-wave and P wave must be separately considered in the analysis. That is to say, for a given incident earthquake wave, one must separate this wave into R-wave, SH-wave, SV-wave and P-wave components and then use the wave number of each wave component to calculate the infinite element stiffness and mass matrices. Consequently, the stiffness and the mass matrices for an infinite element need to be calculated at least four times since the previous 3-D dynamic infinite element can exactly represent only one wave number each time.

6.3.2. Derivation of 3-D Infinite Element

Based on the above considerations, a 3-D dynamic infinite element is discussed below. Since the wave numbers of the R-wave, SH-wave, SV-wave and P-wave are simultaneously used in the present infinite element, it is more economical to use this element to simulate the earthquake wave propagation mechanism in the infinite foundation. In addition, due to the use of a mapping technique, it is feasible to use this element to model arch-dam-foundations in a rectangular co-ordinate system.

Assuming that the foundation is subjected to harmonic loading and the medium of the natural foundation exhibits hysteresis damping, the governing equation of the wave motion of the system can be written as

$$\begin{aligned} G^*\nabla^2 u + (\lambda^* + G^*)\left(\frac{\partial^2 u}{\partial x^2} + \frac{\partial^2 v}{\partial x\,\partial y} + \frac{\partial^2 w}{\partial x\,\partial z}\right) + f_x &= \rho\ddot{u} \\ G^*\nabla^2 v + (\lambda^* + G^*)\left(\frac{\partial^2 u}{\partial x\,\partial y} + \frac{\partial^2 v}{\partial y^2} + \frac{\partial^2 w}{\partial y\,\partial z}\right) + f_y &= \rho\ddot{v} \\ G^*\nabla^2 w + (\lambda^* + G^*)\left(\frac{\partial^2 u}{\partial x\,\partial z} + \frac{\partial^2 v}{\partial y\,\partial z} + \frac{\partial^2 w}{\partial z^2}\right) + f_z &= \rho\ddot{w} \end{aligned} \tag{6.20}$$

$$G^* = G(1 + i\eta_d) \tag{6.21}$$

$$\lambda^* = \lambda(1 + i\eta_d) \tag{6.22}$$

where, G is the shear modulus, λ is the Lame constant, η_d is the hysteresis damping coefficient of the medium, f_x, f_y, f_z are the unit body forces in x, y, z directions, respectively, ρ is the material density and ∇^2 is the second-order 3-D Laplace operator. For instance,

$$\nabla^2 u = \frac{\partial^2 u}{\partial x^2} + \frac{\partial^2 u}{\partial y^2} + \frac{\partial^2 u}{\partial z^2} \tag{6.23}$$

Using the Euler's theorem and ignoring body forces in equation (1.1), the discretized equation of motion of the system can be derived as

$$-\omega^2[M]\{d\} + (1 + i\eta_d)[K]\{d\} = \{F_0\} \tag{6.24}$$

where $\{d\}$ is the unknown nodal displacement vector, ω is the exciting circular frequency, $[M]$ and $[K]$ are global mass and stiffness matrices of the system, respectively, $\{F_0\}$ is the amplitude vector of the applied harmonic load. By Code Number Technique, (Tezcan, 1963), $[M]$ and $[K]$ matrices as well as $\{F_0\}$ can be assembled from the element submatrices and subvectors which have the following form:

$$[M]^e = \iiint_V [N]^T \rho [N] dV$$

$$[K]^e = \iiint_V [B]^T [D][B] dV \tag{6.25}$$

$$\{F_0\} = \iint_A [N]^T \{\bar{x}_0\} dA + [N]^T \{\bar{P}_0\}$$

where *V* and *A* express the volume and area of the element, $\{\bar{x}_0\}$ and $\{\bar{P}_0\}$ are amplitude vectors of boundary traction and concentrated loads, respectively, $[D]$ is the element constitutive matrix, $[B]$ and $[N]$ are the strain matrix and the shape function matrix of the element. It is noted that equation (1.6) holds for both finite and infinite elements. Since the derivation of a 3-D solid finite element is well known, only the necessary formulations of a 3-D dynamic infinite element are given here.

6.3.3. A Seismic 3-D Infinite Element

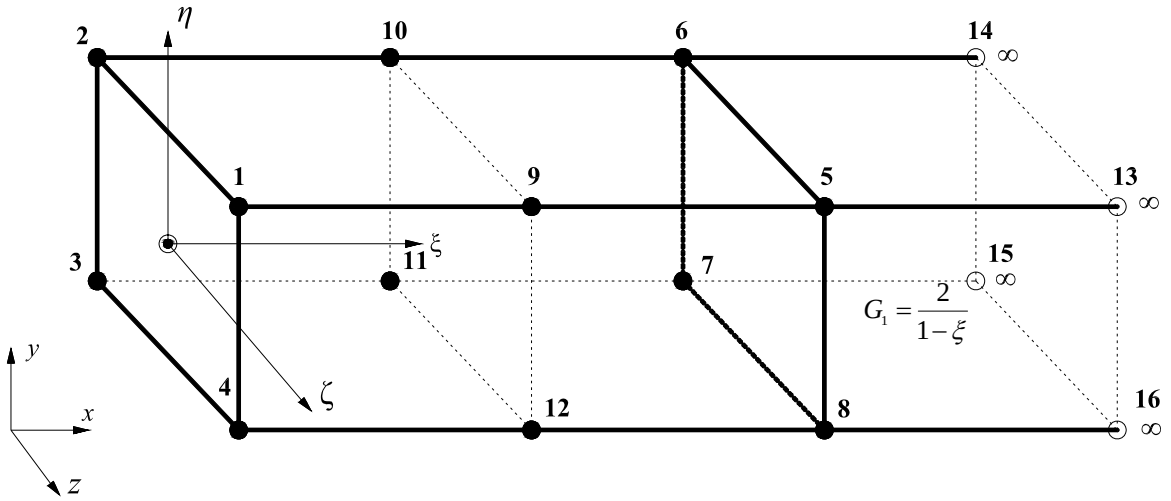

Figure 6.5. A 3-D dynamic infinite element

For the 3-D dynamic infinite element shown in Figure 6.5, since the sides of the element in the infinite direction can be represented by straight lines, only eight nodes are sufficient to describe exactly the geometry of the seismic infinite element in the global co-ordinate system. Therefore, the mapping relationship between the global co-ordinate system and the local co-ordinate system for this element can be defined as

$$\begin{Bmatrix} x \\ y \\ z \end{Bmatrix} = \begin{bmatrix} x_1 & x_2 & . & . & x_8 \\ y_1 & y_2 & . & . & y_8 \\ z_1 & z_2 & . & . & z_8 \end{bmatrix} \begin{Bmatrix} M_1 \\ \vdots \\ M_8 \end{Bmatrix} \tag{6.26}$$

where M_i is the mapping function of the element and it can be expressed as

$$\begin{aligned} M_1 &= \frac{1}{4}(1-\xi)(1+\eta)(1+\zeta) \\ M_2 &= \frac{1}{4}(1-\xi)(1+\eta)(1-\zeta) \\ M_3 &= \frac{1}{4}(1-\xi)(1-\eta)(1-\zeta) \\ M_4 &= \frac{1}{4}(1-\xi)(1-\eta)(1+\zeta) \end{aligned} \tag{6.27}$$

$$M_5 = \frac{1}{4}\xi(1+\eta)(1+\zeta)$$

$$M_6 = \frac{1}{4}\xi(1+\eta)(1-\zeta)$$

$$M_7 = \frac{1}{4}\xi(1-\eta)(1-\zeta)$$

$$M_8 = \frac{1}{4}\xi(1-\eta)(1+\zeta)$$

It is noted that since the mapping functions of the element are different from the displacement functions of the element, the present infinite element is not an isoparametric element. It is a subparametric element.

Considering the compatibility condition of displacement on the connected interface between the finite and infinite element, the displacement field for this 3-D dynamic infinite element can be described as

$$\begin{Bmatrix} u \\ v \\ w \end{Bmatrix} = \begin{bmatrix} u_1 & u_2 & . & . & u_{12} \\ v_1 & v_2 & . & . & v_{12} \\ w_1 & w_2 & . & . & w_{12} \end{bmatrix} \begin{Bmatrix} N_1 \\ \vdots \\ N_{12} \end{Bmatrix} \tag{6.28}$$

where $N_i \ (i = 1, 2, ..., 12)$ are displacement shape functions of the element and can be expressed as

$$N_1 = N_5 = N_9 = P_i(\xi)\left[\frac{1}{4}(1+\eta)(1+\zeta)\right]$$

$$N_2 = N_6 = N_{10} = P_i(\xi)\left[\frac{1}{4}(1+\eta)(1-\zeta)\right]$$

$$N_3 = N_7 = N_{11} = P_i(\xi)\left[\frac{1}{4}(1-\eta)(1-\zeta)\right] \tag{6.29}$$

$$N_4 = N_8 = N_{12} = P_i(\xi)\left[\frac{1}{4}(1-\eta)(1+\zeta)\right]$$

$$P(\xi) = e^{-\alpha\xi}\left(c_1 e^{-i\beta_1\xi} + c_2 e^{-i\beta_2\xi} + c_3 e^{-i\beta_3\xi}\right) \tag{6.30}$$

In which α is a nominal decay coefficient, which is used to express the attenuation of wave amplitude due to the dissipation of wave energy in the material and the geometric divergence of the medium, $\beta_i\,(i=1,2,3)$ are three nominal wave numbers in correspondence to the R-wave, S-wave and P-wave in 3-D domains and these nominal wave numbers are used to express the phase characteristics of the wave during propagation in the medium, $c_i\,(i=1,2,3)$ are the constants to be determined to match the displacement field of the domain.

In order to determine the constants c_1, c_2 and c_3, equation (6.28) should be used. Letting the nodal displacements in any infinite side of the element in the ξ direction equal the displacements expressed by equation (6.28), these constants can be determined. For instance, taking account of one side of the element with node 1, 5 and 9 (see Figure 6.5) the following relationships exist:

$$\begin{Bmatrix} u_1 \\ u_2 \\ u_3 \end{Bmatrix} = \begin{bmatrix} 1 & 1 & 1 \\ -e^{-(1/2)(\alpha+i\beta_1)} & -e^{-(1/2)(\alpha+i\beta_2)} & -e^{-(1/2)(\alpha+i\beta_3)} \\ e^{-(\alpha+i\beta_1)} & e^{-(\alpha+i\beta_2)} & e^{-(\alpha+i\beta_3)} \end{bmatrix} \begin{Bmatrix} c_1 \\ c_2 \\ c_3 \end{Bmatrix} = [C] \begin{Bmatrix} c_1 \\ c_2 \\ c_3 \end{Bmatrix} \tag{6.31}$$

and therefore,

$$\begin{Bmatrix} c_1 \\ c_2 \\ c_3 \end{Bmatrix} = [E] \begin{Bmatrix} u_1 \\ u_5 \\ u_9 \end{Bmatrix} \tag{6.32}$$

where $[E]$ is the inverse matrix of $[C]$. If equation (6.29) is considered $P_i(\xi)\,(i=1,\ 2,...,12)$ can be further expressed as

$$P_i(\xi) = E_{11} e^{-(\alpha+i\beta_1)\xi} + E_{21} e^{-(\alpha+i\beta_2)\xi} + E_{31} e^{-(\alpha+i\beta_3)\xi}\ (i=1,2,3,4)$$

$$P_i(\xi) = E_{12}e^{-(\alpha+i\beta_1)\xi} + E_{22}e^{-(\alpha+i\beta_2)\xi} + E_{32}e^{-(\alpha+i\beta_3)\xi} \quad (i = 5,6,7,8) \tag{6.33}$$

$$P_i(\xi) = E_{13}e^{-(\alpha+i\beta_1)\xi} + E_{23}e^{-(\alpha+i\beta_2)\xi} + E_{33}e^{-(\alpha+i\beta_3)\xi} \quad (i = 9,10,11,12)$$

where

$$\begin{aligned} E_{11} &= \frac{1}{\Delta}e^{-(1/2)(3\alpha+i\beta_2+i\beta_3)}\left(e^{-(i/2)\beta_3} - e^{-(i/2)\beta_2}\right) \\ E_{21} &= \frac{1}{\Delta}e^{-(1/2)(3\alpha+i\beta_1+i\beta_3)}\left(e^{-(i/2)\beta_1} - e^{-(i/2)\beta_3}\right) \\ E_{31} &= \frac{1}{\Delta}e^{-(1/2)(3\alpha+i\beta_1+i\beta_2)}\left(e^{-(i/2)\beta_2} - e^{-(i/2)\beta_1}\right) \end{aligned} \tag{6.34}$$

$$\begin{aligned} E_{12} &= \frac{1}{\Delta}e^{-\alpha}\left(e^{-i\beta_2} - e^{-i\beta_3}\right) \\ E_{22} &= \frac{1}{\Delta}e^{-\alpha}\left(e^{-i\beta_3} - e^{-i\beta_1}\right) \\ E_{32} &= \frac{1}{\Delta}e^{-\alpha}\left(e^{-i\beta_1} - e^{-i\beta_2}\right) \end{aligned} \tag{6.35}$$

$$\begin{aligned} E_{13} &= \frac{1}{\Delta}e^{-(1/2)\alpha}\left(e^{-(i/2)\beta_3} - e^{-(i/2)\beta_2}\right) \\ E_{23} &= \frac{1}{\Delta}e^{-(1/2)\alpha}\left(e^{-(i/2)\beta_1} - e^{-(i/2)\beta_3}\right) \\ E_{33} &= \frac{1}{\Delta}e^{-(1/2)\alpha}\left(e^{-(i/2)\beta_2} - e^{-(i/2)\beta_1}\right) \end{aligned} \tag{6.36}$$

where the Δ =the determinant value of E matrix

$$\begin{aligned} \Delta = e^{-(3/2)\alpha}\Big[& e^{-(i/2)(\beta_2+\beta_3)}\left(e^{-(i/2)\beta_3} - e^{-(i/2)\beta_2}\right) + e^{-(i/2)(\beta_1+\beta_2)}\left(e^{-(i/2)\beta_2} - e^{-(i/2)\beta_1}\right) \\ & + e^{-(i/2)(\beta_1+\beta_3)}\left(e^{-(i/2)\beta_1} - e^{-(i/2)\beta_3}\right)\Big] \end{aligned} \tag{6.37}$$

It is noted that a sufficient condition for the existence of $P_i(\xi)\,(i=1,2,...,12)$ in the infinite element is that β_1, β_2 and β_3 are three different constants. This can be easily satisfied in the infinite-foundation wave problems since the R-wave, S-wave and P-wave have three different wave numbers.

Using the element described above and equation (6.25), it is straightforward to get the mass matrix for the 3-D dynamic infinite element as follows

$$[M]^e = \int_0^{\infty}\int_{-1}^{1}\int_{-1}^{1} [N]^T \rho [N] |J| \, d\xi d\eta d\zeta$$

$$[K]^e = \int_0^{\infty}\int_{-1}^{1}\int_{-1}^{1} [B]^T [D][B] |J| \, d\xi d\eta d\zeta \qquad (6.38)$$

where $|J|$ is the Jacobian determinant which can be determined from the mapping relationship of the element in equations (6.26) and (6.27). Substituting equations (6.27) and (6.29) and related expressions into equation (6.38), the following generalized integral will be encountered in the evaluation of the mass and stiffness matrices of the infinite element:

$$I = \int_0^{\infty} F(\xi) e^{-(2\alpha + i\beta_j + i\beta_k)\xi} d\xi \quad (j=1,2,3,\ k=1,2,3) \qquad (6.39)$$

This generalized integral can be calculated using numerical integration technique.

Consider the set of natural co-ordinates ξ, η, ζ and a corresponding set of global co-ordinates *x, y, z*. By the usual rules of partial differentiation, the ξ derivative can be written as

$$\frac{\partial N_i}{\partial \xi} = \frac{\partial N_i}{\partial x}\frac{\partial x}{\partial \xi} + \frac{\partial N_i}{\partial y}\frac{\partial y}{\partial \xi} + \frac{\partial N_i}{\partial z}\frac{\partial z}{\partial \xi} \qquad (6.40)$$

Performing the same differentiation with respect to the other two co-ordinates and writing in the matrix form:

$$\begin{Bmatrix} \frac{\partial N_i}{\partial \xi} \\ \frac{\partial N_i}{\partial \eta} \\ \frac{\partial N_i}{\partial \zeta} \end{Bmatrix} = \begin{bmatrix} \frac{\partial x}{\partial \xi} & \frac{\partial y}{\partial \xi} & \frac{\partial z}{\partial \xi} \\ \frac{\partial x}{\partial \eta} & \frac{\partial y}{\partial \eta} & \frac{\partial z}{\partial \eta} \\ \frac{\partial x}{\partial \zeta} & \frac{\partial y}{\partial \zeta} & \frac{\partial z}{\partial \zeta} \end{bmatrix} \begin{Bmatrix} \frac{\partial N_i}{\partial x} \\ \frac{\partial N_i}{\partial y} \\ \frac{\partial N_i}{\partial z} \end{Bmatrix} = [J] \begin{Bmatrix} \frac{\partial N_i}{\partial x} \\ \frac{\partial N_i}{\partial y} \\ \frac{\partial N_i}{\partial z} \end{Bmatrix} \tag{6.41}$$

In the above, the left-hand side can be evaluated as the functions N_i are specified in natural co-ordinates. Further as *x*, *y*, *z* are explicitly given, the matrix $[J]$, can be found explicitly in terms of the natural co-ordinates. This matrix is known as the Jacobian matrix.

7. CASE STUDIES

As it was mentioned earlier in Chapter 2, a difficulty is often encountered in finite element analysis in the treatment of an unbounded domain, for which the use of infinite elements offers the most powerful and effective solutions. In the process of developing the stiffness properties of infinite elements, the conventional finite elements are modified to contain some nodes and element boundaries, which model the domain stretching to infinity.

7.1. Boussinesq Problem

In order to compare the predictive capabilities of infinite elements with closed form solutions of the Boussinesq problem, axisymmetric analyses are performed due to the rotational symmetry. A slice of semi-infinite medium, with one *(1)* radian central angle is considered for analysis. A sample mesh suitable for analysis is seen in Figure 7.1.

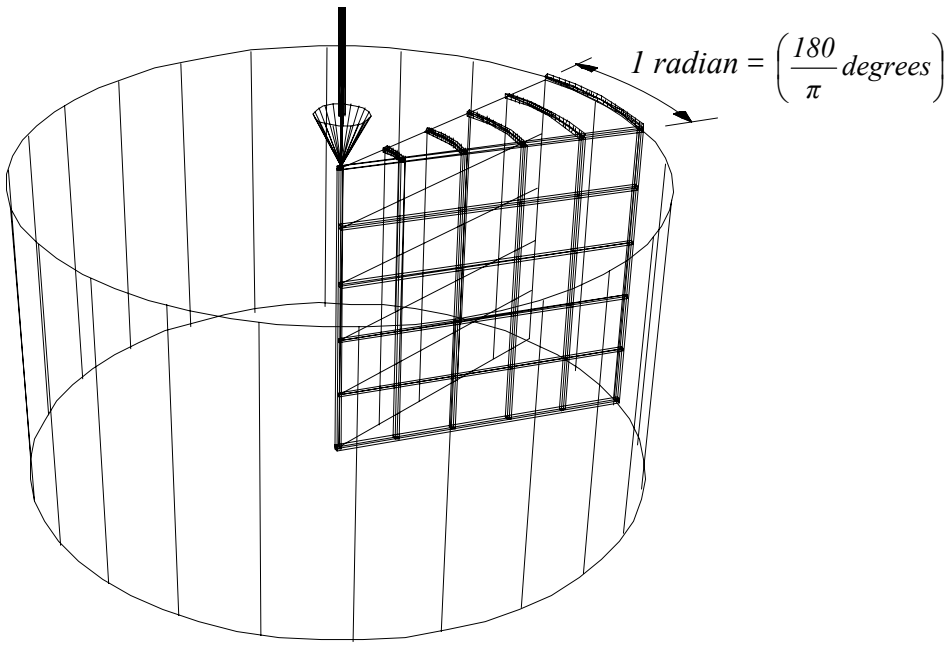

Figure 7.1. Singular load on axi-symmetric semi-infinite medium and a slice taken from it for analysis

In the Finite Element modeling of this Boussinesq problem[*], a 5 by 5 axi-symmetric mesh consisting of eight-node high order quadrilateral elements is generated as shown in Figure 7.2. The computer package program *GeoStudio SIGMA/W* (GeoStudio Analysis Reference and Tutorials, 2004) is used for this purpose. Along the axis of symmetry, coinciding with the vertical truncation boundary, a boundary condition of zero horizontal displacement is imposed throughout. The horizontal truncation boundary at the bottom edge has zero vertical displacements throughout. In fact, typical movable hinge supports are assumed all along the three mutually perpendicular boundary lines.

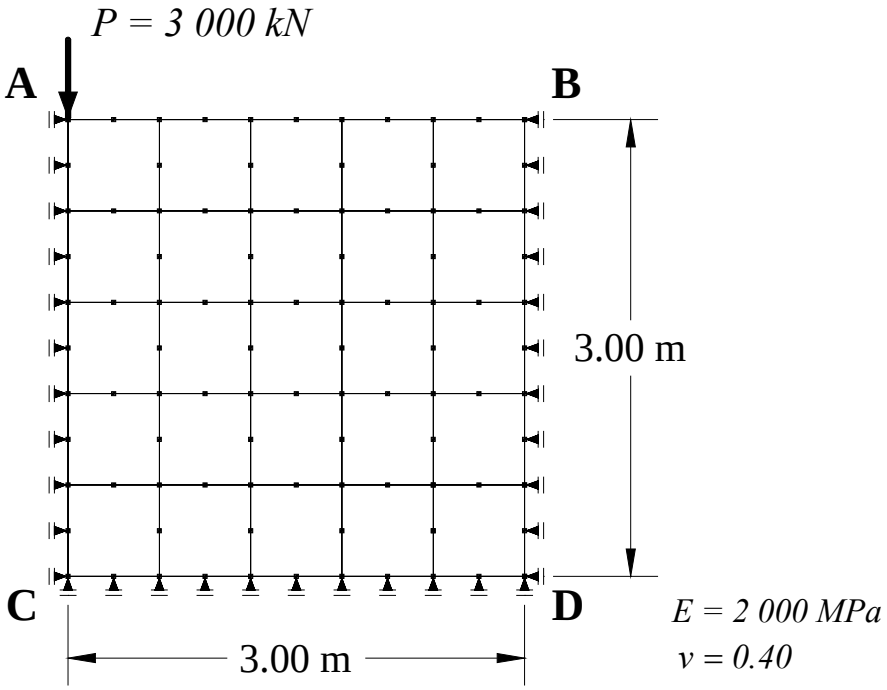

Figure 7.2. Mesh of axi-symmetric body with rigid truncation boundaries

For the purpose of introducing infinite elements at the truncation lines CD and BD, a second model is generated by attaching a corridor of eight-node high order quadrilateral infinite elements to the already existing mesh all along the two truncation boundaries CD and BD as shown in Figure 7.3. The infinite elements are indicated by an arrow head specifying a direction to infinity.

[*] A complete treatment of Boussinesq problem is given in Appendix A

The material is assumed to be linear and isotropic with Young's Modulus *E = 2 000 MPa* and Poisson's ratio *v = 0.40*. The point load acting vertically at the center of a three dimensional elastic half space is *P = 3 000 kN*.

The vertical displacements have been calculated by three distinct methods as follows:

- Finite element modeling with 5 by 5 mesh, using *GeoStudio SIGMA/W* package program;
- The exact formulations by Boussinesq (Jumikis, A. R., 1969);
- Finite element modeling with 5 by 5 mesh with infinite elements attached to the bottom and right-hand side truncation boundaries.

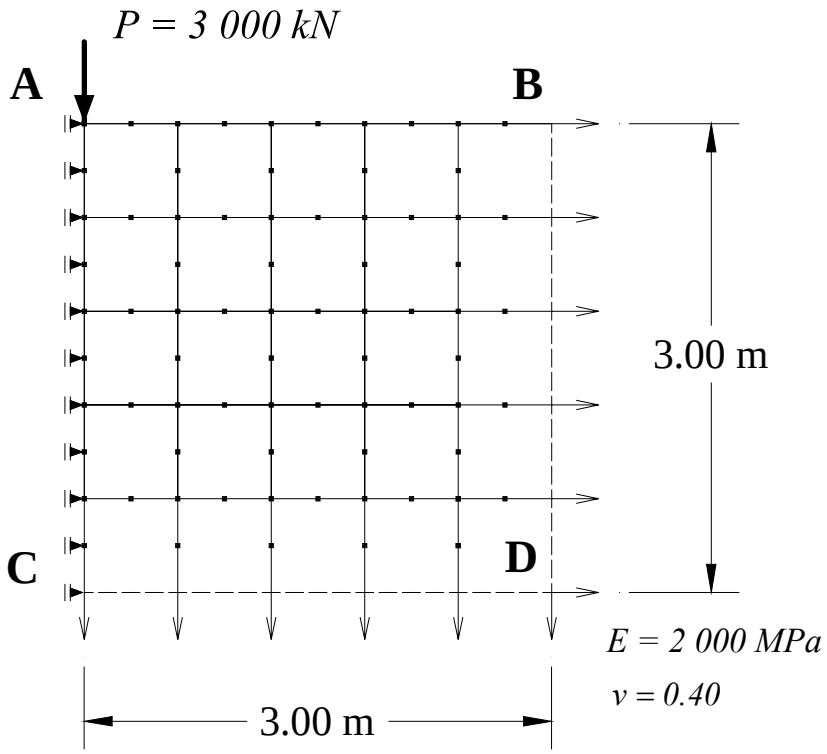

Figure 7.3. Mesh of axi-symmetric body with infinite elements along the truncation boundaries

The vertical displacements calculated by these three methods, all along the two vertical axes at r = 0 m and r = 0.6 m, and also along the horizontal line at z = 1.20 m, are given in Tables 7.1 through 7.3, respectively.

The vertical displacements calculated by these three methods are also illustrated graphically in a comparative fashion, together with the percentages of errors in each case, all along the two vertical and one horizontal lines, as described above, in Figures 7.4 through 7.9, respectively.

Table 7.1. Vertical displacements along the vertical line at r = 0

Depth*(m)*	**Displacements** *(m)* (10^{-4})		
	Finite Elements	***Theory***	***Infinite Elements***
0	55.97	N/A	58.27
0.3	31.82	24.51	34.14
0.6	12.07	12.25	14.40
0.9	6.31	8.17	8.62
1.2	3.61	6.13	5.91
1.5	2.70	4.90	4.97
1.8	1.96	4.08	4.21
2.1	1.25	3.50	3.48
2.4	0.74	3.06	2.97
2.7	0.35	2.72	2.01
3	0.00	2.45	

Table 7.2. Vertical displacements along the vertical line at r = 0.6 m

Depth*(m)*	**Displacements** *(m)* (10^{-4})		
	Finite Elements	***Theory***	***Infinite Elements***
0	5.58	6.68	7.86
0.3	5.36	6.98	7.66
0.6	3.56	6.70	5.86
0.9	3.41	5.85	5.70
1.2	2.81	4.98	5.08
1.5	2.03	4.27	4.26
1.8	1.43	3.70	3.64
2.1	1.00	3.25	3.18
2.4	0.63	2.89	2.80
2.7	0.30	2.60	1.96
3	0.00	2.36	

Table 7.3. Vertical displacements along the horizontal line at z = 1.20 m

Depth*(m)*	**Displacements** *(m)* (10^{-4})		
	Finite Elements	***Theory***	***Infinite Elements***
0	3.61	6.13	5.91
0.3	3.41	5.79	5.70
0.6	2.81	4.98	5.08
0.9	1.80	4.10	4.03
1.2	1.26	3.35	3.44
1.5	0.67	2.77	2.79
1.8	0.31	2.33	2.35
2.1	0.07	2.00	2.02
2.4	-0.07	1.74	1.79
2.7	-0.16	1.54	1.03
3	-0.18	1.38	

7.2. Evaluation of the Results of Boussinesq Problem

Superior degree of accuracy attained by the use of infinite elements is demonstrated clearly when the finite element solutions are compared with those of the exact solution. The solutions by infinite element modeling show a remarkable improvement.

For instance, the vertical displacements obtained by three different methods along the r = 0 axis are illustrated in Figure 7.4. Very good agreements exist with the exact solution when quadratic infinite elements are used. The accuracies improve with larger depths. If we examine the displacement error percentages along this vertical line at r = 0 m in Figure 7.5, it is seen that the errors increase near to the point load due to the effect of singularity of the point load.

Table 7.1 also shows that the displacement values obtained when infinite elements are employed are almost the same as those of the closed form solutions, whereas the pure finite element solutions are relatively very far from the exact theory.

When the displacements along the vertical line at r = 0.6 m and along the horizontal line at z = 1.2 m are examined as shown in Figures 7.6 and 7.8 respectively. It is clearly

seen that the infinite element solutions are in a very good agreement with those of the exact solution. Displacement error percentages given in Figure 7.7 and Figure 7.9 also confirm this conclusion. It is important to recall however that due to stress concentrations in the vicinity of the point load, the accuracy of the numerical solution even with infinite elements may differ slightly from the exact solutions.

In general, the regular finite element solutions underestimate the displacements. The situation is greatly improved however by the introduction of the infinite elements. It is thus proven that the use of infinite elements, provide a significant degree of accuracy at only very little extra computational effort.

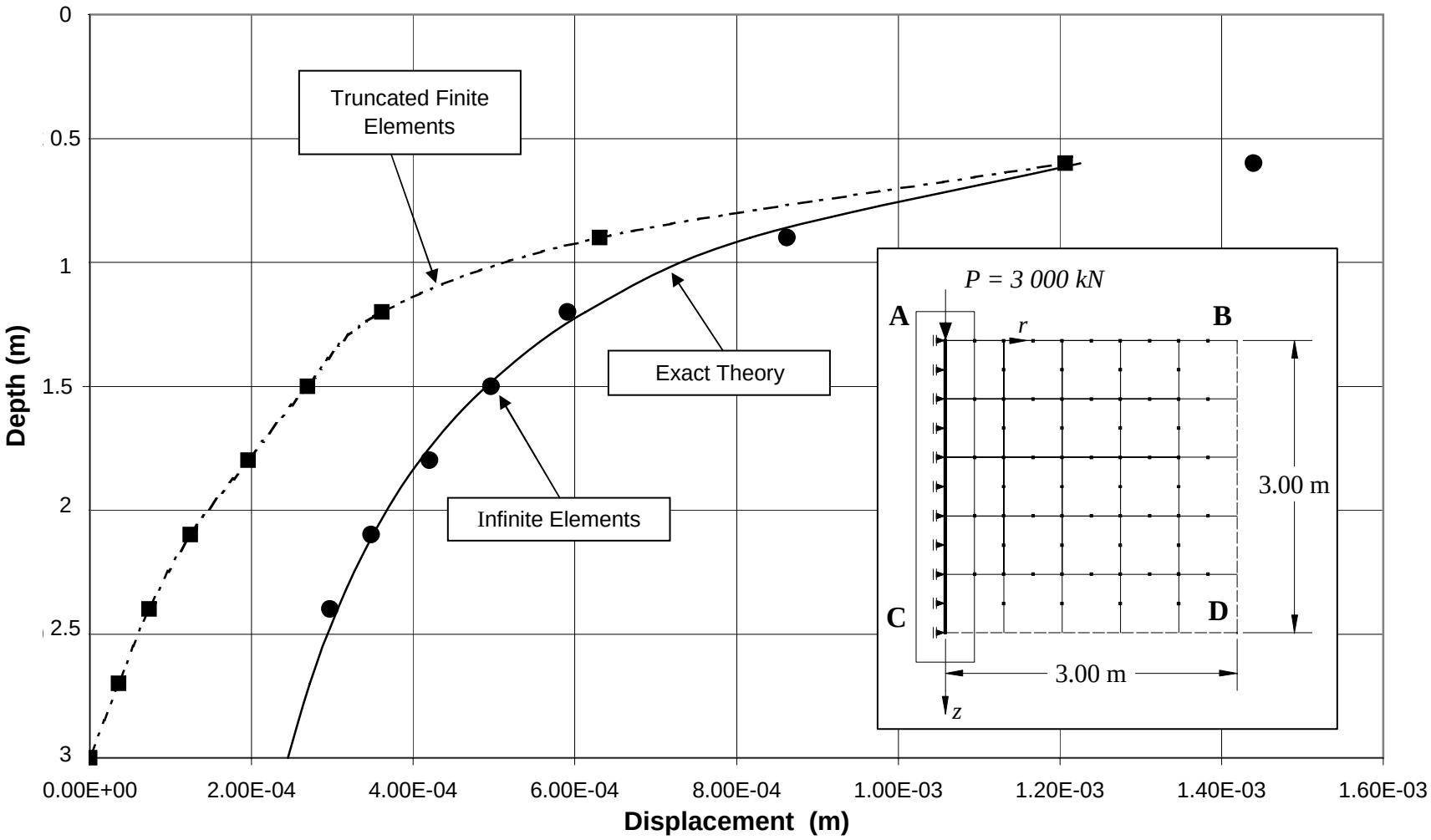

Figure 7.4. Displacements along the vertical line at r = 0

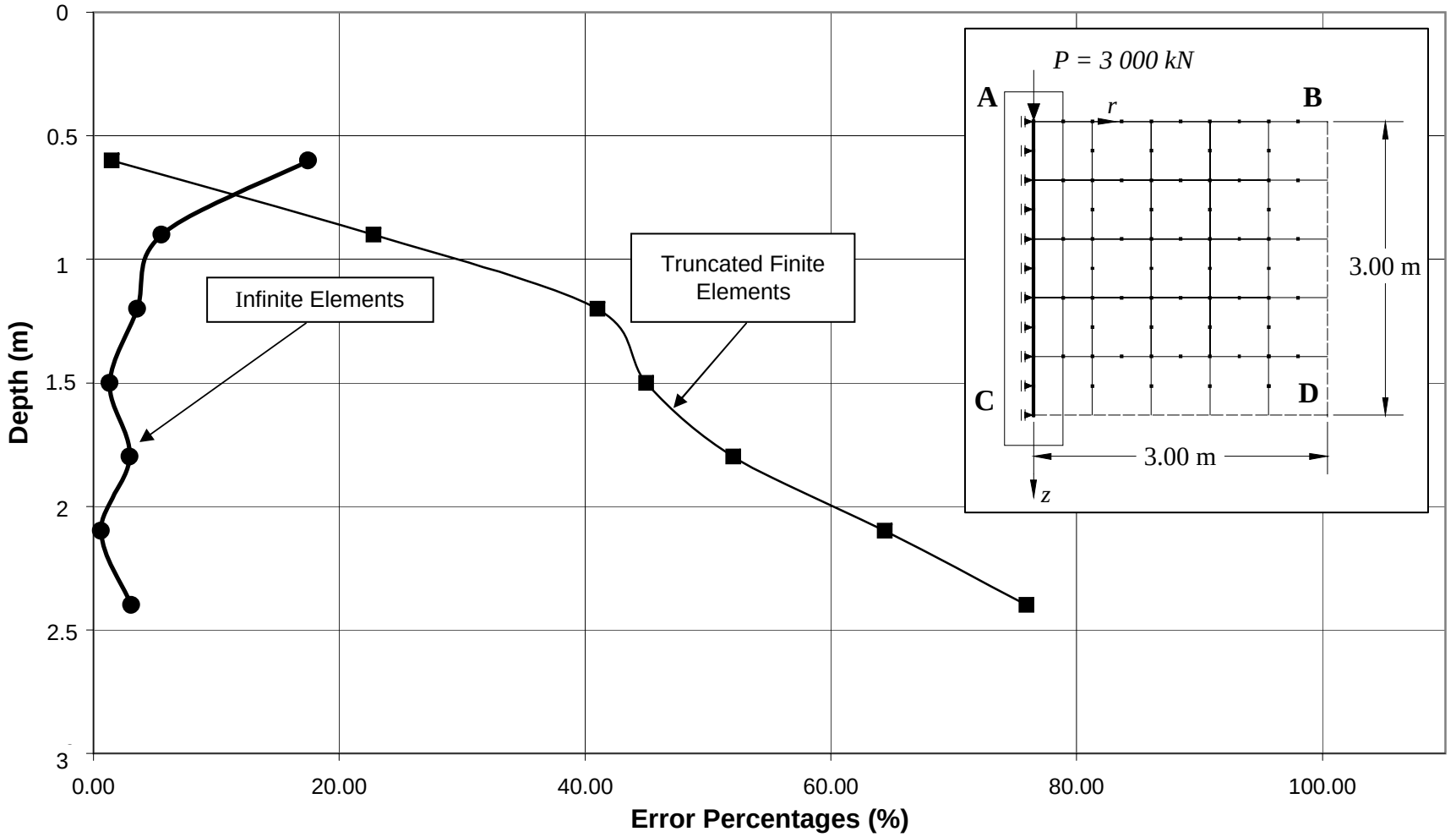

Figure 7.5. Displacement error percentages along the vertical line at r = 0

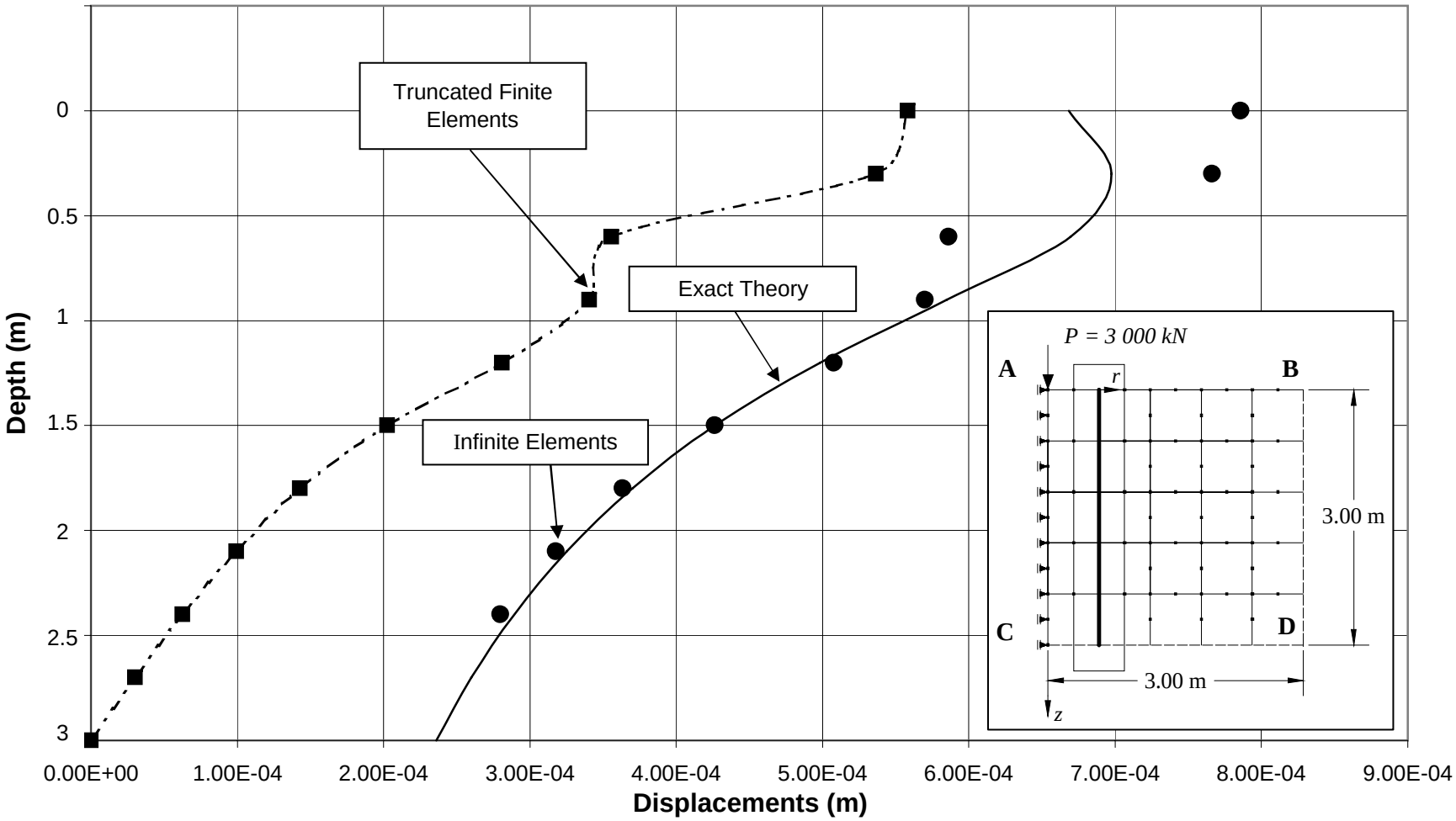

Figure 7.6. Displacements along the vertical line at r = 0.6 m

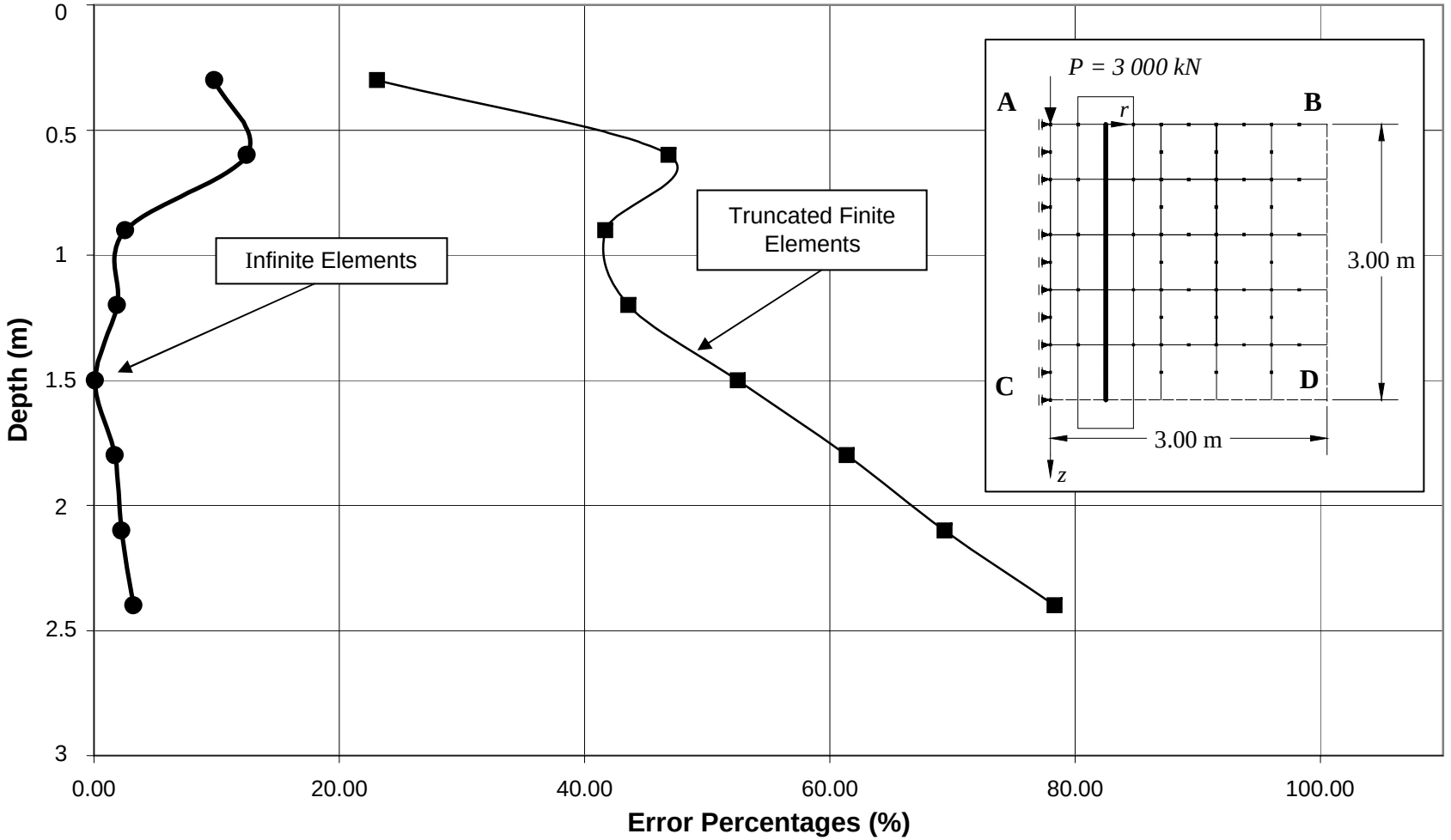

Figure 7.7. Displacement error percentages along the vertical line at r = 0.6 m

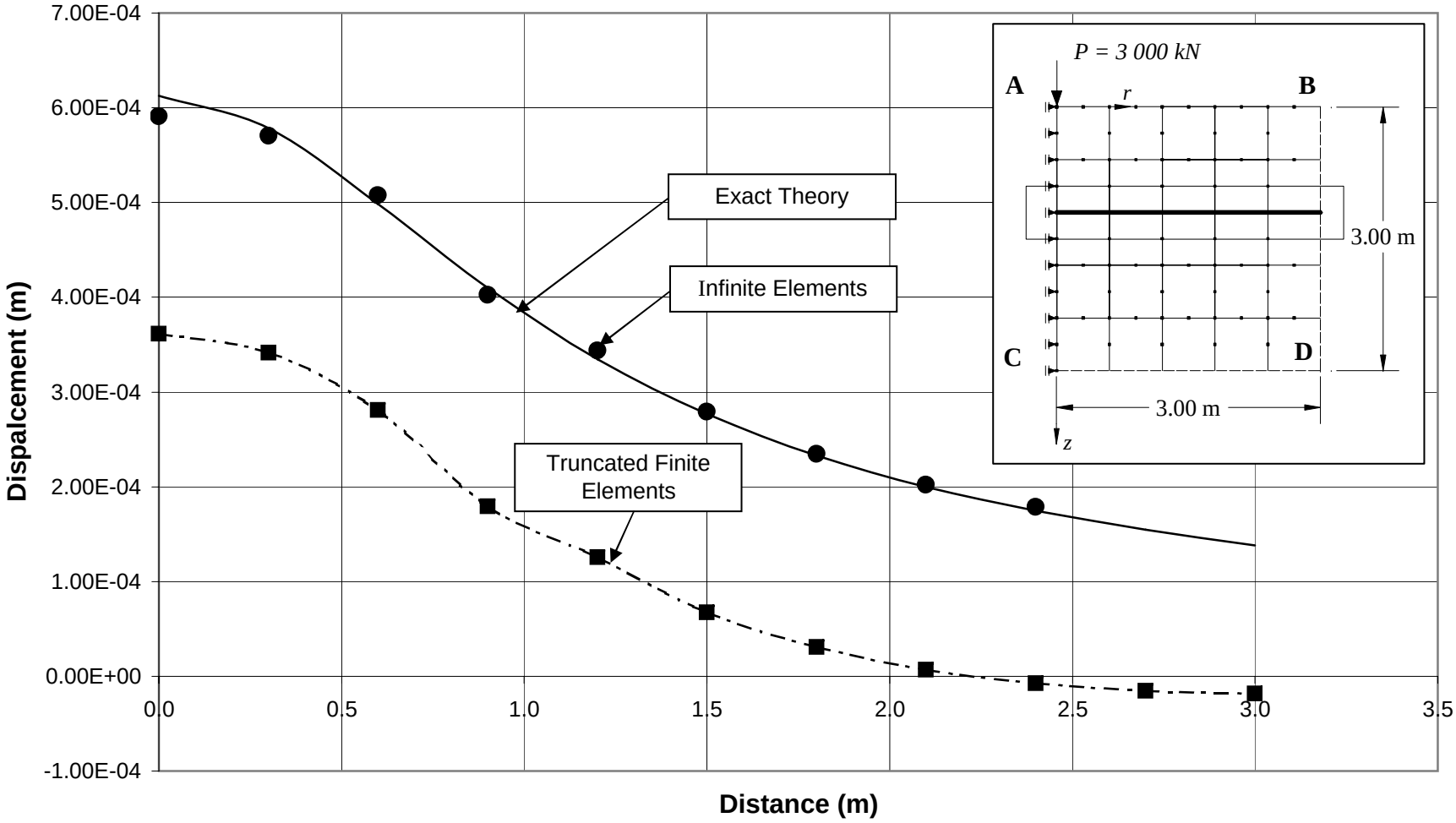

Figure 7.8. Displacements along the horizontal line at z = 1.2 m

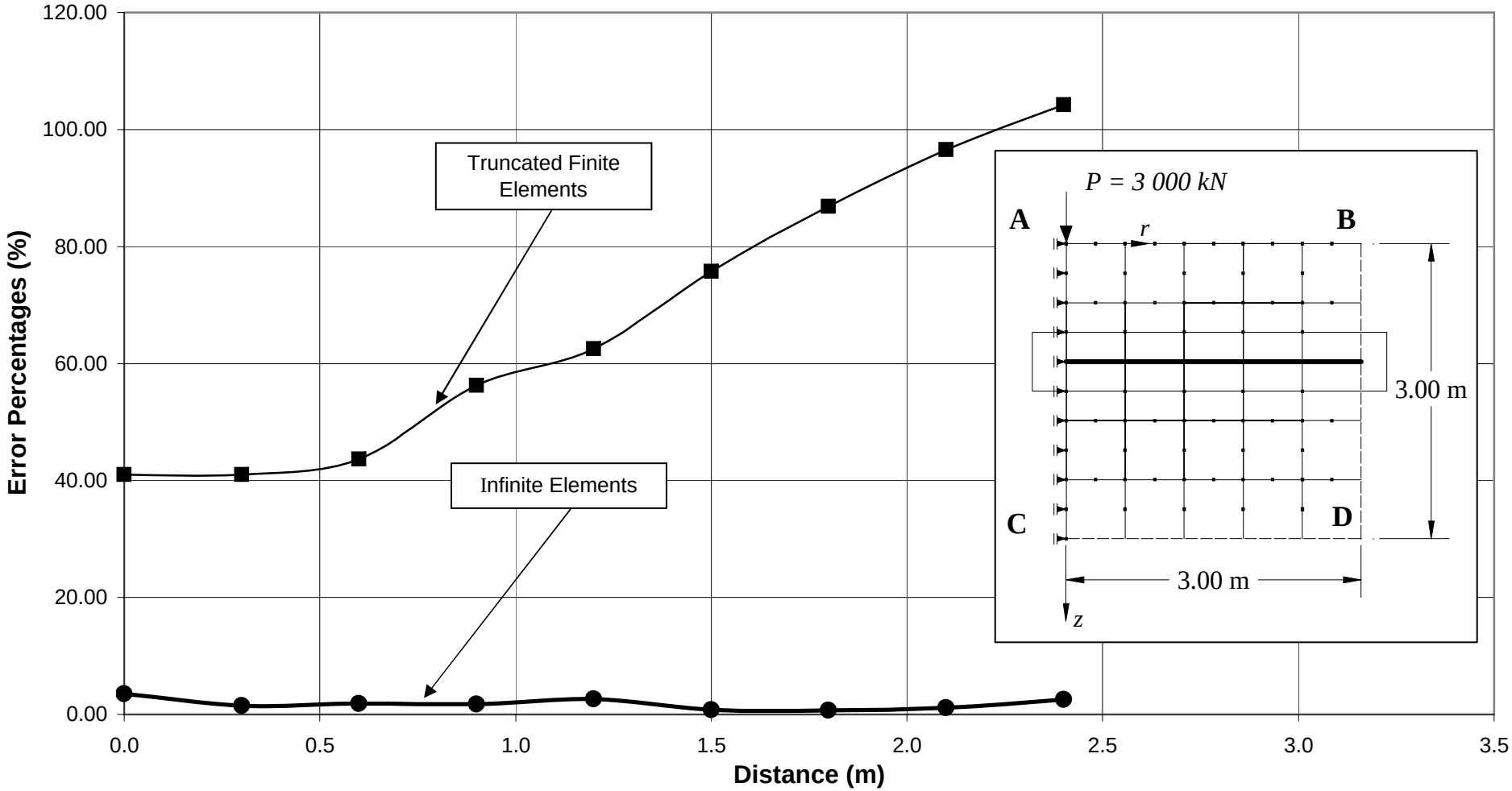

Figure 7.9. Displacement error percentages along the horizontal line at z = 1.2 m

7.3. Circular Uniform Distributed Loading

Uniformly loaded circular foundations are frequently encountered in soil engineering. As a second case study, circular tank on the ground is studied. The tank is *2a=10 m* in diameter; the applied pressure on the ground when the tank is full is 40 kPa. The soil is assumed to be linear and isotropic with Young's Modulus *E = 4 000 kPa* and Poisson's ratio *v = 0.40*. *Since* the problem is rotationally symmetrical about the vertical center-line of the tank, the required finite element grid extends out from the tank center-line and axisymmetric analyses are performed. Figure 7.10 shows schematic diagram of the problem including the foundation region considered in the analysis.

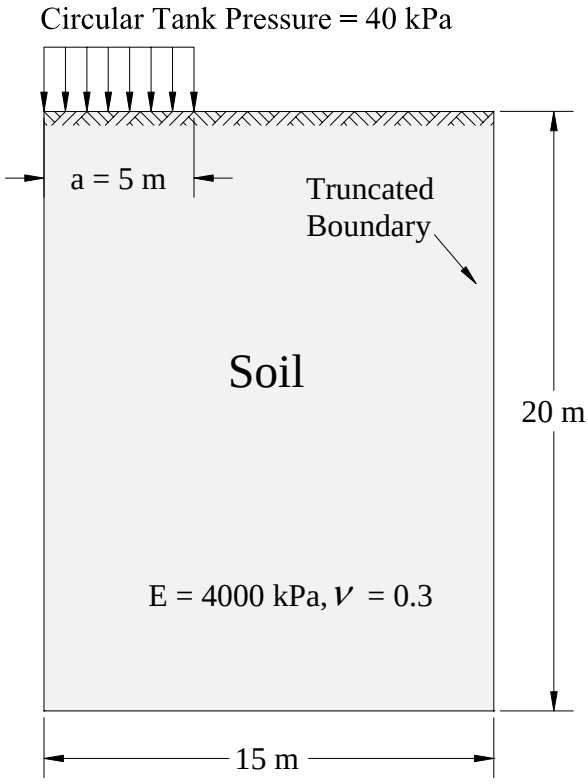

Figure 7.10. Tank on the ground

In the Finite Element modeling of the problem, a 3 by 4 axi-symmetric coarse mesh and 6 by 8 axi-symmetric fine mesh consisting of eight-node high order quadrilateral elements are generated as shown in Figure 7.11 and 7.12. The numerical analyses associated with the problem are carried out using the computer package program *GeoStudio SIGMA/W* (GeoStudio Analysis Reference and Tutorials, 2004). Along the axis

of symmetry, coinciding with the vertical truncation boundary, a boundary condition of zero horizontal displacement is imposed throughout. The horizontal truncation boundary at the bottom edge has zero vertical displacements throughout. In fact, typical movable hinge supports are assumed all along the three mutually perpendicular boundary lines.

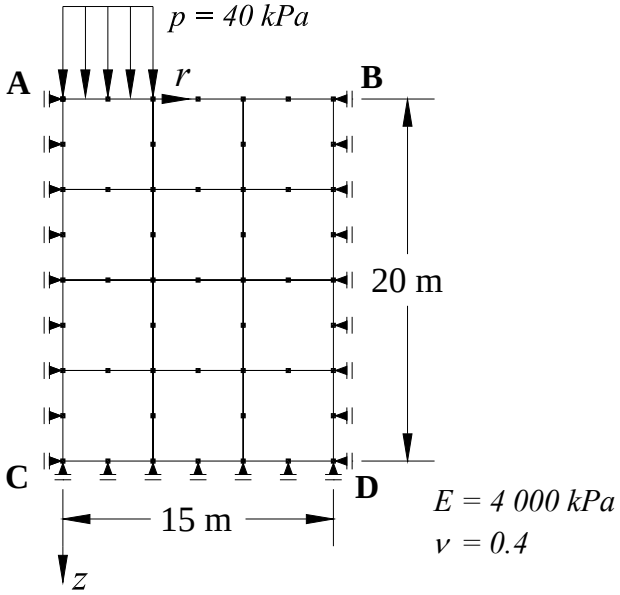

Figure 7.11. Coarse mesh of axi-symmetric body with rigid truncation boundaries

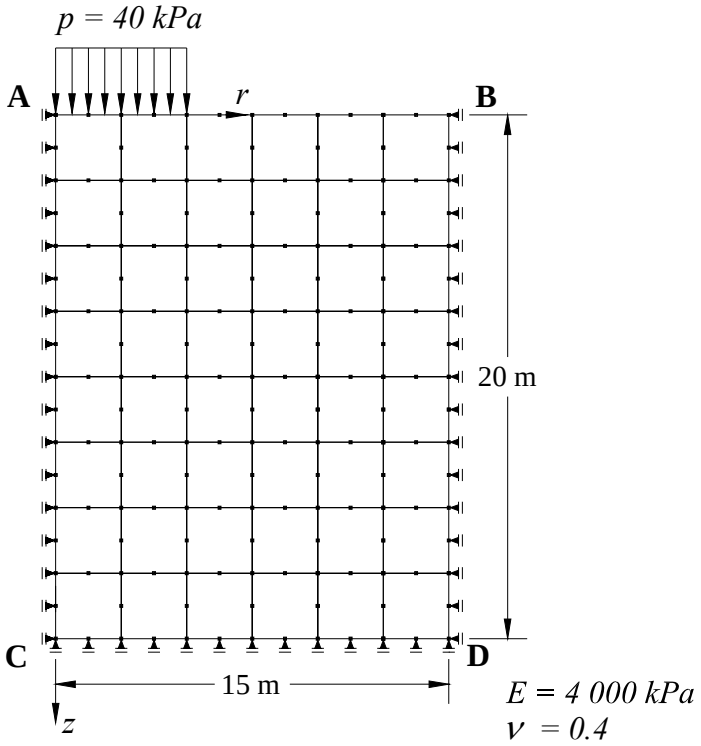

Figure 7.12. Fine mesh of axi-symmetric body with rigid truncation boundaries

For the purpose of introducing infinite elements at the truncation lines CD and BD, a third and fourth models are generated by attaching a corridor of eight-node high order quadrilateral infinite elements to the already existing 3 by 4 coarse mesh and 6 by 8 fine mesh all along the two truncation boundaries CD and BD as shown in Figures 7.13 and 7.14. The infinite elements are indicated by an arrow head specifying a direction to infinity.

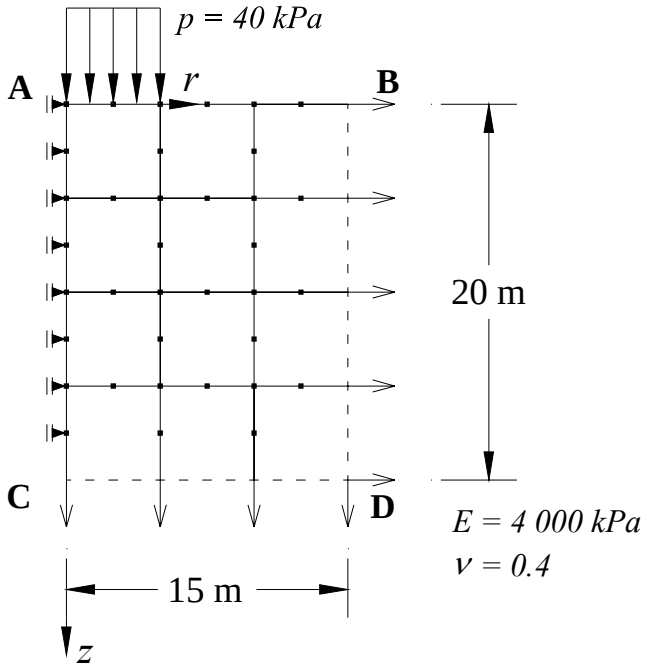

Figure 7.13. Coarse mesh of axi-symmetric body with infinite elements along the truncation boundaries

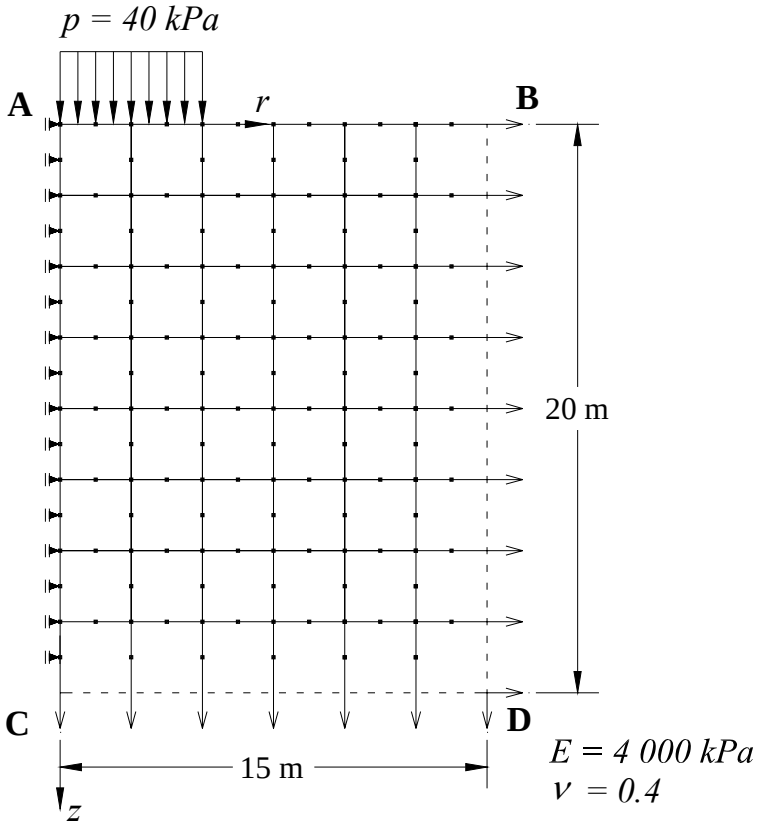

Figure 7.14. Fine mesh of axi-symmetric body with infinite elements along the truncation boundaries

The vertical stresses and the vertical displacements along the vertical, central axis through the center of the circular area have been calculated by three distinct methods as follows:

- Two finite element modelings with 3 by 4 coarse mesh and 6 by 8 fine mesh using GeoStudio SIGMA/W package program;
- The exact formulations (Poulos and Davis, 1974);
- Finite element modeling with 3 by 4 coarse mesh and 6 by 8 fine mesh with infinite elements along the bottom and right-hand side truncation boundaries.

According to analytical solution, the vertical stress and the vertical displacement along the vertical, central axis through the center of the circular area are given in Equations (7.1) and (7.2) respectively.

$$\sigma_z = p\left[1-\left(\frac{1}{1+(a/z)^2}\right)^{3/2}\right] \tag{7.1}$$

$$w = \frac{2pa(1-\nu^2)}{E}\left(\sqrt{1+(z/a)^2}-z/a\right)\left[1+\frac{z/a}{2(1-\nu)\sqrt{1+(z/a)^2}}\right] \tag{7.2}$$

where p is the uniformly distributed loading over the circular bearing area, a is the radius of the circular bearing area, z is the depth, ν is the Poisson's ratio of the medium, and E is the modulus of elasticity of the medium.

The vertical stresses and displacements calculated by these three methods, along the vertical, central axis through the center of the circular area are given in Tables 7.4 and 7.5, respectively and also illustrated graphically in a comparative fashion, for each case in Figures 7.15 and 7.16.

Table 7.4. Vertical stresses along the vertical central axis

Depth *(m)*	**Stresses** *(kPa)*				
	Finite Elements		***Infinite Elements***		***Theory***
	Coarse	Fine	Coarse	Fine	
0.00	55.82	39.36	55.81	39.35	40.00
1.25		39.07		39.09	39.43
2.50	39.18	37.06	39.39	37.13	36.42
3.75		31.60		31.71	31.36
5.00	25.04	27.03	25.33	27.19	25.86
6.25		21.55		21.69	20.95
7.50	19.31	17.06	19.85	17.17	16.96
8.75		14.51		14.52	13.82
10.00	11.53	11.85	12.13	11.76	11.38
11.25		10.34		10.08	9.48
12.50	9.40	8.82	9.43	8.40	7.98
13.75		8.01		7.37	6.80
15.00	7.06	7.17	7.50	6.31	5.85
16.25		6.77		5.66	5.08
17.50	6.63	6.35	4.22	5.43	4.44
18.75		6.23		2.61	3.92
20.00	5.95	6.10	0.03	-0.66	3.48

Table 7.5. Vertical displacements along the vertical central axis

Depth *(m)*	**Displacement** *(m)* (10^{-2})				
	Finite Elements		***Infinite Elements***		***Theory***
	Coarse	Fine	Coarse	Fine	
0.00	7.12	7.35	9.71	9.27	9.10
1.25		6.61		8.54	8.34
2.50	5.54	5.69	8.15	7.63	7.42
3.75		4.78		6.73	6.50
5.00	4.20	3.92	6.79	5.87	5.67
6.25		3.22		5.16	4.97
7.50	2.74	2.65	5.28	4.57	4.39
8.75		2.17		4.07	3.92
10.00	1.80	1.77	4.25	3.66	3.52
11.25		1.44		3.31	3.19
12.50	1.18	1.16	3.56	3.02	2.91
13.75		0.92		2.77	2.68
15.00	0.72	0.71	3.06	2.55	2.48
16.25		0.51		2.36	2.30
17.50	0.34	0.34	2.28	2.19	2.15
18.75		0.17			2.02
20.00	0.00	0.00			1.90

7.4. Evaluation of the Results of Circular Uniform Distributed Loading

Even for a relatively coarse mesh (3 by 4) as shown in Figure 7.13, the improvement of results over a similar analysis but without infinite elements is evident which can be seen from the displacement values along the vertical central axis in Figure 7.16. When fine mesh (6 by 8) is employed, almost no change takes place in the displacements on the other hand the same mesh with infinite elements along the bottom and right-hand side truncation boundaries gives perfect performance as seen in Figure 7.16.

In the case of the stresses, as secondary dependant variables, although the convergence with mesh refinement is observed, no significant improvement of results is seen when employing meshes containing infinite elements as illustrated in Figure 7.15. However, even slightly, the results are still observed to be better when infinite elements are used.

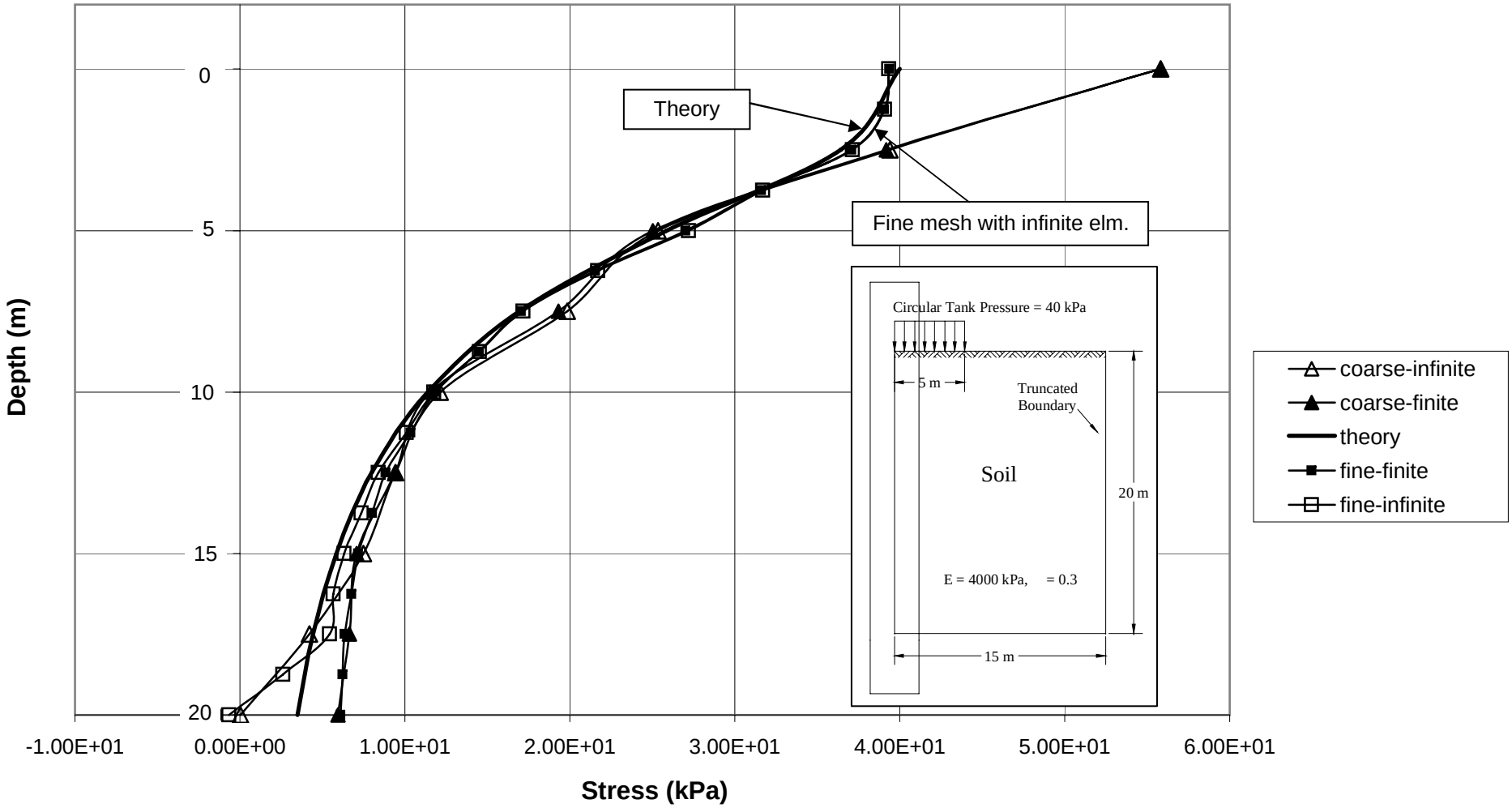

Figure 7.15. Vertical stresses along the vertical central axis

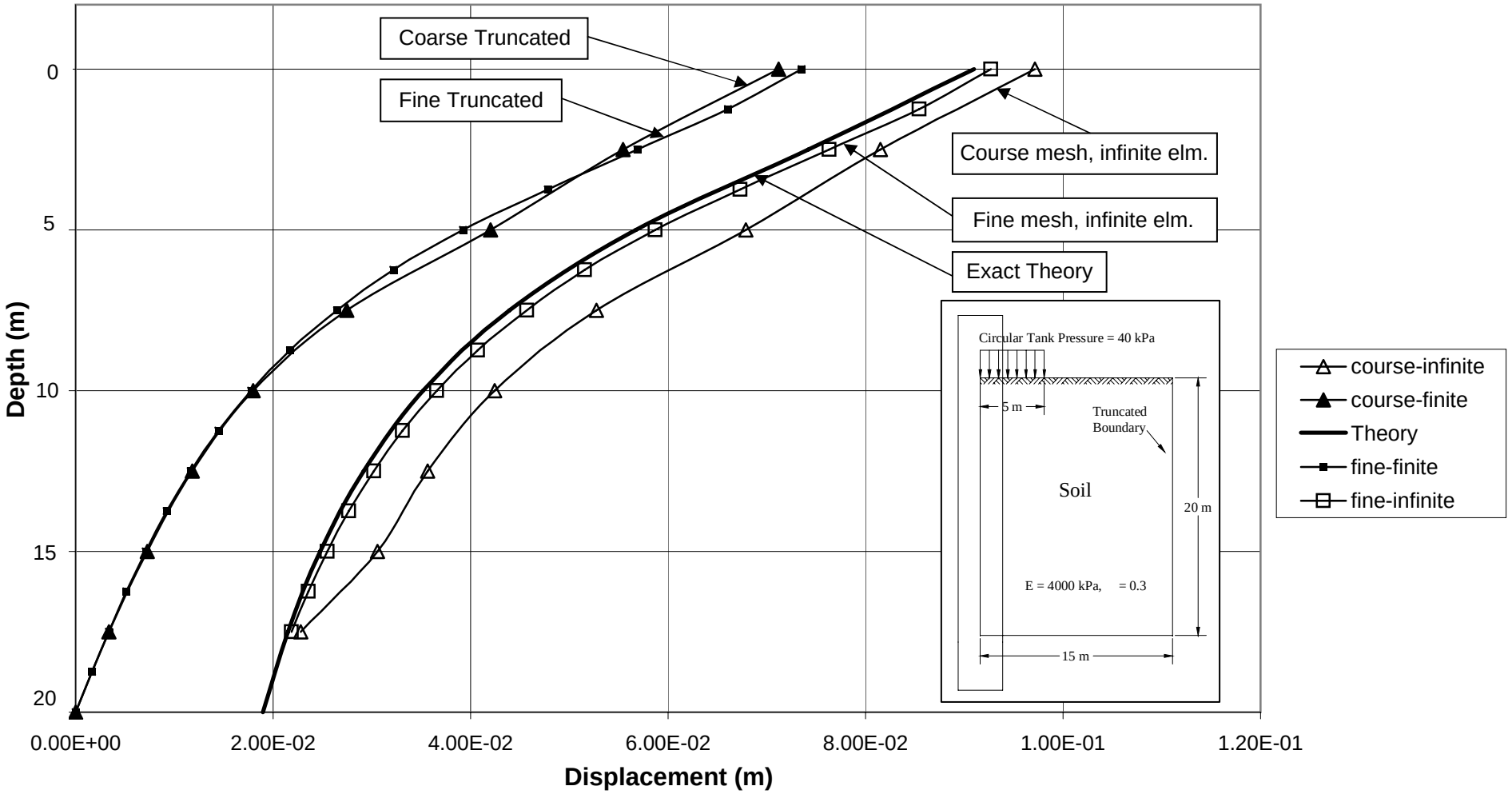

Figure 7.16. Vertical displacements along the vertical central axis

7.5. First Case Study for 3-D Seismic Infinite Element

This numerical example for verifying the 3-D dynamic infinite element is that the calculation of the compliances of a square massless rigid plate resting on an isotropic homogeneous elastic half-space. Figure 7.15 shows the discretization of a plate on the half-space, in which only a quarter of the plate and the half-space is modeled by finite and infinite elements due to the symmetry of the problem. It needs to be mentioned that the symmetry boundary condition is added on the *xz* and *yz* planes since the case was vertical vibration of the plate. In order to compare current numerical results with the previous results, the same assumptions as in the References of Hamidzadeh-Eraghi and Grootenhuis 1981 and Wong and Luco 1976 are adopted and the parameters seen in Table 7.1 are used in the analysis.

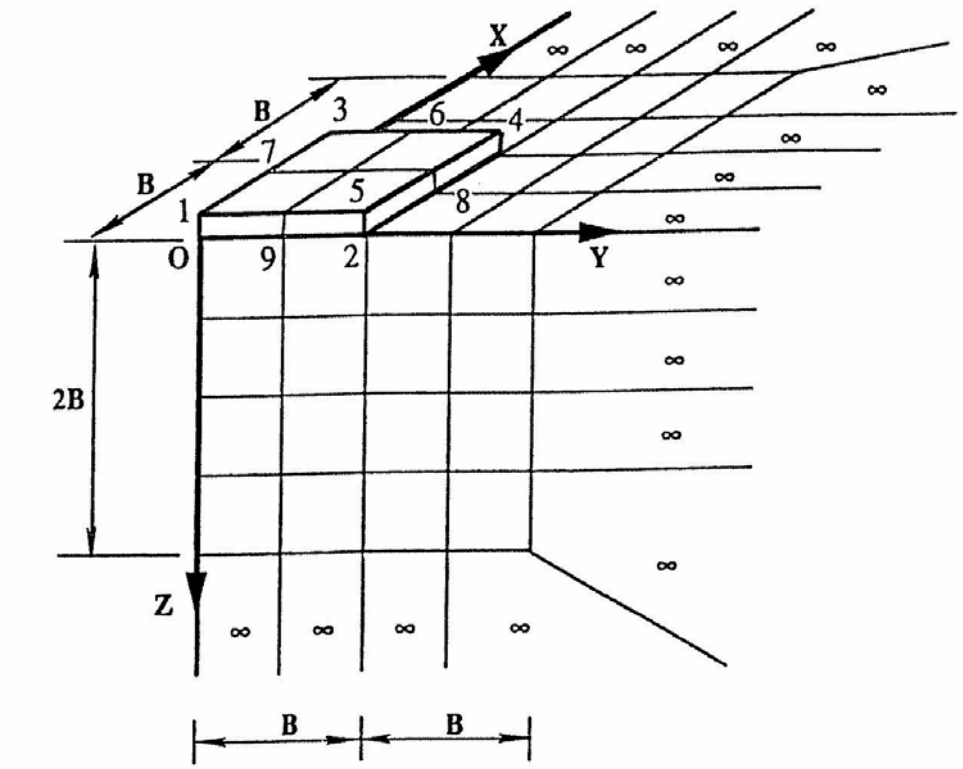

Figure 7.17. Discretization of a plate on the half-space

Table 7.6. Material properties

Plate	**Rock Soil**		
$E_p = 24\times10^{12}\,kPa$	$E_s = 24\times10^{6}\,kPa$	$V_P = 3872\,m/\sec$	$\alpha = 0.028$
$B = 10\,m$	$\mu = 0.333$	$V_S = 1936\,m/\sec$	$G_s = Shear\ Modulus$
$t = 1m$	$\gamma_s = 24kN/m^3$	$V_R = 1804\,m/\sec$	$P_0 = Dynamic\ Load$

In the calculation, the plate is modeled by either thick plate elements or a combination of thick plate elements and plane stress elements. The near field of the foundation is modeled by 3-D solid finite elements and the far field of the foundation is modeled by 3-D dynamic infinite elements. From the wave velocities and the harmonic wave frequency of the foundation, the wave numbers β_i $(i = 1, 2, 3)$ in the infinite element can be evaluated. Besides, the numerical results are expressed as

$$C_X = \frac{U_X}{P_0}(GB), \qquad C_Z = \frac{U_Z}{P_0}(GB) \tag{1.1}$$

where C_X, C_Z are the dimensionless compliances due to the dynamic load of the plate P_0 in x and z directions, Δ_1, Δ_3 are the corresponding complex displacements in x and z directions, G is the shear modulus of the rock medium, $a_0 = \omega B/V_S$ is the dimensionless frequency in which V_S is the S-wave velocity of the rock.

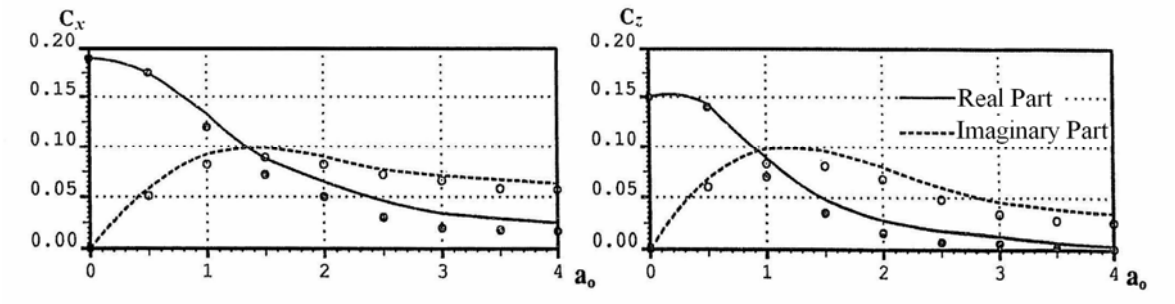

Figure 7.18. Comparison of the current results with the previous results

Figure 7.16 shows a comparison between the current results and the previous results (Hamidzadeh-Eraghi and Grootenhuis 1981 and Wong and Luco 1976) where the solid line

and dashed line for C_X and C_Z are sited from Reference of Wong and Luco, 1976. The solid dot and circle are the numerical results from the present infinite element model in which the plate is modeled using the combination of thick plate elements and plane stress elements. It is noted from Figure 7.16 that there is a very good comparison when the plate is modeled by the combination of thick plate elements and plane stress elements. This demonstrates that accurate results can be obtained from the present finite and infinite element coupling model. Therefore, it is recommended in the seismic analysis of a plate subjected to horizontal earthquakes, shell elements or a combination of thick plate elements and plane stress elements be used in the analysis.

7.6. Second Case Study for 3-D Seismic Infinite Element

This numerical example for verifying the 3-D dynamic infinite element is the calculation of the vertical vibration of a square massless rigid plate resting on a viscoelastic layered foundation, which, in fact, wave propagation problem in the non-homogeneous foundation.

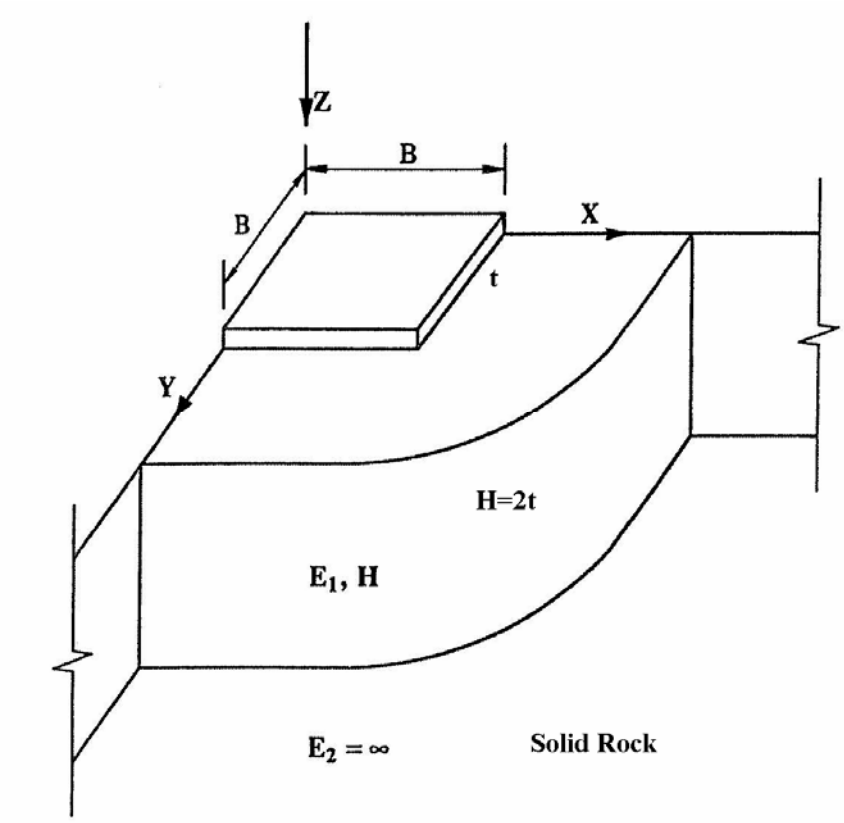

Figure 7.19. Vertical vibration of a rigid plate on a layered foundation

Figure 7.17 shows the discretized model, where only a quarter of the plate and the foundation is considered due to the symmetry of the problem. The selection of the parameters and the considerations are similar as that in the first example, except for the layered foundation is considered resting on a rigid base and the ratio of the layered depth to the plate width is chosen as 2.

A comparison between the current results and the previous results (Chow Y. K., 1987) is shown in Figure 7.18 where *K* and *C* are the damping stiffness coefficient and damping coefficient of the plate, respectively, the solid line expresses the previous results (Chow Y. K., 1987) and the solid circle denotes the current results. It is observed that there exists a good agreement between the current results and previous results. This illustrate that accurate results can be achieved using finite and infinite element coupling model to solve 3-D layered-foundation wave problems.

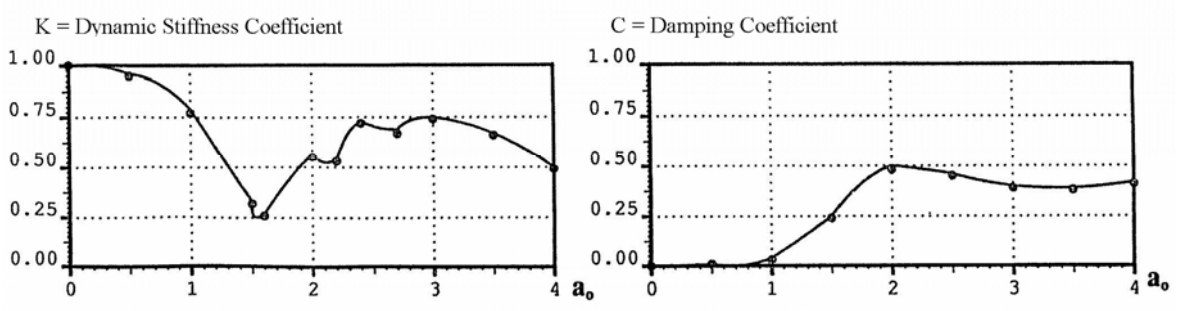

Figure 7.20. Comparison of the current results with the previous results

Thorough the comparison of the numerical results from the present finite and infinite coupling model with previous results for a massless, smooth rigid square plate on a homogeneous elastic half-space or viscoelastic layered foundation, it is demonstrated that accurate results can be obtained using this coupling model to solve 3-D foundation wave problems.

7.7. Sensitivity Analysis of Finite Element Modeling

In order to see the effect of enlargement of domain used in finite element modeling and the effect of springs used all along the truncation boundaries of unbounded domain problems, axisymmetric analyses are performed for Boussinesq problem.

The material is assumed to be linear and isotropic with Young's Modulus $E = 2\,000$ *MPa* and Poisson's ratio $v = 0.40$. The point load acting vertically at the center of a three dimensional elastic half space is $P = 3\,000$ *kN*. The computer package program *GeoStudio SIGMA/W* (GeoStudio Analysis Reference and Tutorials, 2004) is used for this purpose.

The vertical displacements, beneath the point load, have been calculated by five distinct finite element modeling, using the same size finite elements and exact formulation as follows:

- Finite element modeling with 5 by 5 mesh (3m × 3m),
- Finite element modeling with 25 by 25 mesh (15m × 15m),
- Finite element modeling with 50 by 50 mesh (30m × 30m),
- Finite element modeling with 5 by 5 mesh, using springs along the truncated boundaries,
- Finite element modeling with 5 by 5 mesh with infinite elements attached to the bottom and right-hand side of truncated boundaries,
- The exact formulations by Boussinesq (Jumikis, A. R., 1969).

Meshes used for these finite element models may be seen in Figures 7.21 through 7.23.

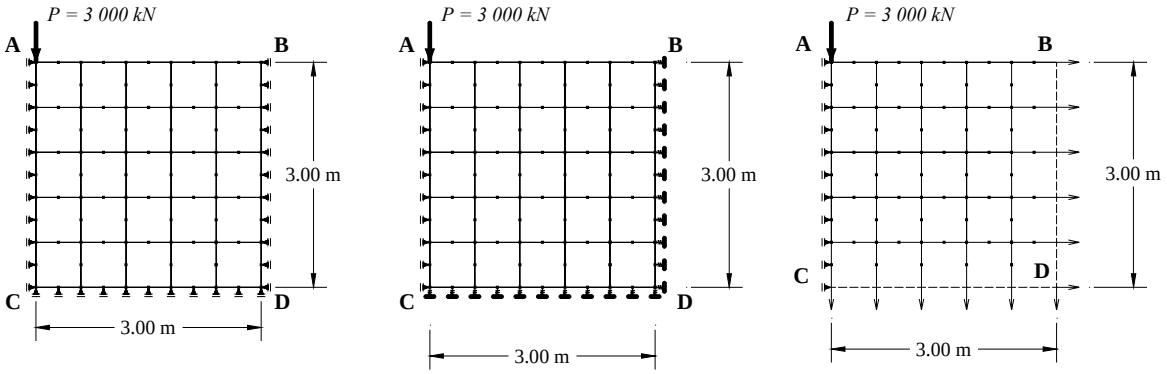

Rigid truncation Springs Infinite elements

Figure 7.21. Meshes of axi-symmetric body (5 by 5)

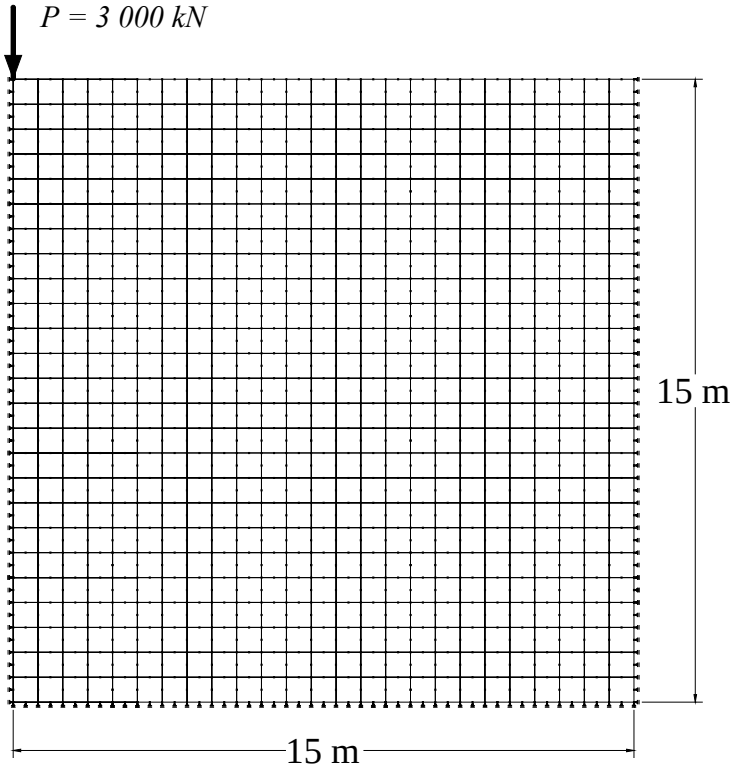

Figure 7.22. Truncated mesh of axi-symmetric body (25 by 25)

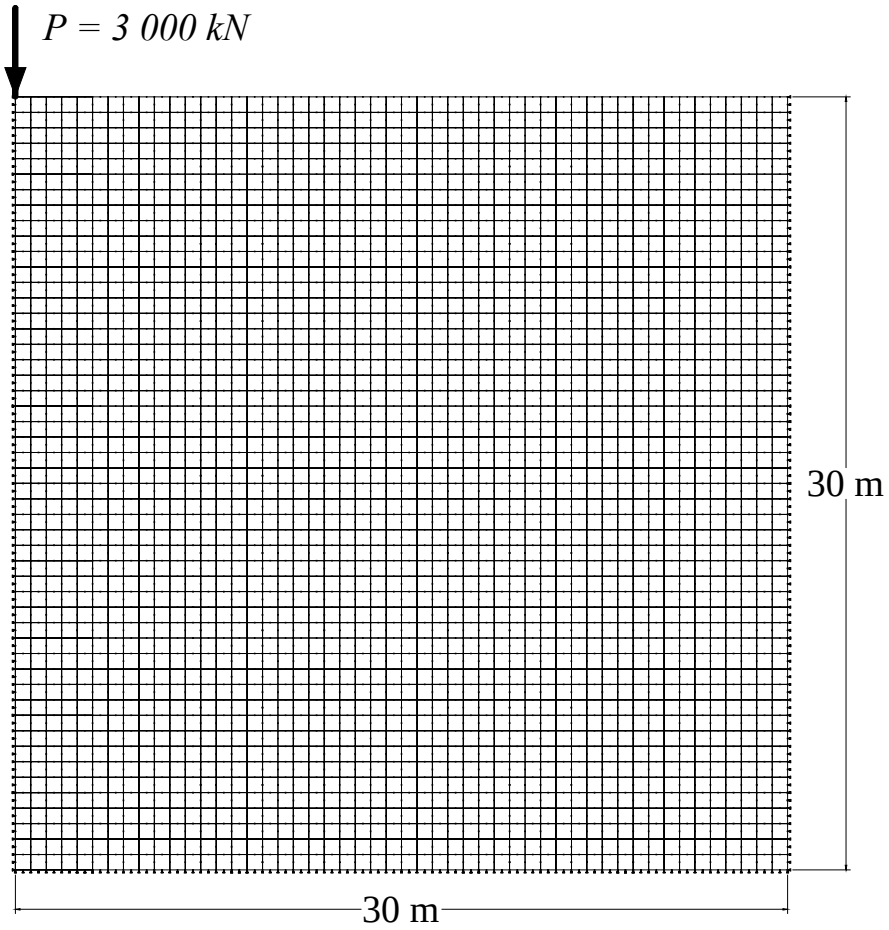

Figure 7.23. Truncated mesh of axi-symmetric body (50 by 50)

The vertical displacements calculated by these six methods, along the vertical axis at r = 0 m are given in Tables 7.7 and illustrated graphically in a comparative fashion in Figure 7.24.

Table 7.7. Vertical displacements along the vertical central axis

Depth*(m)*	**Displacements** *(m)*					
	5x5	***25x25***	***50x50***	***Spring (5x5)***	***Infinite(5x5)***	***exact***
0	1.21E-03	1.39E-03	1.41E-03	1.50E-03	1.44E-03	1.23E-03
0.6	3.61E-04	5.46E-04	5.69E-04	6.54E-04	5.91E-04	6.13E-04
1.2	2.70E-04	4.54E-04	4.77E-04	5.58E-04	4.97E-04	4.90E-04
1.5	1.96E-04	3.80E-04	4.03E-04	4.81E-04	4.21E-04	4.08E-04
1.8	7.38E-05	2.60E-04	2.83E-04	3.45E-04	2.97E-04	3.06E-04
2.4	0.00E+00	2.00E-04	2.23E-04	2.16E-04		2.45E-04

The coarse mesh of 5 by 5 with infinite elements along the truncated boundaries gives consistently the best results, compared with the results of other meshes of 5 by 5, 25 by 25 and 50 by 50 with truncated boundaries. When springs are employed in order to represent the soil conditions all along the truncated boundaries, the results are better than those of the coarse or fine meshes with truncated boundaries. The results of coarse mesh with infinite elements however are the most accurate and closest to the exact solution among all other cases.

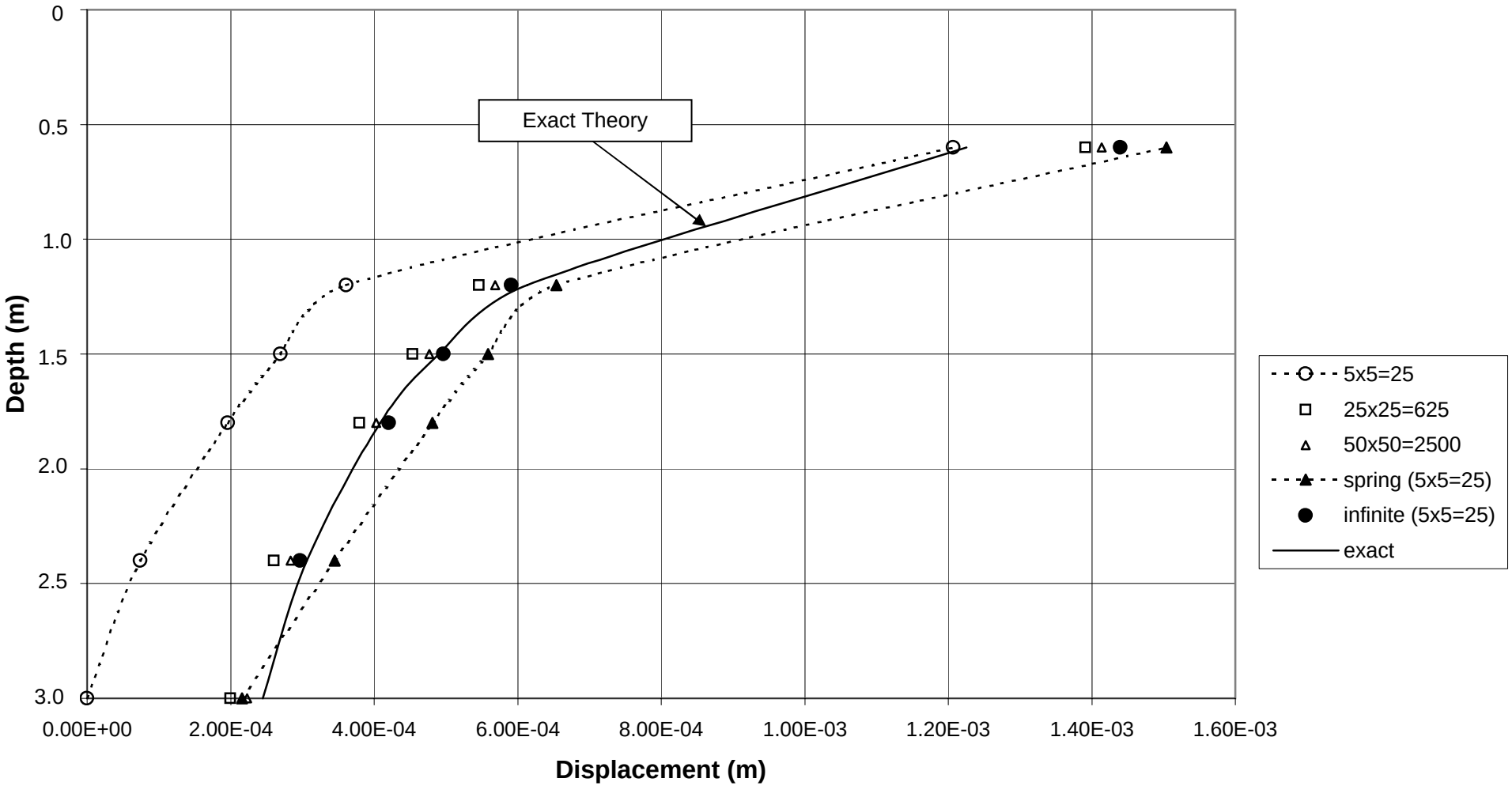

Figure 7.24. Vertical displacements along the vertical central axis

8. CONCLUSIONS

In this Thesis, infinite elements are introduced including a discussion of history and development, fields of application, and their chief merits. Basic classification of infinite elements is given as mapped infinite elements and decay infinite elements with some detailed discussions. General formulations of 1-D, 2-D and 3-D infinite elements are discussed. A comprehensive set of coordinate and field variable mapping functions of 2-D and 3-D infinite elements are presented in practical and explicit fashion. Numerical examples are also supplied to illustrate the use of infinite elements in a variety of problems. Based on the results of the case studies contained herein certain concluding remarks may be stated as follows:

1) The stiffness matrices and all other properties of an infinite element may be formulated in a manner similar to that used for the conventional finite elements. This fact is explicitly demonstrated for the formulation of 1-D, three-node infinite element. In fact, when appropriate isoparametric shape functions are selected for both coordinates and field variables, the derivation of matrix properties of infinite elements of any size and shape becomes a straightforward routine operation.

2) The adaptation of an infinite element into a standard finite element package program does not introduce any special difficulty, simply because the infinite elements retain the narrow band width nature of the master stiffness matrix, and require relatively smaller memory space.

3) The infinite elements provide systematically a very high degree of accuracy even with relatively coarse mesh sizes in unbounded continuum problems. Therefore, the use of infinite elements is indispensable in these categories of problems including the load analysis on semi-infinite medium, soil-structure interaction, seepage and ground water flow, wave propagation, off-shore structures, etc.

4) In order to investigate the relative accuracy supplied by the infinite elements, a sensitivity analysis is performed for the deflections produced by a point load acting on a

semi-infinite elastic half-space. The accuracy of the deflections in the near field is increased steadily if the geometrical size of the finite element modeling of the field is increased. For instance, the error percentage for the vertical deflection at 1.2m depth below surface was 45% when only a 5 by 5 coarse mesh is used. The error is only reduced to 2.7% when a 50 by 50 fine mesh is used 10 times greater field size and 100 times greater number of finite elements. When infinite elements are used however, with only 5 by 5 mesh size, the error is a mere 1.4%. The economy and efficiency gained in computation time and effort, by using infinite elements, are thus unmistakenly proven.

5) Although, the use of equivalent springs all along the truncated boundary provides considerable accuracy compared with cases of enlarged field and mesh size, the use infinite elements gives always superior results.

6) The use of finer mesh size and higher number of finite elements does not increase the accuracy of results as efficiently and drastically as the use of infinite elements. For instance, the vertical deflection at the surface of a semi-infinite medium under a circular loading is 91.0mm by the exact theory. The errors are 21.7% and 19.2% for the 3 by 4 coarse mesh and 6 by 8 fine mesh sizes, respectively. When infinite elements with only 3 by 4 coarse mesh size are used however, the error is drastically reduced to 6.7%.

7) Further research is recommended using 2-D and 3-D infinite elements in a variety of unbounded continuum problems in order to discover the immense versatility of infinite elements.

APPENDIX A: STRESS DISTRIBUTION IN SOILS

Here, stresses and displacements in the soil due to the point load on it will be given. One of the principal problems of soil mechanics relative to the founding of structures is the study of the relationships between the following factors: load, loading area, depth of foundation, settlement, and duration of loading (Jumikis, 1962).

Because of the great diversity in soil properties, and the many variables involved in the stability problems of soil and structure, the relationships between these factors are very complex indeed; and in theoretical studies one is forced in many instances to assume idealized conditions and simplifications, or to study soil mechanics problems experimentally.

A.1. Contact Stresses

The stresses in soil are caused by two principal factors, namely:

1) Self-weight of the soil,

$$\sigma_s = \gamma H \tag{A.1}$$

where, σ_s = stress in soil at depth H, and
γ = unit weight of soil,

2) The stress from the structural load applied to the soil.

A.2. Boussinesq's Theory

Boussinesq's stress distribution theory is based on the results given by the mathematical theory of elasticity for the simplest case of loading of a solid, homogeneous, elastic-isotropic, semi-infinite medium: namely, the case of a single, vertical, point load applied at a point on the horizontal boundary surface (ground surface).

A semi-infinite body is one bounded from one side with a horizontal boundary plane. In the case of soil, the horizontal boundary plane would be the ground surface, and semi-infinite medium is the mass of soil below the ground surface.

Point loads in soil mechanics are single, concentrated loads, and uniformly distributed loads over symmetric polygonal, or circular areas when stresses in soil are considered only at depths greater than threefold diameter of the loaded area. In deriving his stress distribution theory for a single, concentrated load, following assumptions are made:

1) The soil medium is an elastic, homogeneous, isotropic, semi-infinite medium which extends infinitely in all directions from a level surface and which obeys Hooke's law.
2) The soil is weightless.
3) Originally, before the application of the single concentrated load, the soil is not subjected to any other stress, the soil is stress-less or unstressed.
4) The stress distribution from the applied, concentrated load is independent of the type of material of which the homogeneous, elastic-isotropic body is made. Relative to soil the change in volume upon the application of stress to the soil is neglected.
5) The stress-strain relationship is assumed to be linear.
6) There exists a continuity of stress.
7) In such a system the stresses are distributed symmetrically with respect to the z-axis.

The limitations of the theory based on the above assumptions restrict it to the proportionality between stress and deformation. The principles of derivation of Boussinesq's equations are: there are six unknown quantities in the stress distribution problem, seen in Figures A1 and A2 and namely:

the normal stresses: σ_y, σ_t, σ_R ;
the shear stresses: τ, and

displacements: s_l (radial component) and
s_v (vertical component).

Hence, the solution requires 6 independent equations. The equilibrium condition of an elementary material prism renders 2 equations for the axi-symmetrical stress condition. The relationship between stress and strain and the continuity conditions render the other four equations.

A.3. System

In applying Boussinesq's theory to soil, imagine the following system, Figure A.1, the ground surface is the (z = 0)-plane (plane $H_o - H_o$); it is the horizontal boundary of a semi-infinite medium, the medium of soil.

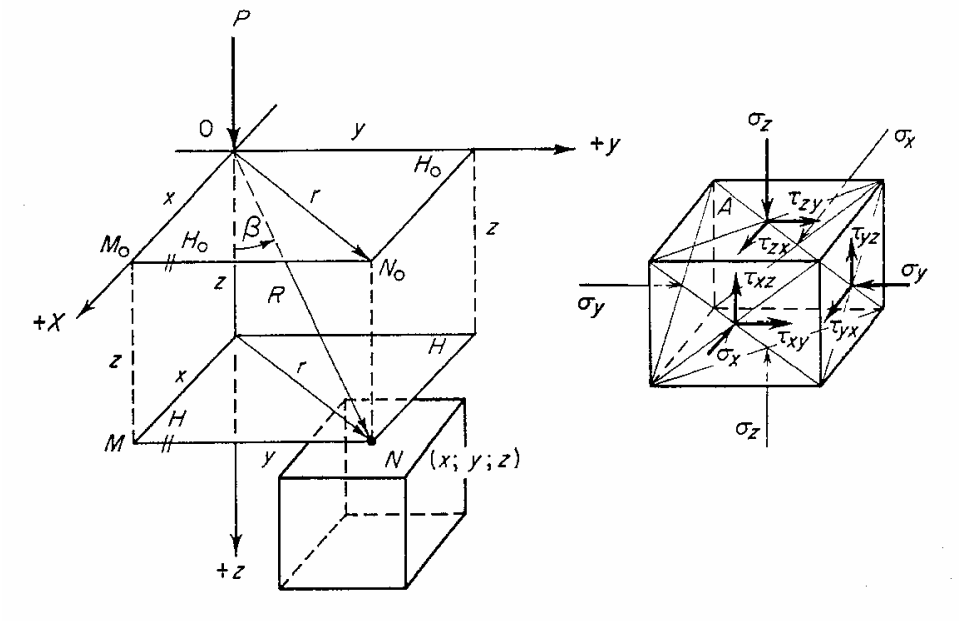

Figure A.1. Orthogonal stresses (Jumikis, 1962)

A single concentrated load, *P*, is acting on this plane at the point of origin of coordinates, *0*, along the *z*-axis. The positive direction of the z-axis is here, for the sake of convenience, directed downwards into the body of the semi-infinite medium to suit the contents of the matter under discussion. The positive branch of the *y*-axis is directed horizontally 90°

counter-clockwise from the *z*-axis. The positive *x*-axis is directed orthogonally to the *y*- and *z*-axes. The +*x* direction is then toward the viewer when viewing the (*z*-*y*)-plane.

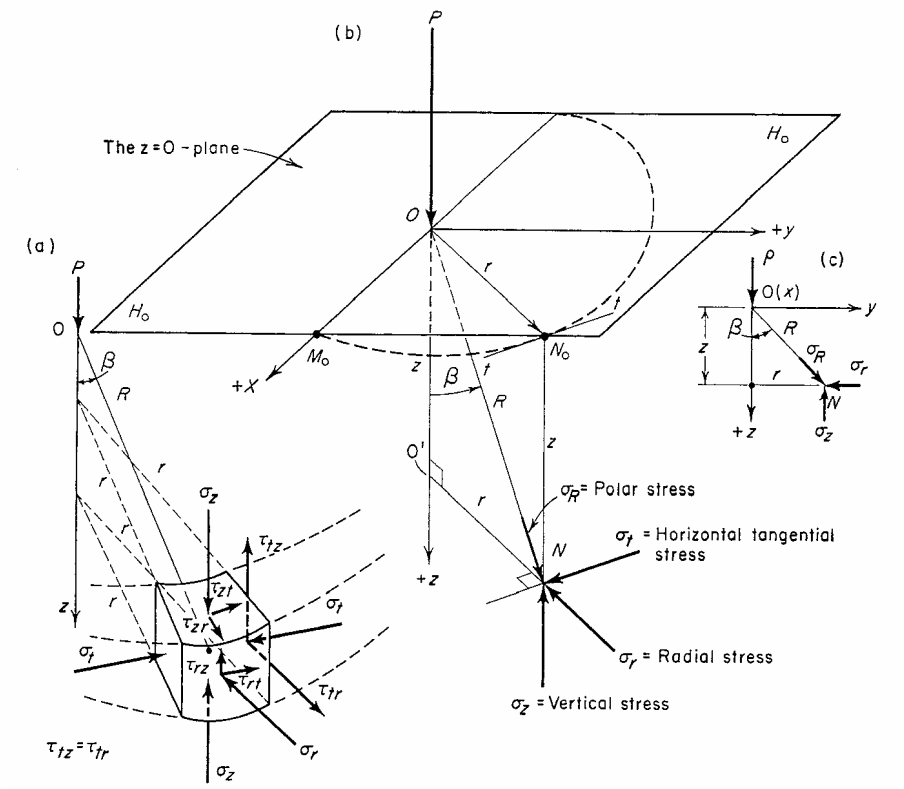

Figure A.2. Loads and stresses in a cylindrical coordinate system (Jumikis, 1962)

In Figure A.1 are shown the orthogonal stresses at point, $N(x; y; z)$, which are the normal and the shear stresses. In Figure A.2 are shown at point $N(R; \beta)$ the polar stress, σ_R; or else, using the cylindrical coordinate system, there is shown the vertical stress, σ_z; the horizontal radial stress, σ_r; and the horizontal tangential stress, σ_t, in the *R*, *z*, *r*, and tangential directions. Here *R* is a radius-vector from *O* to *N*, making an angle, β, with the positive direction of the *z*-axis. The angle, β, is a directed angle and is measured from the +*z*-axis to the radius-vector, *R*, connecting the stressed point, *N*, with the point of origin of coordinates, *O*. The angle, β, is positive when it is followed counterclockwise. The horizontal distance from the z-axis to an arbitrary point, *N*, is designated by *r*.

A.4. Designation of Stresses

The stressed condition of soil at any point is characterized by the stresses acting at that point along the coordinate axis. In the orthogonal coordinate system, the stressed condition of an elementary cube of soil, the faces of which are parallel to the planes of coordinates is characterized by the following stresses Figure A.1 b.

a) Normal Stresses:

σ_z vertical stress

σ_x horizontal normal stress acting along or parallel to the x-axis of coordinates

σ_y horizontal normal stress acting along or parallel to the y-axis of coordinates.

b) Shear Stresses

τ_{xy} and τ_{yx} shear stresses acting in the planes of a cube, planes which are parallel to the z-axis of coordinates. These two shear stresses are acting in mutually perpendicular directions.

τ_{yz} and τ_{zy} shear stresses acting in the planes parallel to the *x*-axis

τ_{zx} and τ_{xz} shear stresses acting in the planes parallel to the *y*-axis

Another mnemonic device for memorizing the shear stress designation is as follows: of the two subscripts to the shear stress symbol, τ, the first one indicates the direction of the plane in which the shear stresses, τ, acts whereas the second subscript indicates the direction in which τ acts.

In the cylindrical coordinate system, the stresses σ_z, σ_r, and σ_t are normal stresses. The shearing stresses are designated by τ. Because of symmetry of the state of stress with respect to the *z*-axis, the shear stresses in the vertical, radial planes, such as the plane ON_oNO', as shown in Figure A.2 are of zero magnitude.

According to the Boussinesq's Theory, the various stresses caused in the semi-infinite medium by a single, concentrated load have the functions summarized as follows:

$$\sigma_x = \frac{P}{2\pi}\left[3\frac{x^2 z}{R^5} - \frac{m-2}{m}\left(\frac{x^2 - y^2}{Rr^2(R+z)} + \frac{y^2 z}{R^3 r^2}\right)\right] \tag{A.2}$$

$$\sigma_y = \frac{P}{2\pi}\left[3\frac{y^2 z}{R^5} - \frac{m-2}{m}\left(\frac{y^2 - x^2}{Rr^2(R+r)} + \frac{x^2 z}{R^3 r^2}\right)\right] \tag{A.3}$$

$$\sigma_z = \frac{3P}{2\pi}\frac{z^3}{R^5} = \frac{3P}{2\pi R^2}\cos^3\beta \tag{A.4}$$

$$\sigma_r = \frac{P}{2\pi}\left[3\frac{r^2 z}{R^5} - \frac{m-2}{m}\left(\frac{R-z}{Rr^2}\right)\right] \tag{A.5}$$

$$\sigma_t = \frac{P}{2\pi}\left[\frac{m-2}{m}\left(\frac{1}{r^2} - \frac{z}{R^3} - \frac{z}{Rr^2}\right)\right] \tag{A.6}$$

$$\tau_{rt} = \tau_{zt} = 0 \tag{A.7}$$

$$\tau_{rz} = \frac{3P}{2\pi}\frac{rz^2}{R^5} \tag{A.8}$$

$$\tau_{zx} = \frac{3P}{2\pi}\frac{z^2 x}{R^5} \tag{A.9}$$

$$\tau_{zy} = \frac{3P}{2\pi}\frac{z^2 y}{R^5} \tag{A.10}$$

In the semi-infinite medium by a single, concentrated load, according to the Boussinesq's Theory, horizontal and vertical displacements are also obtained as follows:

$$u = \frac{(1-2\nu)(1+\nu)P}{2\pi E r}\left[z\left(r^2 + z^2\right)^{-\frac{1}{2}} - 1 + \frac{1}{1-2\nu}r^2 z\left(r^2 + z^2\right)^{-\frac{3}{2}}\right] \tag{A.11}$$

$$w = \frac{P}{2\pi E}\left[(1+\nu)z^2\left(r^2+z^2\right)^{-\frac{3}{2}} + 2(1-\nu^2)\left(r^2+z^2\right)^{-\frac{1}{2}}\right] \quad \text{(A.12)}$$

The stresses in soil at any point $N(R; \beta)$ in polar coordinates are:

$$\sigma_z = \frac{3P}{2\pi R^2}\cos^3\beta \quad \text{(A.13)}$$

$$\sigma_r = \frac{P}{2\pi R^2}\left(3\sin^2\beta\cos\beta - \frac{m-2}{m}\frac{1}{1+\cos\beta}\right) \quad \text{(A.14)}$$

$$\sigma_t = -\frac{m-2}{m}\frac{P}{2\pi R^2}\left(\cos\beta - \frac{1}{1+\cos\beta}\right) \quad \text{(A.15)}$$

For m = 2, $\sigma_t = 0$ (A.16)

$$\tau = \frac{3P}{2\pi R^2}\sin\beta\cos^2\beta \quad \text{(A.17)}$$

A volume-stable soil is characterized by Poisson's coefficient of $m = 2$, in which the cubal deformation is proportional to $(m - 2)$. With $m = 2$, Poisson's ratio is $\mu = 1/m = 0.5$.

Engineers are mostly interested in the vertical, normal, compressive stress, σ_z, particularly as it pertains to the bearing capacity of soil at different depths and on different types of soil layer below the ground surface, and to consolidation settlement analysis of foundation soils. For the same reasons, the derivation of the equation of the σ_z stress for $m = 2$ will now be presented.

A.5. Derivation of σ_z Stress

Deformation: Assume point *N(R; β)* in the mass of soil, Figure A.3, and an elementary area *m – n* at *N*, and thereby $\perp$ *R*. The problem is to express algebraically the

magnitude of the polar stress, σ_R, acting $\perp$ to the area, $m - n$, and then to find an equation for σ_z.

Consider that point N, is now translocated at point N_1, by an amount of dR. Through points N and N_1, two hemispheres can be drawn, the radii of which are R, and $R + dR$, respectively. The change in length of radius is, thus, dR. Note that the farther the point, N, is spaced, along radius from the concentrated load, P, the less is its displacement. The displacement is thought to take place because of the radially distributed stress in the soil. Besides, considering point N translocating along the circle whose radius is R, note that when $\beta = 0$, displacement of point N is larger than at $\beta > 0$. At $\beta = 90°$, displacement of point N approaches to the value of zero.

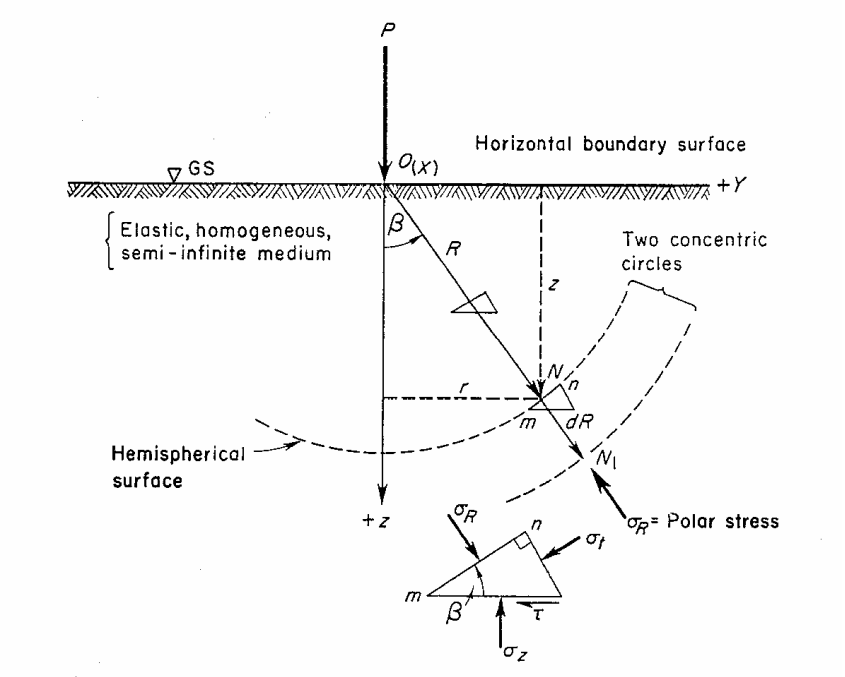

Figure A.3. State of stress at a point (Jumikis, 1962)

Designating displacement by the symbol, s, and noting from the above discussion that displacement is inversely proportional to R, and that displacement for a constant, R, is largest when $\beta = 0$, then displacement, s, can be written as

$$s = C\frac{\cos\beta}{R} \tag{A.18}$$

where C = coefficient of proportionality. At constant, R, when $\beta = 90°$, $s = 0$.

Assume now that point N is displaced at point N_1. Displacement, analogous to equation (A.18), is written as

$$s_1 = C\frac{\cos\beta}{R + dR} \tag{A.19}$$

Strain, ε, or relative deformation, δ/dR, relative to length, dR, where δ is absolute deformation, is

$$\varepsilon = \frac{\delta}{dR} = \frac{s - s_1}{dR} = \frac{C\cos\beta}{R\,dR} - \frac{C\cos\beta}{(R + dR)dR}, \tag{A.20}$$

$$\varepsilon = \frac{C\cos\beta}{R^2 + R\,dR} \tag{A.21}$$

Stress and Strain: Neglecting in the denominator of equation (A.21) the quantity (R dR) which is small as compared with R^2, obtain radial compressive strain

$$\varepsilon = \frac{C\cos\beta}{R^2} \tag{A.22}$$

By Hooke's Law, it can be assumed that stress is proportional to strain

$$\sigma_R = E\,\varepsilon \tag{A.23}$$

where E = modulus of elastisity, then the algebraic expression for polar stress is

$$\sigma_R = \frac{EC\cos\beta}{R^2} \tag{A.24}$$

Equilibrium: The coefficients, α and C, in equation (A.24), and consequently the polar compressive stress, σ_R, can be determined from the equilibrium condition between the single, concentrated load, P, acting normally to the horizontal, semi-infinite plane along the z-axis, and the system of the vertical projections of the upward-directed, polar, compressive stresses (equation A.24), acting with uniform distribution over the hemispherical surface with a radius of R, through point N, for example.

$\sum F_z = 0$

$$P = \int_0^A \sigma_R \cos\beta \; dA \tag{A.25}$$

where $$dA = 2\pi R\, dh = 2\pi R\left(R\, d\beta\right)\sin\beta = 2\pi R^2 \sin\beta\, d\beta \tag{A.26}$$

is the curved surface of the spherical zone, n_1nmm_1, bounded by two parallel planes (nn_1 and mm_1), Figure A.4.

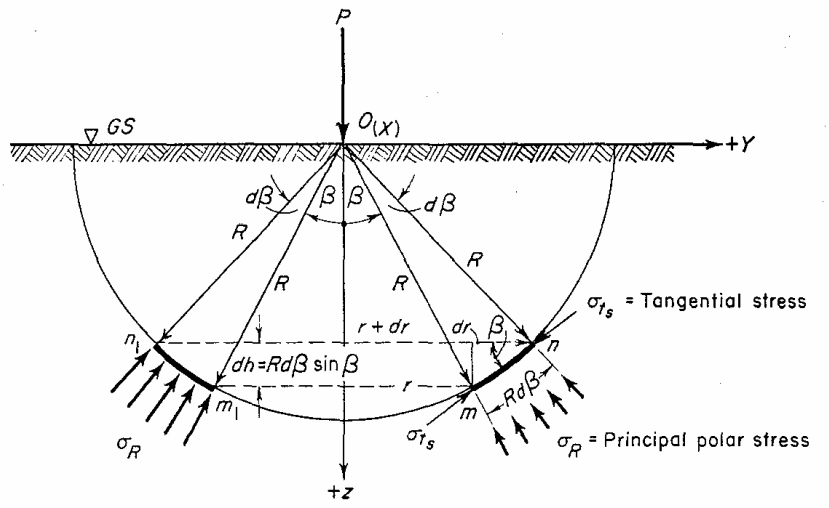

Figure A.4. Equilibrium conditions

Equation (A.25) is now rewritten as

$$P = 2\pi R^2 \int_0^{\pi/2} \sigma_R \sin\beta \cos\beta \, d\beta \tag{A.27}$$

or, after integration,

$$P = \frac{2}{3}\pi E C\,, \tag{A.28}$$

$$E C = \frac{3}{2}\left(P/\pi\right) \text{ and } C = \frac{3P}{2\pi E}\,. \tag{A.29}$$

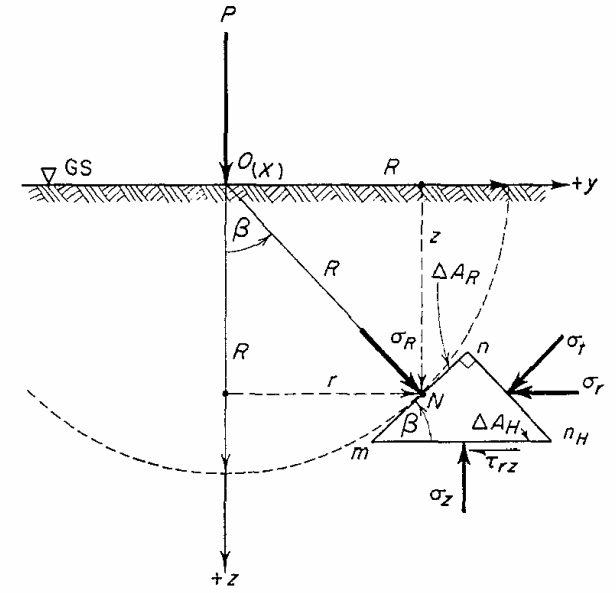

Figure A.5. Relation of vertical stresses to polar stresses

Polar Stress: Substituting equation (A.29) into equation (A.24), obtain the expression for polar stress

$$\sigma_R = \frac{3}{2}\frac{P}{\pi}\frac{\cos\beta}{R^2} \tag{A.30}$$

This equation reads that the polar stress, σ_R, varies inversely as the square of the distance, R^2, from the point of application of the concentrated load, P, at the ground surface.

Vertical Normal Stress: In foundation engineering engineers are interested more in the vertical, normal, compressive stress, σ_z, acting on a horizontal area rather than in the polar stress. To find the vertical, normal, compressive stress, σ_z, Figure A.5, use is now made of Mohr's graphical stress circle, Figure A.6. By means of this construction,

$$\sigma_z = \sigma_R \cos^2 \beta \tag{A.31}$$

Note from Figure A.6 that angle β determines the magnitude of σ_z ; σ_R is here known from equation A.30.

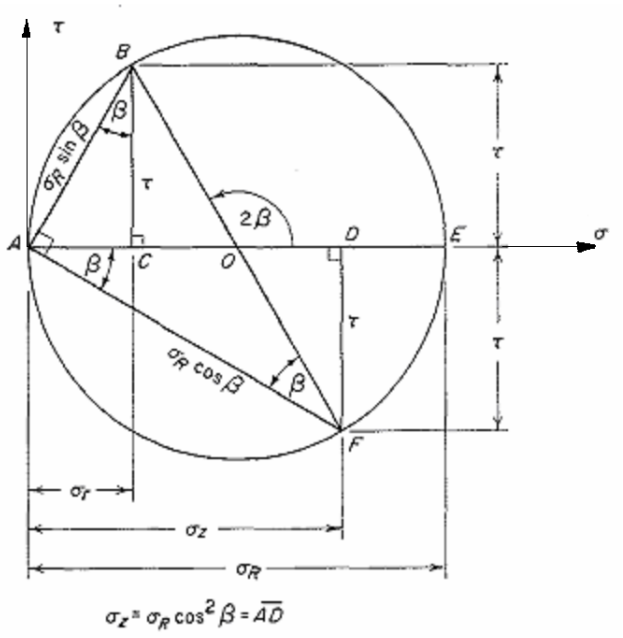

Figure A.6. Finding vertical stresses σ_z , from Mohr's circle (Jumikis, 1962)

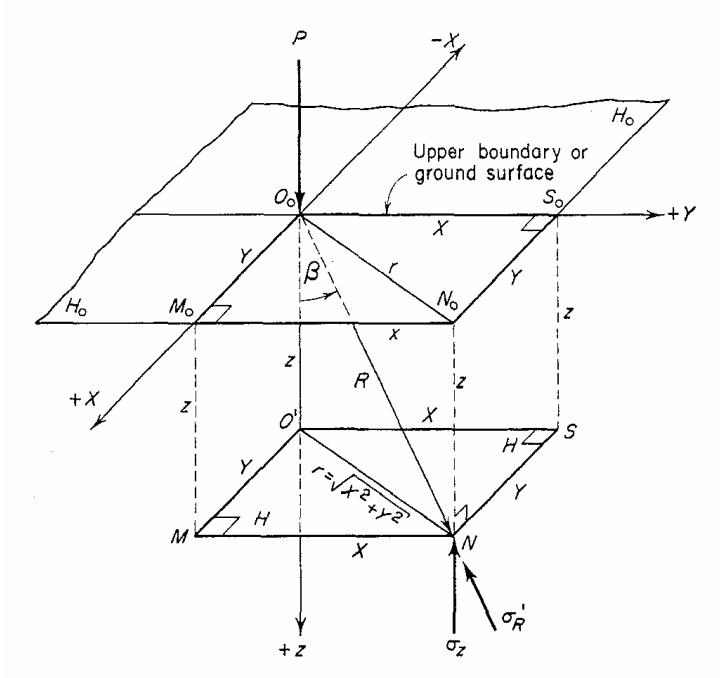

Figure A.7. Coordinates of point N, the point of application of σ_z (Jumikis, 1962)

Because $\cos\beta = z/R$,

$$\sigma_z = \sigma_R \left(\frac{z}{R}\right)^2 \tag{A.32}$$

or substituting equation (A.30) into equation (A.32), obtain

$$\sigma_z = \frac{3}{2}\frac{P}{\pi}\frac{z^3}{R^5} \tag{A.33}$$

With $R^2 = z^2 + r^2$, and with $r^2 = x^2 + y^2$, where *x*, *y*, and *z* are the coordinates of point *N*, Figure A.7, the vertical, normal, compressive stress, σ_z, is calculated as

$$\sigma_z = \frac{3P}{2\pi z^2}\frac{1}{\left[1+\left(\frac{r}{z}\right)^2\right]^{5/2}} \tag{A.34}$$

or

$$\sigma_z = K\frac{P}{z^2} \tag{A.35}$$

where

$$K = \frac{3}{2\pi}\frac{1}{\left[1+\left(\frac{r}{z}\right)^2\right]^{5/2}} = \frac{0.478}{\left[1+\left(\frac{r}{z}\right)^2\right]^{5/2}} \tag{A.36}$$

is the Boussinesq vertical stress coefficient.

Thus, equation (A.1) permits the calculation of the vertical, normal, compressive stress, σ_z, caused by concentrated load, P, at any point N, below the boundary surface, H_o-H_o of a semi-infinite medium.

When point N is on the z-axis, on the line of action of P, then $\beta = 0$, $r = 0$, and σ_z has a maximum value of

$$\sigma_z = \frac{3P}{2\pi z^2} = (0.478)\frac{P}{z^2} \tag{A.37}$$

Note that Boussinesq's equations give the stresses in a semi infinite medium caused by the surface loads only and the medium is weightless and the load P is a concentrated point load.

APPENDIX B: NUMERICAL INTEGRATION FORMULAS

Table B.1. The Gaussian quadrature formulas for constant weight function (Krylov, 1962)

$$\int_{-1}^{1} f(x)\,dx \approx \sum_{k=1}^{n} A_k^{(n)} f(x_k^{(n)})$$

$x_k^{(n)}$	$A_k^{(n)}$
$n = 2$	
0.57735 02691 89625 76451	1.00000 00000 00000 00000
$n = 3$	
0.77459 66692 41483 37704	0.55555 55555 55555 55556
0.00000 00000 00000 00000	0.88888 88888 88888 88889
$n = 4$	
0.86113 63115 94052 57522	0.34785 48451 37453 85737
0.33998 10435 84856 26480	0.65214 51548 62546 14263
$n = 5$	
0.90617 98459 38663 99280	0.23692 68850 56189 08751
0.53846 93101 05683 09104	0.47862 86704 99366 46804
0.00000 00000 00000 00000	0.56888 88888 88888 88889
$n = 6$	
0.93246 95142 03152 02781	0.17132 44923 79170 34504
0.66120 93864 66264 51366	0.36076 15730 48138 60757
0.23861 91860 83196 90863	0.46791 39345 72691 04739
$n = 7$	
0.94910 79123 42758 52453	0.12948 49661 68869 69327
0.74153 11855 99394 43986	0.27970 53914 89276 66790
0.40584 51513 77397 16691	0.38183 00505 05118 94495
0.00000 00000 00000 00000	0.41795 91836 73469 38776
$n = 8$	
0.96028 98564 97536 23168	0.10122 85362 90376 25915
0.79666 64774 13626 73959	0.22238 10344 53374 47054
0.52553 24099 16328 98582	0.31370 66458 77887 28734
0.18343 46424 95649 80494	0.36268 37833 78361 98297
$n = 9$	
0.96816 02395 07626 08984	0.08127 43883 61574 41197
0.83603 11073 26635 79430	0.18064 81606 94857 40406
0.61337 14327 00590 39731	0.26061 06964 02935 46232
0.32425 34234 03808 92904	0.31234 70770 40002 84007
0.00000 00000 00000 00000	0.33023 93550 01259 76316

Table B.2. The Gaussian Laguerre quadrature formulas (Krylov, 1962)

$$\int_0^\infty x^a e^{-x} f(x)\,dx \approx \sum_{k=1}^{n} A_k^{(n)} f(x_k^{(n)})$$

$x_k^{(n)}$	$A_k^{(n)}$
$n = 1$	
1.00000 00000 00	1.00000 00000 00
$n = 2$	
0.58578 64376 27	0.85355 33905 93
3.41421 35623 73	0.14644 66094 07
$n = 3$	
0.41577 45567 83	0.71109 30099 29
2.29428 03602 79	0.27851 77335 69
6.28994 50829 37	(−1) 0.10389 25650 16
$n = 4$	
0.32254 76896 19392 312	0.60315 41043 41633 602
1.74576 11011 58346 58	0.35741 86924 37799 687
4.53662 02969 21127 98	(−1) 0.38887 90851 50053 843
9.39507 09123 01133 13	(−3) 0.53929 47055 61327 450
$n = 5$	
0.26356 03197 18	0.52175 56105 83
1.41340 30591 07	0.39866 68110 83
3.59642 57710 41	(−1) 0.75942 44968 17
7.08581 00058 59	(−2) 0.36117 58679 92
12.64080 08442 76	(−4) 0.23369 97238 58
$n = 6$	
0.22284 66041 79	0.45896 46739 50
1.18893 21016 73	0.41700 08307 72
2.99273 63260 59	0.11337 33820 74
5.77514 35691 05	(−1) 0.10399 19745 31
9.83746 74183 83	(−3) 0.26101 72028 15
15.98287 39806 02	(−6) 0.89854 79064 30
$n = 7$	
0.19304 36765 60	0.40931 89517 01
1.02666 48953 39	0.42183 12778 62
2.56787 67449 51	0.14712 63486 58
4.90035 30845 26	(−1) 0.20633 51446 87
8.18215 34445 63	(−2) 0.10740 10143 28
12.73418 02917 98	(−4) 0.15865 46434 86
19.39572 78622 63	(−7) 0.31703 15479 00
$n = 8$	
0.17027 96323 05101 000	0.36918 85893 41637 530
0.90370 17767 99379 912	0.41878 67808 14342 956
2.25108 66298 66130 69	0.17579 49866 37171 806
4.26670 01702 87658 79	(−1) 0.33343 49226 12156 515
7.04590 54023 93465 70	(−2) 0.27945 36235 22567 252
10.75851 60101 80995 2	(−4) 0.90765 08773 35821 310
15.74067 86412 78004 6	(−6) 0.84857 46716 27253 154
22.86313 17368 89264 1	(−8) 0.10480 01174 87151 038

REFERENCES

Abdel-Fattah, T. T., H. A. Hodhod, A. Y. Akl, 2000, "A Novel Formulation of Infinite Elements for Static Analysis", *Computers & Structures*, Vol. 77, pp. 371-379.

Anderson, D. L. and R. L. Ungless, 1977, "Infinite finite elements", *Int. Symp. Innovative Num. Anal. Appl. Eng. Sci*., France.

Askar, H. G. and P. P. Lynn, 1984, "Infinite Elements for Ground Freezing Problems", *Journal of Engineering Mechanics*, Vol. 110, pp. 157-172.

Astley, R. J., 2000, "Infinite elements for wave problems: a review of current formulations and an assessment of accuracy", *International Journal of Numerical Methods in Engineering*, Vol. 49, pp. 951-976.

Beer, G. and J. L. Meek, 1981, "Infinite Domain Elements", *International Journal for Numerical Methods in Engineering*, Vol. 17, pp. 43-52.

Bettess, P., 1977, "Infinite elements", *International Journal for Numerical Methods in Engineering*, Vol. 11, pp. 53-64.

Bettess, P., 1980, "More on infinite elements", *International Journal for Numerical Methods in Engineering*, Vol. 15, pp. 1613-1626.

Bettess, P., 1992, *Infinite Eleements*, Penshaw Press, U.K.

Bettess, P., C. Emson, and K. Baldo, 1982, "Some Useful Techniques for Testing Infinite Elements", *Applied Mathematical Modeling*, Vol. 6, pp. 436-440.

Bettess, P., and O. C. Zienkiewicz, 1977, "Diffraction and refraction of surface waves using finite and infinite elements", *International Journal of Numerical Methods in Engineering*, Vol. 11, pp. 1271-1290.

Bolza, O., 1973, *Lectures on the Calculus of Variations*, Chelsea Publishing Company, New York.

Booker, J. R. and J. C. Small, 1981, "Finite Element Analysis of Problems with Infinitely Distant Boundaries", *International Journal of Numerical Methods in Engineering*, Vol. 5, pp. 345-368.

Cheng, Y. M., 1996, "The Use of Infinite Elements", *Computers and Geotechnics*, Vol. 18, No. 1, pp. 65-70.

Cheung Y. K., S. H. Lo, A. Y. T. Leung, 1996, *Finite Element Implementation*, Blackwell Scince Ltd.

Chow Y. K., 1987, "Vertical vibration of three-dimensional rigid foundation on layered media", *Earthquake Eng. Struct. Dyn*., Vol. 15, pp. 585-594.

Chow Y. K., and I. M. Smith, 1981, "Static and Periodic Infinite Elements", *International Journal for Numerical Methods in Engineering*, Vol. 17, pp. 503-526.

Chuhan Z. and Z. Chongbin, 1987, "Coupling Method of Finite and Infinite Elements for Strip Foundation Wave Problems", *Earthquake Engineering and Structural Dynamics*, Vol. 15, pp. 839-851.

Clough, R. W., 1960, "The Finite Element Method in Plane Stress Analysis", *Proceedings, American Society of Civil Engineers, 2nd Conference on Electronic Computation*, Pittsburgh, pp. 345-378.

Cook, R. D., D. S. Malkus, and M. E. Plesha, 1989, *Concepts and Applications of Finite Element Analysis*, John Wiley & Sons, Inc., USA.

Courant, R., 1943, "Variational Methods for the Solution of Problems of Equilibrium and Vibrations", *Bulletin of the American Mathematical Society*, Vol. 49, pp.1-23.

Curnier, A., 1983, "A Static Infinite Element", *International Journal for Numerical Methods in Engineering*, Vol. 19, pp. 1479-1488.

Damjanıć, F., D. R. J. Owen, 1984, "Mapped Infinite Elements in Transient Thermal Analysis", *Computers & Structures*, Vol. 19, No. 4, pp. 673-687.

Elsgolc, L. E., 1962, *Calculus of Variations*, Addison-Wesley Publishing Company Inc., Massachusetts.

Fish, J., T. Belytschko, 2007, *A First Course in Finite Elements*, John Wiley & Sons, Inc., England.

Gelfand, I. M. and S. V. Fomin, 1963, *Calculus of Variations*, Prentice-Hall, Englewood Cliffs, N.J.

GeoStudio Version 6.02, *Stress and Deformation Modeling with SIGMA/W*, GEO-SLOPE International Ltd, Calgary, Alberta, Canada, 2004.

GeoStudio, *Analysis Reference*, Stress and Deformation Modeling with SIGMA/W, GEO-SLOPE International Ltd, Calgary, Alberta, Canada, 2004.

GeoStudio, *Tutorials*, GEO-SLOPE International Ltd, Calgary, Alberta, Canada, 2004.

Gökhan, G., 1978, *Varyasyonlar Hesabı*, Kutulmuş Matbaası, İstanbul.

Hamidzadeh-Eraghi, H., R. and P. Grootenhuis, 1981, "The dynamics of a rigid foundation on the surface of an elastic half-space", *Earthquake Eng. Struct. Dyn.*, Vol. 9, pp.505-515.

Harmandar, E., 2002, *Performance of Higher Order Finite Elements*, M.S. Thesis, Boğaziçi University.

Hrennikoff, A., 1941, "Solution of Problems in Elasticity by the Frame Work Method", *Journal of Applied Mechanics*, Vol. 8, No: 4, pp. 169-175.

Jumikis, A. R., 1969, *Theoretical Soil Mechanics : with practical applications to soil mechanics and foundation engineering*, Van Nostrand Reinhold Co., New York.

Jumikis, A. R., 1962, *Soil Mechanics*, D. Van Nostrand Company, Inc., New Jersey.

Kaplan, W., 1980, *Advanced Mathematics for Engineers*, Addison-Wesley Publishing Company, USA.

Khalili, N., M. Yazdchi and S. Valliappan, 1999, "Wave Propagation Analysis of Two-Face Saturated Porous Media Using Coupled Finite-Infinite Element Method", *Soil Dynamics and Earthquake Engineering*, Vol. 18, pp. 533-553.

Krasnov, M. L., G. I. Makarenko and A. I. Kiselev, *Problems and Exercises in the Calculus of Variations*, MIR Publishers, Moscow.

Kreyszig, E., 1962, *Advanced Engineering Mathematics*, John Wiley and Sons, New York.

Krylov, V. I., 1962, *Approximate Calculation of Integrals*, The Macmillan Company, New York.

Kumar P., 1985, "Static Infinite Element Formulation", *Journal of Structural Engineering*, Vol. 111, pp. 2355-2372.

Kumar P., 1986, "Numerical Modeling Criterion for the Analysis of Underground Openings using Infinite Elements", *Applied Mathematical Modeling*, Vol. 10, pp. 357-366.

Kumar P., 2000, "Infinite Elements for Numerical Analysis of Underground Excavations", *Tunneling and Underground Space Technology*, Vol. 15, pp. 117-124.

Logan, D. L., 2002, *A First Course in the Finite Element Method*, Thomson Learning, California.

Lynn P. P., and H. A. Hadid, 1981, "Infinite elements with $1/r^n$ type decay", *International Journal for Numerical Methods in Engineering*, Vol. 17, pp. 347-355.

Lysmer, J., and R. L. Kuhlemeyer, 1969, "Finite Dynamic Model for Infinite Media", *Journal of the Engineering Mechanics Division of the ASCE*, pp. 859-877, August.

McHenry, D., 1943, "A Lattice Analogy for the Solution of Plane Stress Problems", *Journal of Institution of Civil Engineers*, Vol. 21, pp. 59-82.

Medina, F., 1981, "An axisymmetric infinite element", *International Journal for Numerical Methods in Engineering*, Vol. 17, pp. 1177-1185.

Medina, F., 1983, "Finite Element Techniques for Problems of Unbounded Domains", *International Journal for Numerical Methods in Engineering*, Vol. 19, pp. 1209-1226.

Noor, A. K., 1991, *Bibliography of books and monographs on finite element technology*, Appl. Mech. Rev., pp. 307-317.

Pissanetzky, S., 1983, "An Infinite Element and a Formula for Numerical Quadrature over an Infinite Interval", *International Journal for Numerical Methods in Engineering*, Vol. 19, pp. 913-927.

Poulos, H. G. and E. H. Davis, 1974, *Elastic Solutions for Soil and Rock Mechanics*, John Wiley & Sons, Inc, New York.

Rajapakse, R. K. N. D. and P. Karasudhi, 1986, "An efficient Elastodynamic Infinite Element", *International Journal of Solids and Structures*, Vol. 22, No. 6, pp. 643-657.

Rao, S. S., 1989, *The Finite Element Method in Engineering*, Pergamon Press, Oxford.

Sadecka, L., 2000, "A Finite / Infinite Element Analysis of Thick Plate on a Layered Foundation", *Computers and Structures*, Vol. 76, pp. 603-610.

Simoni, L. and B. A. Schrefler, 1987, "Mapped Infinite Elements in Soil Consolidation" *International Journal for Numerical Methods in Engineering*, Vol. 24, pp. 513-527.

Tezcan, S. S., 1963, "Simplified Formulation of Stiffness Matrices", *Journal of the Structural Division*, ASCE, pp. 445-449.

Turner, M. J., R. W. Clough, H. C. Martin, and L. J. Topp, 1956, "Stiffness and Deflection Analysis of Complex Structures", *Journal of Aeronautical Sciences*, Vol. 23, No. 9, pp. 805-824.

Ungless, R. L., 1973, *An infinite finite element*, M.S. Thesis, University of British Columbia.

Wong, H. L. and J. E. Luco, 1976, "Dynamic response of rigid foundations of arbitrary shape", *Earthquake Eng. Struct. Dyn.*, Vol. 4, pp.579-587.

Wood, W. L., 1976, "On the finite element solution of an exterior boundary value problem", *International Journal for Numerical Methods in Engineering*, Vol. 10, pp. 885-891.

Yong, S. C., and C. B. Yun, 1992, "Axisymmetric infinite elements for soil-structure interaction analysis", *Engineering Structures*, Vol. 14, pp. 361-370.

Yun, C., D. Kim and J. Kim, 2000, "Analytical Frequency-Dependent Infinite Elements for Soil-Structure Interaction Analysis in Two-Dimensional Medium", *Engineering Structures*, Vol. 22, pp. 258-271.

Zhao, C. and S. Valliappan, 1993, "A Dynamic Infinite Element for Three-Dimensional Infinite Domain Wave Problems", *International Journal for Numerical Methods in Engineering*, Vol. 36, pp. 2567-2580.

Zhao, C. and S. Valliappan, 1993, "Transient Infinite Elements for Seepage Problems in Infinite Media", *International Journal for Numerical Methods in Engineering*, Vol. 17, pp. 323-341.

Zhao, C. and S. Valliappan, 1994, "Transient Infinite Elements for Contaminant Transport Problems", *International Journal for Numerical Methods in Engineering*, Vol. 37, pp. 1143-1158.

Zhao, C., C. Zang, and G. Zang, 1987, "Study on the characteristics of mapping dynamic infinite elements", *Earthquake Eng. Eng. Vib.,* , Vol. 7, pp. 1-15.

Zienkiewicz, O. C., 1971, *The Finite Element Method in Engineering Science*, McGraw-Hill Publishing Company, London.

Zienkiewicz, O. C. and Y. K. Cheung, 1965, "Finite Elements in the Solution of Field Problems", *The Engineer*, pp. 507-510.

Zienkiewicz, O. C. and Y. K. Cheung, 1967, *The Finite Element Method in Structural and Continuum Mechanics*, McGraw-Hill Publishing Company, London.

Zienkiewicz, O. C., C. Emson and P. Bettess, 1983, "A Novel Boundary Infinite Element", *International Journal for Numerical Methods in Engineering*, Vol. 19, pp. 393-404.

Zienkiewicz, O. C. and P. Bettess, 1977, "Diffraction and Refraction of Surface Waves Using Finite and Infinite Elements", *International Journal for Numerical Methods in Engineering*, Vol. 11, pp. 1271-1290.

Zienkiewicz, O. C., K. Bando, P. Bettess, C. Emson, and T. C. Chiam, 1985, "Mapped Infinite Elements for Exterior Wave Problems" ,*International Journal for Numerical Methods in Engineering*, Vol. 21, pp. 1229-1251.

Zienkiewicz, O. C. and P. Bettess, 1975, “Infinite elements in the study of fluid structure interaction problems”, *Proc. 2nd Int. Symp. On Comp. Methods Appl. Sci.*, Versailles, also published in Lecture Notes in Physics, Vol. 58, Eds. J. Ehlers et al., Springer-Verlag, Berlin, 1976.

Zienkiewicz, O. C. and Y. K. Cheung, 1967, *The Finite Element Method in Structural and Continuum Mechanics*, McGrow-Hill Publishing Company, London.